SLAC-233
UC-34d
(T/E)

PARITY VIOLATING ASYMMETRIES AND WEAK NEUTRAL CURRENTS*

Thomas Tsao

Stanford Linear Accelerator Center
Stanford University
Stanford, California 94305

December 1980

Prepared for the Department of Energy

under contract number DE-AC03-76SE00515

Printed in the United States of America. Available from the National Technical Information Service, U.S. Department of Commerce, 5285 Port Royal Road, Springfield, VA 22161. Price: Printed Copy A06; Microfiche A01.

---

* Ph.D. dissertation.

PARITY VIOLATING ASYMMETRIES AND

WEAK NEUTRAL CURRENTS

Thomas Tsao, Ph.D.
Stanford University, 1980

The vector and axial couplings of leptons and quarks to the weak neutral current are studied by focusing on the parity violating asymmetries which arise in the following scattering processes: polarized-electron nucleon elastic collisions, dilepton production in polarized-proton proton scattering, polarized-electron positron annihilation into fermion pairs, and polarized-electron electron collisions. Numerical results are presented for the Weinberg-Salam model of electroweak interactions. It is found that at $q^2 = 1$ GeV^2, the parity violating asymmetries for elastic electron nucleon collisions are typically $\mathcal{O}(10^{-5})$ for proton, neutron, and deuteron targets. For dilepton production at presently available energies of $s = 10^3$ GeV^2, the parity violating asymmetries are $\mathcal{O}(10^{-2})$ while at much higher energies $s = 6.4 \times 10^5$ GeV^2, the asymmetries are $\mathcal{O}(10^{-1})$. Electron positron annihilation into $\mu^+\mu^-$, $q\bar{q}$ and e^+e^- give parity violating asymmetries that are typically $\mathcal{O}(10^{-1}$ to 1) for s near the Z^o pole. Polarized-electron electron scattering yields parity violating asymmetries of $\mathcal{O}(10^{-2})$ at $s \approx 10^4$ GeV^2.

The restrictions imposed on the parameters of the six-quark model by the neutral kaon system are discussed - with QCD effects included in the leading logarithmic approximation. The dependence of the CP violation parameter ϵ', the b-quark lifetime, and the ratio of decay widths $\Gamma(b \to ux)/\Gamma(b \to cx)$ on the six-quark model parameters is also discussed.

DEDICATION

To the memory of my father, Wei Yi Tsao, and to my mother, Nancy Shih Cheng Tsao, for making these years worthwhile.

ACKNOWLEDGMENTS

Several people contributed significantly toward the completion of this thesis. I am deeply grateful to my research advisor, Fred Gilman, for providing me with the opportunity to do high-energy theory during these past three years. His patient teaching, steady encouragement, and warm support have made this a valuable and enriching experience. In addition, I would like to acknowledge Brad Gaiser and Mark Wise for many helpful suggestions and useful technical discussions. I would expecially like to thank Rich McCord for numerous assistances and illuminating conversations. Finally, I am grateful to Sharon Jensen for her assistance in preparing a preliminary version of this thesis.

TABLE OF CONTENTS

CHAPTER I

INTRODUCTION

A research area of considerable interest to high energy physicists during the past decade has been the subject of neutral current interactions. This new type of weak interaction was first discovered[1] in 1973 in the particle reaction $\nu p \rightarrow \nu x$. Unlike the familiar weak beta decay in which the charge Q of the nucleon in the system undergoes a change of one unit ($\Delta Q = +1$), this new interaction does not change the charge of the hadronic system ($\Delta Q = 0$). The ordinary beta decay with $\Delta Q \neq 0$ is a charged current weak interaction, which proceeds via the exchange of a very massive charged intermediate vector boson W. This newly discovered weak interaction with $\Delta Q = 0$ has come to be called the neutral current interaction, since it is mediated by a massive neutral intermediate vector boson (known as the Z^o). As a matter of fact, the carrier of this new force had been conjectured by Weinberg and Salam[2] in their gauge theory of electroweak interactions, prior to 1973.

As with charged current interactions, the investigation into the structure of neutral current interactions has been rewarding for both experimental and theoretical workers. The experimentalists have conducted precise and beautiful measurements confirming the existence of the weak neutral current in a wide variety of particle reactions.[3] These range from the initial discovery of the neutral current in the pioneering neutrino scattering experiment done at Gargamelle, to the recent results from the SLAC polarized-electron experiment -- which eliminated most of the competing gauge models. Spurred on by the

experimental discoveries, the theorists have gained deeper understanding of the structure of non-abelian gauge theories, spontaneous symmetry breaking, renormalization, etc. By combining the electromagnetic and weak forces into a single electroweak force, the theorists have attained partial success in the unification of the four fundamental interactions.

Of the many possible gauge models of the electroweak interaction, the Weinberg-Salam (WS) theory is the simplest. At present, it can successfully account for all the phenomenology of neutral current processes. Indeed, it has become the 'standard' model with which theoretical analyses of available experimental information on neutral current processes are based.

Two methods of analysis of experimental data are currently in vogue. The first approach is to view the neutral current as a totally new phenomenon, with the goal being the determination of the unknown effective couplings of the new interaction. The second method is to assume that the WS theory gives the correct description of nature. Theoretical predictions based on the WS model are calculated in lowest-order perturbation theory, and then compared with the experimental data. These comparisons have verified the consistency of the WS model to within some minor discrepancies, which are assumed to be due to additional, higher-order corrections to the lowest-order results.

A combination of these two points of view is taken in this report. However, the purpose here is not to analyze experimental data. Rather, new reactions which involve the neutral current are proposed and analyzed with the aim of providing alternate measurements of the effective couplings of fermions to the weak neutral current. For the purpose of predicting actual numbers for cross sections and asymmetries, the WS model is

applied -- with the latest experimental value for the weak mixing angle $\sin^2\theta_W$ being used as input.

At present laboratory energies, the effects of the weak neutral current in most physical processes are largely overshadowed by the ever-present electromagnetic current. One way of overcoming the effects of the competing electromagnetic interaction is to look for explicitly parity violating quantities. Since the electromagnetic coupling of the photon to matter is parity conserving, observation of parity violation is a direct way of eliminating the bothersome electromagnetic background.

In Chapter II the parity violating difference in the elastic scattering of right-handed and left-handed longitudinally polarized electrons with a nucleon is studied. It is found that neutron targets yield larger parity violating asymmetries (by about a factor of three for $\sin^2\theta_W = \frac{1}{4}$) than proton targets -- mainly because the d quark has a larger vector coupling to the Z^o than the u quark. The parity violating asymmetry for polarized-electron deuteron scattering is also derived. All electron-nucleon asymmetries are $\mathcal{O}(10^{-5})$ at SLAC energies. In Chapter III, the parity violating asymmetries in dilepton production by polarized protons are examined. Because larger collision energies are accessible in pp collisions, and also because the vector coupling of quarks to the Z^o is much larger in magnitude than the electron vector coupling, the dilepton asymmetries ($\mathcal{O}(10^{-2})$ at present laboratory energies of $s = 10^4$ GeV^2) are much larger than the previously considered electron-nucleon asymmetries. In addition, asymmetries for very energetic collisions (energies large compared to the Z^o mass) are considered. In the following chapter, the cross sections, parity violating and angular asymmetries for polarized-

electron positron annihilation into $\mu^+\mu^-$, $q\bar{q}$ and e^+e^- are studied. For completeness, the reaction $e^-e^- \to e^-e^-$ is also discussed in Chapter IV.

In Chapter V, we turn to a somewhat different topic -- that of determining the angular parameters of the six-quark model. The K^o-$\bar{K}^o$ system has traditionally been used to derive constraints on the six-quark model parameters. The transformation of the K^o into a $\bar{K}^o$ is a second-order weak effect which occurs through a box diagram involving the exchange of two charged W's inside a loop. There is no first-order diagram since the single Z^o cannot make the required change in quark flavors. Nevertheless, the second-order box diagram with the two W's may be considered an effective neutral current interaction.

Two measurable quantities of the K^o-$\bar{K}^o$ system are the mass difference and the CP violation parameter. These two quantities are related to the real and imaginary parts, respectively, of the effective Hamiltonian for K^o-$\bar{K}^o$ transition. The two equations have a complicated dependence on the six-quark model angular parameters. Experimental values for the mass difference and CP violation parameter consequently impose constraints on the values that can be taken on by these six-quark parameters. In Chapter V we consider the effects of quantum chromodynamic (QCD) corrections (calculated in the leading logarithmic approximation) on the constrained parameters. Since there are three unknown parameters -- the two Cabibbo-like mixing angles θ_2, θ_3 and the single phase angle δ -- but only two coupled equations relating these parameters, the two QCD-modified constraining equations can at best only be "solved" for two angles as functions of a third angle. Here $\sin\theta_3$ has been chosen as the independent parameter, and $\sin\theta_2$ and $\sin\delta$ are expressed in terms

of this parameter. We conclude Chapter V by using our results for the six-quark model parameters to calculate the dependence on $\sin\theta_3$ of the CP violation parameter ε', the b-quark lifetime, and the ratio of decay widths $\Gamma(b \to ux)/\Gamma(b \to cx)$.

REFERENCES AND FOOTNOTES FOR CHAPTER I

1. For reviews and references on the subject of weak neutral currents, see L. M. Sehgal, Status of Neutral Currents in Neutrino Interactions, Neutrino-78 Conference Proceedings, Purdue University; J. J. Sakurai, Neutral Currents and Gauge Theories, Conference in honor of P. Dirac, Florida State University, April 1978.
2. S. Weinberg, Phys. Rev. Lett. 19, 1264 (1967); A. Salam in Elementary Particle Theory: Relativistic Groups and Analyticity (Nobel Symposium No. 8), edited by N. Svartholm (Almqvist and Wiksell, Stockholm, 1968), p. 367.
3. See J. J. Sakurai and references contained within.

CHAPTER II

POLARIZED-ELECTRON ELASTIC SCATTERING ASYMMETRIES IN SU(2) × U(1)*

1. Introduction

An interference between the weak and electromagnetic interactions can give rise to a difference between the cross sections for scattering of right- and left-handed electrons on either leptonic or hadronic targets. The measurement[1] of deep inelastic asymmetries to the required level of accuracy increases the interest in the theoretical predictions for both elastic and inelastic electron-nucleon scattering asymmetries.

The consequences of weak-electromagnetic interference for electron scattering experiments have been explored over the last several years since gauge theories in general, and the Weinberg-Salam SU(2) × U(1) model[2] in particular, have become central to understanding the weak interactions. The asymmetry expected in polarized electron elastic scattering has been calculated in several papers.[3,4,5] Recently predictions for elastic electron-proton scattering, Δ electroproduction, and deep inelastic scattering were brought up-to-date in terms of gauge theories of present interest.[6]

However, in the case of elastic scattering Ref. 6 was restricted in that only elastic electron-proton scattering was considered, certain approximations were made which are relevant to high energy ($E_{beam} \approx$ 20 GeV) experiments done at SLAC, and results were presented only for $\sin^2\theta_W = 1/3$. Here we remove these restrictions. In Sect. 2 we calculate both electron-proton and electron-neutron elastic scattering for a range

of values of $\sin^2\theta_W$. Furthermore, we calculate the terms neglected in Ref. 6 within an $SU(2) \times U(1)$ gauge theory and show their quantitative effect. While at low energy they turn out to be of considerable importance,[7] we show they truly are negligible for most SLAC energies when the right-handed electron is a singlet under the gauge group, as in the original Weinberg-Salam model. When the electron is assigned to a right-handed doublet the previously neglected terms give the whole asymmetry, and it is an order of magnitude smaller. Elastic electron-neutron scattering turns out to give an asymmetry many times bigger than that for elastic electron-proton scattering for typical values of the kinematic and $SU(2) \times U(1)$ model parameters.

With some quite general assumptions about the gauge theory transformation properties of the quarks making up the neutron and proton in the deuteron, we rederive in Sect. 3 a very simple form[5] for the asymmetry in elastic electron-deuteron scattering. It is relatively large in magnitude and opposite in sign to that predicted for elastic or inelastic scattering on protons and neutrons separately. Finally in Sect. 4 we present a discussion of our results.

2. Polarized-Electron Nucleon Elastic Scattering Asymmetries

As noted above, the asymmetry between the cross sections for elastic scattering of right- and left-handed electrons on nucleons expected because of the interference between exchange of a photon and a weak neutral boson, Z^o, has been calculated previously.[3-6] Taking the couplings at the nucleon vertex to be the usual Dirac $\left(eF_1^\gamma(q^2)\right)$ and Pauli $\left(eF_2^\gamma(q^2)/2M_N\right)$ ones for the photon, and correspondingly, $F_1^Z(q^2)$

and $F_2^Z(q^2)$ as well as $G_A^Z(q^2)$ (the coefficient of $\gamma_\mu\gamma_5$) for the Z^o, one finds the asymmetry:[8,9]

$$A_{eN\to eN} = \frac{d\sigma_R - d\sigma_L}{d\sigma_R + d\sigma_L} = \left(\frac{2q^2}{e^2 M_Z^2}\right)\left\{-g_A\left[\frac{q^4}{4M_N^2}\left(F_1^\gamma + F_2^\gamma\right)\left(F_1^Z + F_2^Z\right)\right.\right.$$
$$\left.\left. + \left(2EE' - \frac{q^2}{2}\right)\left(F_1^\gamma F_1^Z + \frac{q^2}{4M_N^2} F_2^\gamma F_2^Z\right)\right] - g_V G_A^Z\left(F_1^\gamma + F_2^\gamma\right)\left(E^2 - E'^2\right)\right\}$$
$$\times\left\{\frac{q^4}{4M_N^2}\left(F_1^\gamma + F_2^\gamma\right)^2 + \left(2EE' - \frac{q^2}{2}\right)\left[\left(F_1^\gamma\right)^2 + \frac{q^2}{4M_N^2}\left(F_2^\gamma\right)^2\right]\right\}^{-1} \quad . \qquad (2.1)$$

Here E and E' are the initial and final electron energies and g_V and g_A are the vector and axial-vector couplings of the Z^o with mass M_Z to the (assumed) point-like electron.

In Ref. 6 the limit $q^2/2M_N E \to 0$, or equivalently $E \to \infty$, was taken in Eq. (2.1). In that limit, argued in Ref. 6 to be a good approximation in the SLAC experimental regime, Eq. (2.1) simplifies dramatically to[9]

$$A_{eN\to eN} \approx -\left(\frac{2q^2}{e^2 M_Z^2}\right)\frac{g_A\left[F_1^\gamma F_1^Z + \frac{q^2}{4M_N^2} F_2^\gamma F_2^Z\right]}{\left(F_1^\gamma\right)^2 + \frac{q^2}{4M_N^2}\left(F_2^\gamma\right)^2} \quad . \qquad (2.2)$$

We now wish to examine this high energy approximation in some detail. Specifically, we investigate quantitatively how big the terms proportional to the axial-vector coupling of the nucleon can be in various cases. Of course, when g_A of the electron vanishes, these previously neglected terms are the only contributions to the asymmetry in lowest order. To investigate this, and to calculate asymmetries with neutron as well as proton targets, we need the couplings of the Z^o to the nucleon.

For the sake of completeness, we review here the usual procedure[10] for obtaining these couplings.

We first recall that F_1^Z and F_2^Z, or equivalently G_E^Z and G_M^Z are dependent on the particular gauge theory. Their magnitude is most directly obtained by considering the coupling of the γ and Z^o to quarks. In terms of quark fields the electromagnetic current is

$$\frac{2e}{3}\,\bar{u}\gamma_\mu u - \frac{e}{3}\,\bar{d}\gamma_\mu d - \frac{e}{3}\,\bar{s}\gamma_\mu s + \frac{2e}{3}\,\bar{c}\gamma_\mu c \quad .$$

Neglecting the contribution of strange and charmed quarks to the nucleon's electromagnetic properties, we have[11]

$$\begin{aligned} \langle p \,|\, \tfrac{2e}{3}\,\bar{u}\gamma_\mu u - \tfrac{e}{3}\,\bar{d}\gamma_\mu d \,|\, p\rangle &= eG_p^\gamma \\ = \langle n \,|\, \tfrac{2e}{3}\,\bar{d}\gamma_\mu d - \tfrac{e}{3}\,\bar{u}\gamma_\mu u \,|\, n\rangle &\quad , \end{aligned} \tag{2.3a}$$

and

$$\begin{aligned} \langle n \,|\, \tfrac{2e}{3}\,\bar{u}\gamma_\mu u - \tfrac{e}{3}\,\bar{d}\gamma_\mu d \,|\, n\rangle &= eG_n^\gamma \\ = \langle p \,|\, \tfrac{2e}{3}\,\bar{d}\gamma_\mu d - \tfrac{e}{3}\,\bar{u}\gamma_\mu u \,|\, p\rangle &\quad , \end{aligned} \tag{2.3b}$$

where an isospin rotation has been used to obtain the last equalities in Eqs. (2.3a) and (2.3b). Thus,

$$\langle p|\bar{u}\gamma_\mu u|p\rangle = \langle n|\bar{d}\gamma_\mu d|n\rangle = 2G_p^\gamma + G_n^\gamma \quad , \tag{2.4a}$$

and

$$\langle p|\bar{d}\gamma_\mu d|p\rangle = \langle n|\bar{u}\gamma_\mu u|n\rangle = G_p^\gamma + 2G_n^\gamma \quad . \tag{2.4b}$$

Now in terms of right- and left-handed weak charges, Q_R and Q_L, of the quarks, which are determined by the gauge theory model, the weak vector current is

$$\frac{1}{2}\left(Q_{R,u}^Z + Q_{L,u}^Z\right)\bar{u}\gamma_\mu u + \frac{1}{2}\left(Q_{R,d}^Z + Q_{L,d}^Z\right)\bar{d}\gamma_\mu d \quad .$$

Combining this with Eq. (2.4) we have,

$$G^Z_{E,p} = \frac{1}{2}\left(Q^Z_{R,u} + Q^Z_{L,u}\right)\left(2G^\gamma_{E,p} + G^\gamma_{E,n}\right)$$

$$+ \frac{1}{2}\left(Q^Z_{R,d} + Q^Z_{L,d}\right)\left(G^\gamma_{E,p} + 2G^\gamma_{E,n}\right) \quad , \tag{2.5a}$$

$$G^Z_{M,p} = \frac{1}{2}\left(Q^Z_{R,u} + Q^Z_{L,u}\right)\left(2G^\gamma_{M,p} + G^\gamma_{M,n}\right)$$

$$+ \frac{1}{2}\left(Q^Z_{R,d} + Q^Z_{L,d}\right)\left(G^\gamma_{M,p} + 2G^\gamma_{M,n}\right) \quad , \tag{2.5b}$$

and similar equations for the vector couplings of the Z^o to the neutron.

The axial-vector couplings of the Z^o to the nucleon are determined in a similar manner. We first recall that the isovector axial-vector current is measured in weak neutron beta decays:

$$\langle p|\bar{u}\gamma_\mu\gamma_5 u - \bar{d}\gamma_\mu\gamma_5 d|p\rangle$$

$$= -\langle n|\bar{u}\gamma_\mu\gamma_5 u - \bar{d}\gamma_\mu\gamma_5 d|n\rangle = G_A(q^2) \quad , \tag{2.6}$$

where $G_A(0) = +1.24$. The isoscalar portion of the axial-vector current is determined by demanding that the ratio of isoscalar and isovector matrix elements be the same as that for total magnetic moments:[10]

$$\langle p|\bar{u}\gamma_\mu\gamma_5 u + \bar{d}\gamma_\mu\gamma_5 d|p\rangle$$

$$= \frac{3(\mu_p + \mu_n)}{\mu_p - \mu_n}\ \langle p|\bar{u}\gamma_\mu\gamma_5 u - \bar{d}\gamma_\mu\gamma_5 d|p\rangle \quad , \tag{2.7}$$

where

$$\mu_p = G^\gamma_{M,p}(0) = 2.79 \quad \text{and} \quad \mu_n = G^\gamma_{M,n}(0) = -1.91 \quad .$$

This is supported by the F/D ratio in SU(3) being nearly the same for the weak axial-vector current and the total magnetic moment. Such an equality is predicted by the quark model,[12] where F/D = 2/3; and indeed, the factor $3(\mu_p + \mu_n)/(\mu_p - \mu_n)$ in Eq. (2.7) could be replaced to high accuracy by its quark model value of 3/5.

Putting together the results for matrix elements of the axial-vector current yields:

$$\langle p|\bar{u}\gamma_\mu\gamma_5 u|p\rangle = \langle n|\bar{d}\gamma_\mu\gamma_5 d|n\rangle = G_A(q^2)\left(\frac{2\mu_p + \mu_n}{\mu_p - \mu_n}\right) \tag{2.8a}$$

and

$$\langle p|\bar{d}\gamma_\mu\gamma_5 d|p\rangle = \langle n|\bar{u}\gamma_\mu\gamma_5 u|n\rangle = G_A(q^2)\left(\frac{\mu_p + 2\mu_n}{\mu_p - \mu_n}\right) \quad . \tag{2.8b}$$

The axial-vector couplings of the Z^o in a particular gauge theory are then related back to the quark charges: Since the axial-vector quark current is

$$\frac{1}{2}\left(Q^Z_{R,u} - Q^Z_{L,u}\right)\bar{u}\gamma_\mu\gamma_5 u + \frac{1}{2}\left(Q^Z_{R,d} - Q^Z_{L,d}\right)\bar{d}\gamma_\mu\gamma_5 d \quad ,$$

we have

$$G^Z_{A,p} = \frac{1}{2}\left(Q^Z_{R,u} - Q^Z_{L,u}\right)G_A\left(\frac{2\mu_p + \mu_n}{\mu_p - \mu_n}\right) + \frac{1}{2}\left(Q^Z_{R,d} - Q^Z_{L,d}\right)G_A\left(\frac{\mu_p + 2\mu_n}{\mu_p - \mu_n}\right) \tag{2.9a}$$

and

$$G^Z_{A,n} = \frac{1}{2}\left(Q^Z_{R,u} - Q^Z_{L,u}\right) G_A\left(\frac{\mu_p + 2\mu_n}{\mu_p - \mu_n}\right)$$

$$+ \frac{1}{2}\left(Q^Z_{R,d} - Q^Z_{L,d}\right) G_A\left(\frac{2\mu_p + \mu_n}{\mu_p - \mu_n}\right) \quad . \tag{2.9b}$$

All that remains is to specify the weak quark charges. We concentrate on SU(2)×U(1), where

$$\begin{aligned}
Q^Z_{R,u} &= \frac{e}{2\,\sin\theta_W \cos\theta_W}\left(2T^u_{3R} - \frac{4}{3}\sin^2\theta_W\right) \quad , \\
Q^Z_{L,u} &= \frac{e}{2\,\sin\theta_W \cos\theta_W}\left(1 - \frac{4}{3}\sin^2\theta_W\right) \quad , \\
Q^Z_{R,d} &= \frac{e}{2\,\sin\theta_W \cos\theta_W}\left(2T^d_{3R} + \frac{2}{3}\sin^2\theta_W\right) \quad , \\
Q^Z_{L,d} &= \frac{e}{2\,\sin\theta_W \cos\theta_W}\left(-1 + \frac{2}{3}\sin^2\theta_W\right) \quad ,
\end{aligned} \tag{2.10}$$

for the quarks, and

$$\begin{aligned}
Q^Z_{R,e} &= \frac{e}{2\,\sin\theta_W \cos\theta_W}\left(2T^e_{3R} + 4\sin^2\theta_W\right) \quad , \\
Q^Z_{L,e} &= \frac{e}{2\,\sin\theta_W \cos\theta_W}\left(-1 + 4\sin^2\theta_W\right) \quad ,
\end{aligned} \tag{2.11}$$

for the electron. Here θ_W is the Weinberg angle; recent neutrino experiments[13] determine $\sin^2\theta_W$ to be in the neighborhood of 0.25. T^i_{3R} is the value of the third component of weak isospin for a right-handed fermion i, which is zero in the original Weinberg-Salam model. The most popular alternative is to put fermions in right-handed doublets, so that $T^i_{3R} = \pm\frac{1}{2}$.

However, an analysis[14] of a combination of neutrino induced neutral current processes (as well as results of Ref. 1) are inconsistent with either $T_{3R}^{u} = \frac{1}{2}$ or $T_{3R}^{d} = -\frac{1}{2}$. Henceforth we take $T_{3R}^{u} = T_{3R}^{d} = 0$, but leave open the two possibilities, $T_{3R}^{e} = 0$ or $-\frac{1}{2}$.

We now employ Eqs. (2.5), (2.9), (2.10), and (2.11) to calculate the asymmetry in Eq. (2.1). For this purpose we assume that all the vector current form factors G_E^{γ}, G_M^{γ}, G_E^{Z}, and G_M^{Z}, have the same dipole q^2 dependence:

$$G(q^2) = G(0) \Big/ \left[1 + \frac{q^2}{0.71\ \text{GeV}^2}\right] \quad . \tag{2.12}$$

Similarly, we take the axial-vector form factors to be of the form[10,15]

$$G_A(q^2) = G_A(0) \Big/ \left[1 + \frac{q^2}{0.9\ \text{GeV}^2}\right] \quad . \tag{2.13}$$

For the Weinberg-Salam model with $\sin^2\theta_W = \frac{1}{3}$ we display in Fig. 2.1 the asymmetry in electron-proton and electron-neutron elastic scattering when the incident beam energy is 3.23 GeV, 19.38 GeV, and infinity. The first two values of beam energy are of particular relevance to SLAC, where the spin of the electron precesses by an additional 180° between the linear accelerator and the end station for each 3.23 GeV of beam energy. In the limit of infinite energy Eq. (2.1) reduces to Eq. (2.2); the latter being the equation used in Ref. 6 to predict the elastic asymmetry. In fact, the curve in Fig. 2.1 for the elastic electron-proton scattering asymmetry at $E = \infty$ is precisely the Weinberg-Salam model curve in Fig. 3 of Ref. 6.

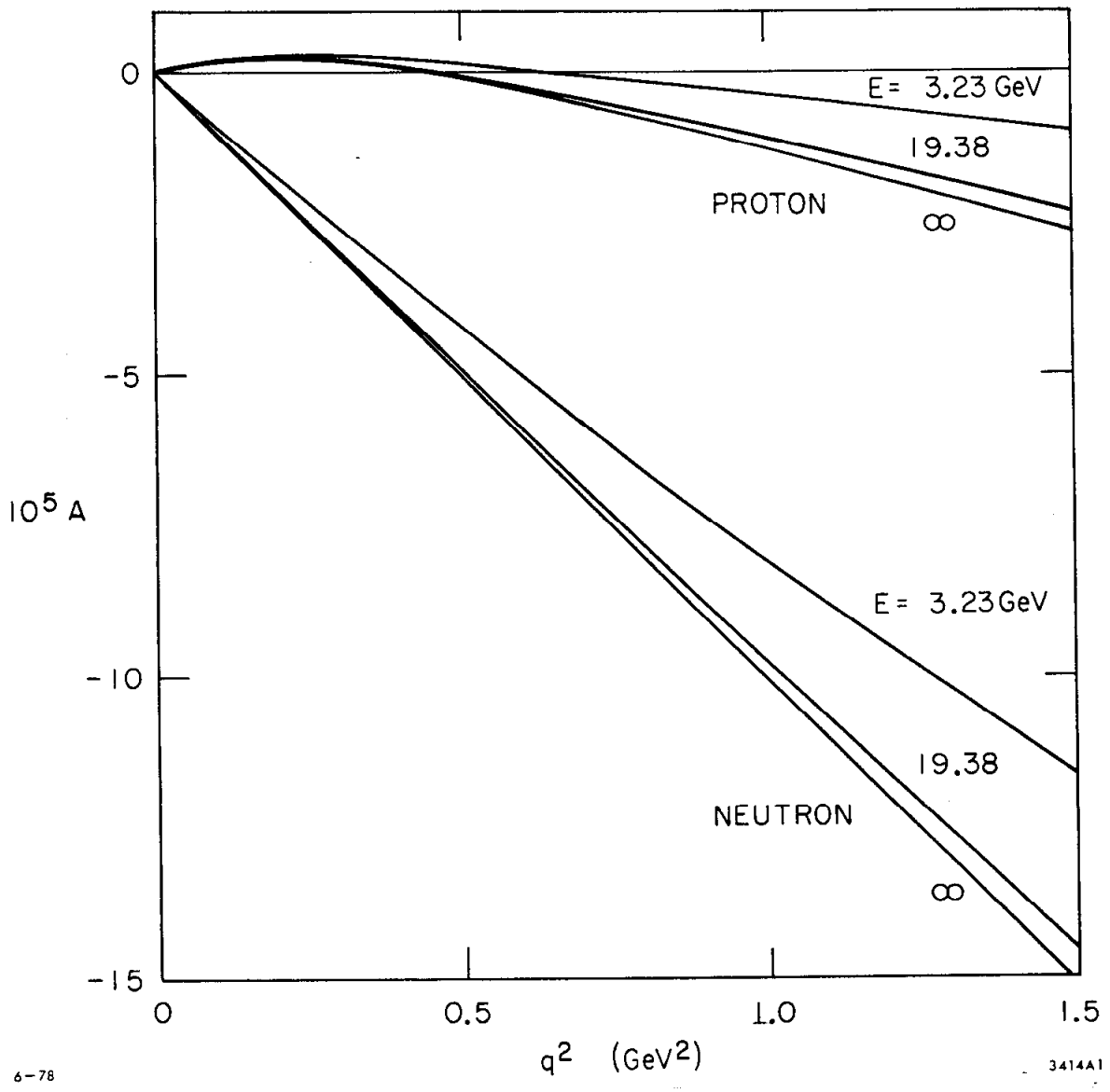

Fig. 2.1. The asymmetry in polarized electron-proton and electron-neutron elastic scattering for electron beam energies of 3.23 GeV, 19.38 GeV, and infinity. All predictions are for the Weinberg-Salam model with $\sin^2\theta_W = 1/3$.

We see that the approximation used in Ref. 6 to compute the elastic asymmetry at high energies is very good. Only at the lowest SLAC energies does there appear to be a noticeable, and perhaps measurable, deviation. Since most of the difference between the exact Eq. (2.1) and the approximate Eq. (2.2) comes from dropping the term proportional to $g_V G_A^Z$, we see that the actual value of $g_V G_A^Z$ has little effect on the predicted magnitude of the asymmetry in the original Weinberg-Salam model at high energies. However, at low energies, particularly below 1 GeV, the asymmetry generally does depend quite strongly on the term proportional to $g_V G_A^Z$, as shown in recent calculations.[4,7] It is in this way that lower energy elastic scattering experiments are of special importance.

On the other hand, if the electron is in a right-handed doublet $\left(T_{3R}^e = -\frac{1}{2}\right)$ then $g_A = 0$ and the dominant contribution to the high energy elastic asymmetry vanishes. Everything now comes from the term proportional to $g_V G_A^Z$. Using the exact Eq. (2.1), the resulting elastic electron-proton scattering asymmetry is a factor of about three to ten smaller than when $T_{3R}^e = 0$. This can be seen by direct comparison of Figs. 2.2 and 2.3 in which the elastic scattering asymmetry is computed for $\sin^2\theta_W = 0.20$, 0.25, and 0.30 and $T_{3R}^e = 0$ and $-\frac{1}{2}$, respectively.[16]

Figures 2.1, 2.2, and 2.3 also contain predictions for polarized electron-neutron elastic scattering asymmetries for the same range of parameters in $SU(2) \times U(1)$ as above. The most dramatic and important difference between a neutron and a proton target is the magnitude of the predicted asymmetries. The neutron asymmetries are much larger. For $\sin^2\theta_W = \frac{1}{3}$ and $T_{3R}^e = 0$ there is an order of magnitude difference at $q^2 = 1$ GeV^2. For $\sin^2\theta_W = \frac{1}{4}$ it is factor of about three at the same q^2.

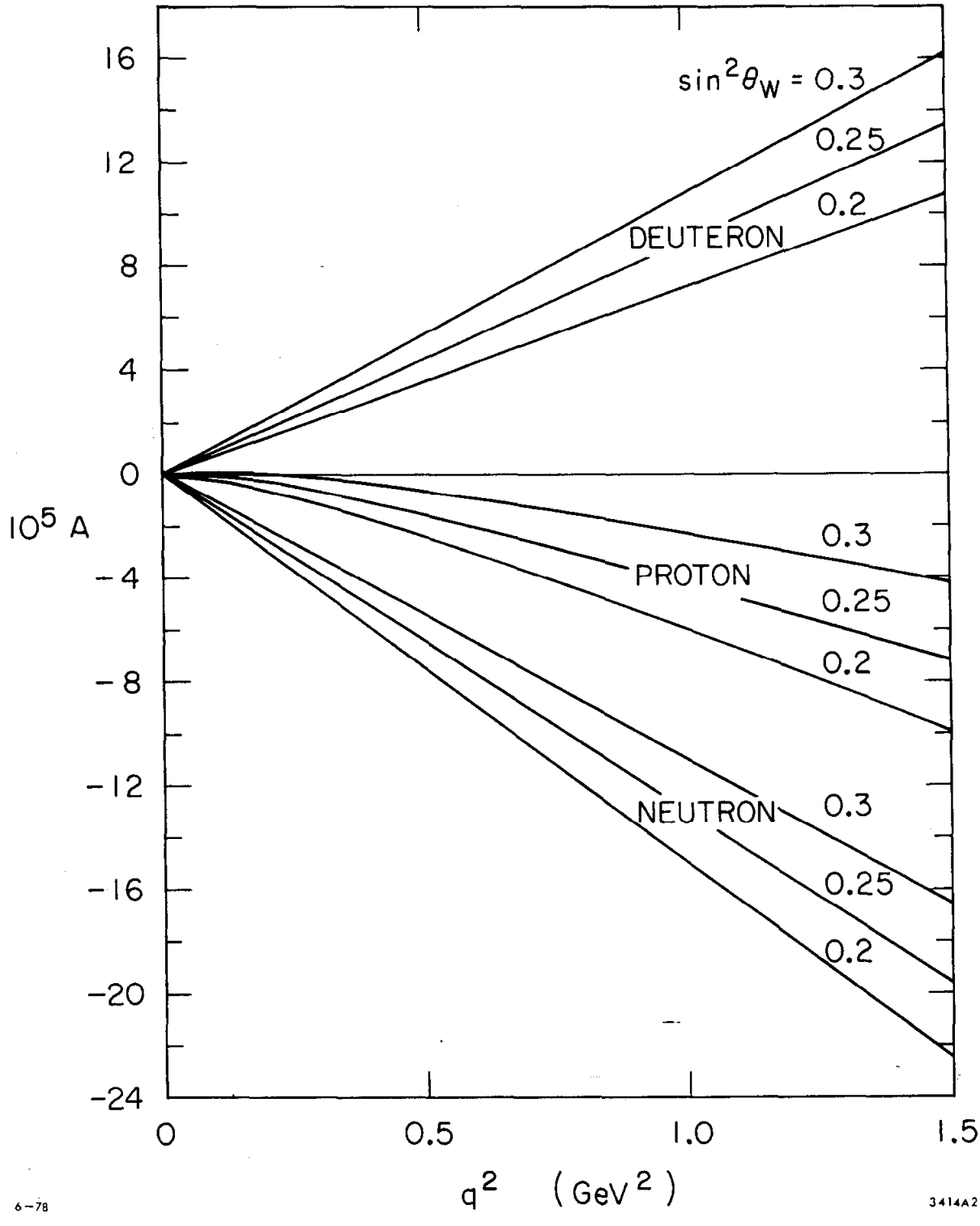

Fig. 2.2. The asymmetry in polarized electron-proton, electron-neutron, and electron-deuteron elastic scattering at a beam energy of 19.38 GeV for the Weinberg-Salam model ($T^e_{3R} = 0$) and $\sin^2\theta_W = 0.20$, 0.25, and 0.30.

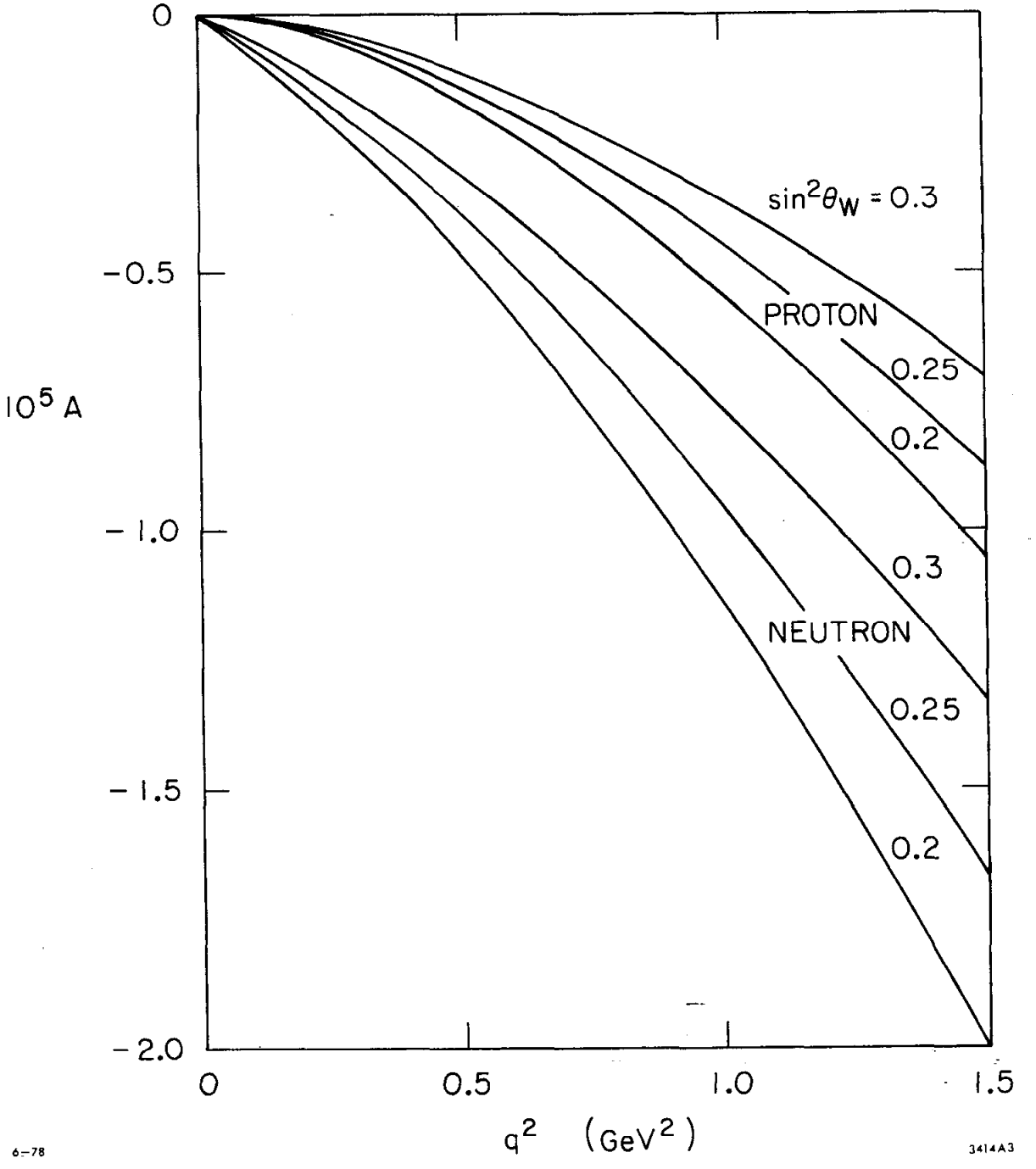

Fig. 2.3. The asymmetry in polarized electron-proton and electron-neutron elastic scattering at a beam energy of 19.38 GeV in SU(2) × U(1) with the right-handed electron in a doublet ($T^e_{3R} = -1/2$) and $\sin^2\theta_W = 0.20$, 0.25, and 0.30.

Even when $T^e_{3R} = -\frac{1}{2}$ and both the neutron and proton asymmetries are much smaller in magnitude, the neutron asymmetries are still a factor of two or so bigger. This difference originates in $SU(2) \times U(1)$ primarily because the d quark has a larger vector coupling to the Z^o than the u quark, and shows up more dramatically in elastic than in inelastic scattering.

3. Polarized Electron-Deuteron Elastic Scattering Asymmetries

Since elastic electron-neutron scattering will be accomplished by measuring the quasi-elastic scattering on the neutron (and proton) in deuterium, the question comes to mind as to what true elastic electron-deuteron scattering will yield. The asymmetry for polarized electron scattering on isospin zero nuclei has been considered previously.[5] We review the argument briefly here.

If we neglect the strange and charmed quarks in the nucleon, and hence in the deuteron, the up and down quarks (or antiquarks) in a deuteron together have net third component of weak isospin equal to zero in $SU(2) \times U(1)$. This holds for the right- and left-handed quarks separately.[17] The weak charges, Q^Z_R and Q^Z_L, of the deuteron then only get contributions in $SU(2) \times U(1)$ from the term proportional to $Q^\gamma \sin^2\theta_W$. More generally, the local current J^Z_μ to which the Z^o couples, when taken between deuteron states is proportional to that for the photon:

$$\langle D|J^Z_\mu|D\rangle = -\frac{e \sin^2\theta_W \langle D|J^\gamma_\mu|D\rangle}{\sin\theta_W \cos\theta_W} \quad . \tag{2.14}$$

As a result there are no axial-vector couplings of the Z^o to the deuteron and the vector couplings, being proportional to the electron-

magnetic ones, exactly cancel between the numerator and denominator in the expression for the asymmetry. The final result[5] for the elastic electron-deuteron asymmetry in SU(2) × U(1) is then:

$$A_{eD \to eD} = +\left(\frac{Gq^2}{2\sqrt{2}\,\pi\alpha}\right)\left(1 + 2T^e_{3R}\right)\left(2\sin^2\theta_W\right) \quad . \tag{2.15}$$

Values of this asymmetry when $T^e_{3R} = 0$ are shown in Fig. 2.2, along with those for elastic electron-proton and electron-neutron scattering. The magnitude is relatively large, and very importantly, positive. With $\sin^2\theta_W \lesssim 0.3$ this is the only elastic or inelastic electron scattering asymmetry in SU(2) × U(1) which is expected to be positive at high energies. Furthermore it gives a very clean measurement of $\sin^2\theta_W$. Unfortunately, the rapid fall-off of the deuteron form factor makes it problematic as to whether this will prove to be a practical way of extracting $\sin^2\theta_W$ with high accuracy.

4. Discussion

We have calculated elastic electron-proton, electron-neutron, and electron-deuteron scattering asymmetries in detail within the context of the SU(2) × U(1) gauge theory of weak and electromagnetic interactions. Asymmetries of the same magnitude as in deep inelastic scattering are generally found.

The terms in the elastic electron-proton (or neutron) asymmetry proportional to G_A^Z, the axial-vector coupling of the Z^o to the nucleon, are found quantitatively to give negligible contributions at beam energies of ~20 GeV. Only low energy (below a few GeV) experiments are sensitive to such terms and can be used to determine their value in the original Weinberg-Salam model.

The asymmetries for elastic electron-neutron scattering for $\sin^2\theta_W < 0.3$ are of the same sign, but much larger in magnitude, when compared to those for electron-proton elastic scattering. Electron-deuteron scattering, however, gives asymmetries of similar magnitude but opposite sign to other predicted elastic or inelastic asymmetries within $SU(2) \times U(1)$.

In contrast to deep inelastic polarized electron scattering asymmetry measurements, elastic scattering offers two advantages in testing the underlying gauge theory of weak and electromagnetic interactions. First, one does not need to depend on the applicability of the quark-parton model in general, or knowledge of quark flavor distributions in the nucleon in particular, in order to interpret the results. One only needs to relate mostly measured elastic form factors of the nucleon, often at small values of q^2, to the quark couplings of the γ and Z^o. While some theoretical assumptions are necessary to carry this out, they seem relatively well founded and, importantly, different from those required to interpret deep inelastic scattering.

Second, at SLAC energies elastic scattering is very much like doing a measurement at $y = (E-E')/E \approx 0$ for deep inelastic scattering. In fact, for a given scattering angle as y decreases one passes from the deep inelastic region, to that of resonance electroproduction, and finally to elastic scattering. We recall[6] that in deep inelastic scattering the asymmetry is proportional to g_A of the electron at $y = 0$; if g_A vanishes so does the asymmetry. Contrasting Figs. 2.2 and 2.3 we see a similar effect in elastic scattering; if g_A vanishes ($T^e_{3R} = -\frac{1}{2}$, as in Fig. 2.3), then the asymmetry in elastic scattering at SLAC energies drops by roughly

an order of magnitude. Polarized electron-nucleon elastic scattering is then an alternative, or at least complementary, method to measuring a y distribution in true deep inelastic scattering in order to determine the singlet or doublet assignment of the right-handed electron in $SU(2) \times U(1)$.

REFERENCES AND FOOTNOTES FOR CHAPTER II

* Most of the material in this chapter is published in F. Gilman and T. Tsao, Phys. Rev. D19, 790 (1978).

1. C. Prescott et al. (SLAC-Yale-Bielifeld collaboration), SLAC proposal E-122, 1975 (unpublished) and C. Prescott et al., Phys. Lett. 77B, 347 (1978).

2. S. Weinberg, Phys. Rev. Lett. 19, 1264 (1967); A. Salam, in Elementary Particle Theory: Relativistic Groups and Analyticity (Nobel Symposium No. 8), edited by N. Svartholm (Almqvist and Wiksell, Stockholm, 1968), p. 367.

3. Ya. B. Zeldovich and A. M. Perelomov, Zh. Eksp. Teor. Fiz. 39, 1115 (1960) [Sov. Phys. - JETP 12, 777 (1961)]; S. M. Bilenkii et al., Yad. Fiz. 21, 1271 (1975) [Sov. J. Nucl. Phys. 21, 657 (1976)]; S. G. Grigoryan and S. V. Esaibegyan, Izv. Akad. Navk. Arm. SSR 11, 11 (1976).

4. E. Reya and K. Schilcher, Phys. Rev. D10, 952 (1974), and in Interaction Studies in Nuclei, edited by H. Jochim and B. Ziegler (North-Holland, Amsterdam, 1975), p. 291; D. Cuthiell and J. N. Ng, Phys. Rev. D16, 3225 (1977).

5. G. Feinberg, Phys. Rev. D12, 3575 (1975). See also J. D. Valecka, Nucl. Phys. A285, 349 (1977).

6. R. N. Cahn and F. J. Gilman, Phys. Rev. D17, 1313 (1978).

7. E. Hoffmann and E. Reya, Phys. Rev. D18, 3230 (1978).

8. The sign of the term proportional to $g_V G_A^Z$ in Eq. (2.1) is opposite to that in Ref. 6 due to a sign error there. Since this term was

dropped in Ref. 6 because it gives a negligible contribution at high energy, it makes no difference in any of the numerical results or conclusions of that paper.

9. The q^2 dependence of the form factors in Eq. (2.1) and many of the following equations is suppressed for the sake of clarity.

10. See the lectures by J. D. Bjorken, in Proceedings of the SLAC Summer Institute on Particle Physics, edited by M. C. Zipf (SLAC, Stanford, California, 1976), SLAC Report No. 198, p. 1.

11. The space-time dependence in Eq. (2.3) and some of the later equations is suppressed: G^γ represents both G_E^γ and G_M^γ times the appropriate gamma matrices taken between nucleon spinors.

12. See, for example, the review by J. J. J. Kokkedee, The Quark Model (Benjamin, New York, 1969).

13. M. Holder et al., Phys. Lett. 71B, 222 (1977); P. Wanderer et al., Phys. Rev. D17, 1679 (1978); P. C. Bosetti et al., Oxford University preprint 20/78, 1978 (unpublished).

14. L. Abbott and R. M. Barnett, Phys. Rev. Lett. 40, 1303 (1978); L. Langacker and P. Sidhu, Phys. Lett. 74B, 233 (1978); and P. Q. Hung and J. J. Sakurai, Phys. Lett. 72B, 208 (1977).

15. The mass squared characterizing the dipole form chosen for $G_A(q^2)$ has somewhat arbitrarily been chosen as 0.9 GeV^2, as in Ref. 10. Other values between the vector form factor dipole mass squared of 0.71 GeV^2 and 1.1 GeV^2 make only minor changes in our numerical results.

16. In some models where parity is conserved in lowest order, radiative corrections give rise to sizeable asymmetries. In general, such

radiative corrections may give rise to non-negligible effects in the present case where the dominant contribution to the high energy elastic asymmetry vanishes in lowest order. See W. J. Marciano and A. I. Sanda, Phys. Rev. D17, 3055 (1978).

17. This is true only if the right-handed u and d quarks are both in doublets or both in singlets in $SU(2) \times U(1)$. We of course assume the left-handed u and d quarks share a doublet.

CHAPTER III

PARITY VIOLATING ASYMMETRIES IN DILEPTON PRODUCTION BY POLARIZED PROTONS*

1. Introduction

The Drell-Yan model[1] for production of high invariant mass lepton pairs in hadron-hadron collisions has become the standard with which continuum dilepton data is compared.[2] Basic features of the model such as the predicted scaling behavior of the cross section are in agreement with the results of experiments with proton beams. Other features such as the angular distribution of the pair and the ratio of π^+ to π^- induced cross sections are found to follow theoretical predictions as well. While the transverse momentum distribution of the dilepton pair and the absolute magnitude of the cross section point to possible higher order quantum chromodynamic (QCD) corrections to the model,[2] we shall use it as a lowest order mechanism in order to see what the size of weak-electromagnetic interference effects will be.

These effects arise in lowest order from interference between diagrams with a virtual photon, γ, and that with a neutral weak vector boson, Z^o. Such is the case for the asymmetry in the angular distribution of the lepton (or antilepton) with respect to the beam direction in dilepton production by hadrons.[3] This may arise from interference between the amplitude for $q\bar{q} \to \gamma \to \ell\bar{\ell}$ and for $q\bar{q} \to Z^o \to \ell\bar{\ell}$ with axial-vector coupling of the Z^o to both quarks and leptons. Such an asymmetry is completely analogous to that predicted in $e^-e^+ \to \mu^-\mu^+$, which is expected to be observed at PEP and PETRA. It has the disadvantage that

an asymmetry of this type also occurs from higher order electromagnetic effects. These latter must be subtracted from the observed asymmetry to isolate the part due to weak-electromagnetic interference and thence permit extraction of Z^o couplings.

These last problems may be avoided by considering an explicitly parity violating asymmetry which is forbidden to arise from electromagnetic effects in any order. Here we consider such asymmetries in dilepton production by polarized protons incident on nucleon targets. These are directly analogous to the asymmetry seen[4] in deep inelastic scattering of polarized electrons. Because of the large dilepton mass accessible in proton-nucleon collisions, however, one might expect asymmetries of order 10^{-2} or more, rather than those of order 10^{-4} measured[4] at SLAC in deep inelastic electron scattering.

In the next section, assuming the Drell-Yan mechanism, we calculate the form of the expected effects and show that there are two different cross section asymmetry terms. The relation of each to the quark distributions in a polarized proton and to the Z^o couplings to quarks and leptons is given. In Sect. 3 we use these formulae together with known quark-parton distributions and Z^o couplings in the Weinberg-Salam model to give numerical predictions of the asymmetries for present laboratory energies $s = 10^3$ GeV^2, and also for Isabelle energies $s = 6.4 \times 10^5$ GeV^2. We conclude in Sect. 4 with a discussions of our results and their experimental implications.

2. Polarized Beam Asymmetries in Dilepton Production

It is most convenient in deriving the polarization asymmetry to work first at the quark level. We assume that the dileptons are generated via the Drell-Yan mechanism[1] of quark-antiquark annihilation through a virtual γ or Z^0. The vector or axial-vector nature of γ and Z^0 couplings, together with neglect of quark masses, implies that right-handed and left-handed quarks annihilate with left-handed and right-handed antiquarks, respectively. Similarly, with neglect of lepton masses right-handed (left-handed) leptons are produced only with left-handed (right-handed) anti-leptons. The cross sections for $q\bar{q} \to \ell\bar{\ell}$ may then be labeled by just the initial quark and final lepton helicities, λ_q and λ_ℓ, respectively, the antiquark and anitlepton helicities being implied.

The derivation then proceeds in a manner which is in direct analogy to that for the asymmetry in polarized electron scattering.[5] With cross sections $\sigma_{\lambda_q,\lambda_\ell}$ written in terms of couplings of the γ and Z^0 to right-handed (left-handed) quarks and leptons, $Q_{R,q}$ and $Q_{R,\ell}$ $\left(Q_{L,q} \text{ and } Q_{L,\ell}\right)$, and the rotation group d functions, we have:[6]

Right-handed quark, right-handed lepton,

$$\sigma_{RR} \propto \left| Q^{\gamma}_{R,q} \frac{1}{q^2} Q^{\gamma}_{R,\ell} + Q^{Z}_{R,q} \frac{1}{q^2+M_Z^2} Q^{Z}_{R,\ell} \right|^2 \left| d^1_{1,1}(\theta) \right|^2 \quad ; \quad (3.1a)$$

Right-handed quark, left-handed lepton,

$$\sigma_{RL} \propto \left| Q^{\gamma}_{R,q} \frac{1}{q^2} Q^{\gamma}_{L,\ell} + Q^{Z}_{R,q} \frac{1}{q^2+M_Z^2} Q^{Z}_{L,\ell} \right|^2 \left| d^1_{1,-1}(\theta) \right|^2 \quad ; \quad (3.1b)$$

Left-handed quark, right-handed lepton,

$$\sigma_{LR} \propto \left| Q^{\gamma}_{L,q} \frac{1}{q^2} Q^{\gamma}_{R,\ell} + Q^{Z}_{L,q} \frac{1}{q^2 + M_Z^2} Q^{Z}_{R,\ell} \right|^2 |d^1_{-1,1}(\theta)|^2 \; ; \quad (3.1c)$$

Left-handed quark, left-handed lepton,

$$\sigma_{LL} \propto \left| Q^{\gamma}_{L,q} \frac{1}{q^2} Q^{\gamma}_{L,\ell} + Q^{Z}_{L,q} \frac{1}{q^2 + M_Z^2} Q^{Z}_{L,\ell} \right|^2 |d^1_{-1,-1}(\theta)|^2 . \quad (3.1d)$$

The angle θ is that between the incoming quark and outgoing lepton in the $q\bar{q}$ (or $\ell\bar{\ell}$) center-of-mass system. The right- and left-handed couplings of the photon are equal and are just the charges 2e/3, -e/3, and -e/3 for the u,d, and s quarks, respectively. Similarly, $Q^{\gamma}_{R,\ell} = Q^{\gamma}_{L,\ell} = -e$ for the charged leptons.

If we form the parity-violating asymmetry from the difference of cross sections for initial quarks with positive and negative helicities (and summed over final lepton helicities), we have

$$A = \frac{\sigma_{RR} + \sigma_{RL} - \sigma_{LR} - \sigma_{LL}}{\sigma_{RR} + \sigma_{RL} + \sigma_{LR} + \sigma_{LL}} \quad . \quad (3.2)$$

For the present, we consider the low energy case $|q^2/M_Z^2| << 1$. Thus, expanding to first order in q^2/M_Z^2, the γ-Z interference terms give the leading contribution to the numerator while the square of the photon amplitudes gives the leading contribution to the denominator:

$$A \overset{|q^2/M_Z^2| \ll 1}{\approx} -\frac{|q^2|}{2M_Z^2} \times Q_q^\gamma Q_\ell^\gamma \Big[\Big(Q_{R,q}^Z Q_{R,\ell}^Z + Q_{R,q}^Z Q_{L,\ell}^Z - Q_{L,q}^Z Q_{R,\ell}^Z - Q_{L,q}^Z Q_{L,\ell}^Z\Big)(1+\cos^2\theta) + \Big(Q_{R,q}^Z Q_{R,\ell}^Z - Q_{R,q}^Z Q_{L,\ell}^Z + Q_{L,q}^Z Q_{R,\ell}^Z - Q_{L,q}^Z Q_{L,\ell}^Z\Big)(2\cos\theta)\Big] \times \Big[\Big(Q_q^\gamma Q_\ell^\gamma\Big)^2 (1+\cos^2\theta)\Big]^{-1} \quad . \tag{3.3}$$

This formula takes on a somewhat neater appearance in terms of vector and axial-vector coupling constants,

$$Q_R^Z = g_V + g_A$$

$$Q_L^Z = g_V - g_A \quad , \tag{3.4}$$

for both the Z^o couplings to quarks and leptons. The formula for the asymmetry then becomes

$$A \overset{|q^2/M_Z^2| \ll 1}{\approx} -\frac{2|q^2|}{M_Z^2} \cdot \frac{Q_q^\gamma Q_\ell^\gamma \big[g_{A,q} g_{V,\ell}(1+\cos^2\theta) + g_{V,q} g_{A,\ell}(2\cos\theta)\big]}{\Big(Q_q^\gamma Q_\ell^\gamma\Big)^2 (1+\cos^2\theta)} \quad . \tag{3.5}$$

Notice that there are two distinct terms which are coefficients of different angular factors. Averaging over center-of-mass angles just leaves a term proportional to $g_{A,q} g_{V,\ell}$.

The asymmetry to be observed in hadron-hadron collisions may now be obtained by folding the quark level cross sections and resulting asymmetry in Eq. (3.5) with the quark and antiquark distributions in the initial

hadrons. We consider in particular collisions of longitudinally polarized protons with unpolarized nucleons. The probability of finding a quark of type i in the incident longitudinally polarized proton with spin parallel (antiparallel) to that of the proton and with momentum fraction x_1 is defined to be $f^+_{i/p}(x_1)$ ($f^-_{i/p}(x_1)$). Clearly $f^+_{i/p}(x_1) + f^-_{i/p}(x_1) = f_{i/p}(x_1)$, the probability of finding a quark of type i with any spin direction. A quark of type i in the proton annihilates with its corresponding anti-quark, $\bar{i}$, in the nucleon target, which occurs[7] with momentum fraction x_2 with probability $f_{\bar{i}/N}(x_2)$.

Defining the asymmetry in polarized proton + nucleon $\to \ell\bar{\ell}$ + ... collisions as the difference over the sum of cross section for proton helicity +1/2 and -1/2, we then find[8]

$$A(x_1,x_2,\theta) \overset{|q^2/M_Z^2| \ll 1}{\approx} -\frac{2|q^2|}{M_Z^2} \times \frac{\sum_i Q_i^\gamma Q_\ell^\gamma \left[f^+_{i/p}(x_1) - f^-_{i/p}(x_1)\right] f_{\bar{i}/N}(x_2) \left[g_{A,i} g_{V,\ell} + g_{V,i} g_{A,\ell} \frac{2\cos\theta}{1+\cos^2\theta}\right] + i \leftrightarrow \bar{i}}{\sum_i \left(Q_i^\gamma Q_\ell^\gamma\right)^2 f_{i/p}(x_1)\, f_{\bar{i}/N}(x_2) + i \leftrightarrow \bar{i}} \tag{3.6}$$

The sum over i includes all types of quarks u,d,s,c,.... For all leptons $Q^\gamma_\ell = -e$. In terms of s, the square of the center-of-mass energy of the p-N system, we have the kinematic relation $|q^2| = x_1 x_2 s$. We then rewrite Eq. (3.6) as

$$A(x_1,x_2,\theta) \overset{|q^2/M_Z^2| << 1}{\approx} \frac{x_1 x_2 s}{2\pi\alpha M_Z^2} \tag{3.7}$$

$$\times \frac{\sum_i \left(Q_i^\gamma/e\right)\left[f^+_{i/p}(x_1) - f^-_{i/p}(x_1)\right] f_{\bar{i}/N}(x_2)\left[g_{A,i}g_{V,\ell} + g_{V,i}g_{A,\ell}\,\frac{2\cos\theta}{1+\cos^2\theta}\right] + i\leftrightarrow\bar{i}}{\sum_i \left(Q_i^\gamma/e\right)^2 f_{i/p}(x_1)\, f_{\bar{i}/N}(x_2) + i\leftrightarrow\bar{i}}$$

The numerator of Eq. (3.7) is composed of pieces containing $g_{A,i}g_{V,\ell}$ and $g_{V,i}g_{A,\ell}$ which have different angular properties. The asymmetry which survives integration over θ is

$$A_1(x_1,x_2) \overset{|q^2/M_Z^2| << 1}{\approx} \frac{x_1 x_2 s}{2\pi\alpha M_Z^2} \tag{3.8}$$

$$\times \frac{\sum_i \left(Q_i^\gamma/e\right) g_{A,i}g_{V,\ell}\left[f^+_{i/p}(x_1) - f^-_{i/p}(x_1)\right] f_{\bar{i}/N}(x_2) + i\leftrightarrow\bar{i}}{\sum_i \left(Q_i^\gamma/e\right)^2 f_{i/p}(x_1)\, f_{\bar{i}/N}(x_2) + i\leftrightarrow\bar{i}}$$

Isolating the term which is odd in $\cos\theta$ (by forming a forward-backward lepton angualr asymmetry on top of the polarization asymmetry) gives the independent asymmetry:

$$A_2(x_1,x_2) \overset{|q^2/M_Z^2| << 1}{\approx} \frac{x_1 x_2 s}{2\pi\alpha M_Z^2} \tag{3.9}$$

$$\times \frac{\sum_i \left(Q_i^\gamma/e\right) g_{V,i}g_{A,\ell}\left[f^+_{i/p}(x_1) - f^-_{i/p}(x_1)\right] f_{\bar{i}/N}(x_2) + i\leftrightarrow\bar{i}}{\sum_i \left(Q_i^\gamma/e\right)^2 f_{i/p}(x_1)\, f_{\bar{i}/N}(x_2) + i\leftrightarrow\bar{i}}$$

The decomposition

$$A(x_1,x_2,\theta) = A_1(x_1,x_2) + \frac{2\cos\theta}{1+\cos^2\theta} A_2(x_1,x_2) \quad , \qquad (3.10)$$

into θ independent and θ dependent terms is in complete analogy to the situation[5] in polarized electron deep inelastic scattering where the asymmetry has y independent and y dependent terms. In fact, since the y variable is directly related to the angle of scattering in the electron-quark center-of-mass, it is more than just an analogy. There is, however, an important difference. Because in the present case the asymmetry is based on the difference of quark polarizations rather than lepton polarizations, the positions of $g_{A,q}g_{V,\ell}$ and $g_{V,q}g_{A,\ell}$ are flipped. The θ independent term here involves $g_{A,q}g_{V,\ell}$, while the y independent term in the asymmetry for deep inelastic polarized electron scattering involves $g_{V,q}g_{A,\ell}$, and vice versa for the θ and y dependent terms. This is of major importance for the predicted magnitude at low energies of A_1 relative to that of A_2 which is calculated in the next section.

However, before proceeding to the numerical results for A_1 and A_2 at low energies, we also consider the other extreme case of very high energies -- when $|q^2/M_Z^2| >> 1$. Since at very high energies the weak force becomes comparable in strength to the electromagnetic force, this means that that Z^{o2} terms in the polarized cross sections (3.1) can no longer be neglected. Rather, Z^{o2} terms must now be included in both the numerator and denominator terms of the asymmetry A. Because it involves little extra work, and for the sake of completeness, we first present the exact, lowest-order results for the asymmetries near the Z^o pole ($-q^2 \approx M_Z^2$), and then consider the limiting high energy case $\left(|q^2/M_Z^2| >> 1\right)$.

The derivation proceeds in analogy to before, except that all Z^{o2} terms are kept, and the propagator replacement

$$\frac{1}{q^2 + M_Z^2} \rightarrow \frac{1}{q^2 + M_Z^2 + iM_Z\Gamma}$$

is made to account for the finite decay width Γ of the Z^o when $-q^2 \approx M_Z^2$. The exact lowest order result for the parity violating asymmetry is then

$$\begin{aligned} A = & \left\{ 2 \sum_i \left(f^+_{i/p}(x_1) - f^-_{i/p}(x_1) \right) f_{\bar{i}/N}(x_2) \right. \\ & \times \left[\left(|\eta|^2 \hat{s}^2 \frac{g_{V,i} g_{A,i} \left(g^2_{V,e} + g^2_{A,e} \right)}{e^4} - \left(Q^\gamma_i / e \right) \mathrm{Re}\, \eta\, \hat{s}\, \frac{g_{A,i} g_{V,e}}{e^2} \right) \right. \\ & + \left(|\eta|^2 \hat{s}^2 \frac{g_{V,e} g_{A,e} \left(g^2_{V,i} + g^2_{A,i} \right)}{e^4} - \left(Q^\gamma_i / e \right) \mathrm{Re}\, \eta\, \hat{s}\, \frac{g_{V,i} g_{A,e}}{e^2} \right) \\ & \left. \left. \times \frac{2\cos\theta}{1 + \cos^2\theta} \right] + i \leftrightarrow \bar{i} \right\} \\ & \times \left\{ \sum_i f_{i/p}(x_1)\, f_{\bar{i}/N}(x_2) \left[\left(\left(Q^\gamma_i / e \right)^2 + |\eta|^2 \hat{s}^2 \frac{\left(g^2_{V,i} + g^2_{A,i} \right)\left(g^2_{V,e} + g^2_{A,e} \right)}{e^4} \right. \right. \\ & - 2 \left(Q^\gamma_i / e \right) \Big) + 2 \left(|\eta|^2 \hat{s}^2 \frac{g_{V,i}\, g_{V,e}\, g_{A,i}\, g_{A,e}}{e^4} - \left(Q^\gamma_i / e \right) \mathrm{Re}\, \eta\, \hat{s}\, \frac{g_{A,e} g_{A,i}}{e^2} \right) \\ & \left. \left. \times \frac{2\cos\theta}{1 + \cos^2\theta} \right] + i \leftrightarrow \bar{i} \right\}^{-1} . \end{aligned} \tag{3.11}$$

In Eq. (3.11) we have defined for convenience

$$\eta = \frac{1}{q^2 + M_Z^2 + iM_Z\Gamma} , \tag{3.12}$$

and

$$\hat{s} = |q|^2 . \tag{3.13}$$

If we integrate over θ as before, we find

$$A_1 = \Big\{ 2 \sum_i \Big(f^+_{i/p}(x_1) - f^-_{i/p}(x_1) \Big) f_{\bar{i}/N}(x_2)$$

$$\times \left[|\eta|^2 \hat{s}^2 \frac{g_{V,i} g_{A,i} \left(g^2_{V,e} + g^2_{A,e} \right)}{e^4} - \left(Q^\gamma_i / e \right) \mathrm{Re}\, \eta\, \hat{s}\, \frac{g_{A,i} g_{V,e}}{e^2} \right] + i \leftrightarrow \bar{i} \Big\}$$

$$\times \Big\{ \sum_i f_{i/p}(x_1) f_{\bar{i}/N}(x_2) \Big[\left(Q^\gamma_i / e \right)^2 + |\eta|^2 \hat{s}^2 \frac{\left(g^2_{V,i} + g^2_{A,i} \right)\left(g^2_{V,e} + g^2_{A,e} \right)}{e^4}$$

$$- 2 \left(Q^\gamma_i / e \right) \mathrm{Re}\, \eta\, \hat{s}\, \frac{g_{V,i} g_{V,e}}{e^2} \Big] + i \leftrightarrow \bar{i} \Big\}^{-1} \quad . \tag{3.14}$$

As before, we also define A_2 by forming a forward-backward asymmetry on top of the polarization asymmetry:

$$A_2 = \Big\{ 2 \sum_i \Big(f^+_{i/p}(x_1) - f^-_{i/p}(x_1) \Big) f_{\bar{i}/N}(x_2)$$

$$\times \left[|\eta|^2 \hat{s}^2 \frac{g_{V,e} g_{A,e} \left(g^2_{V,i} + g^2_{A,i} \right)}{e^4} - \left(Q^\gamma_i / e \right) \mathrm{Re}\, \eta\, \hat{s}\, \frac{g_{V,i} g_{A,e}}{e^2} \right] + i \leftrightarrow \bar{i} \Big\}$$

$$\times \Big\{ \sum_i f_{i/p}(x_1) f_{\bar{i}/N}(x_2) \Big[\left(Q^\gamma_i / e \right)^2 + |\eta|^2 \hat{s}^2 \frac{\left(g^2_{V,i} + g^2_{A,i} \right)\left(g^2_{V,e} + g^2_{A,e} \right)}{e^4}$$

$$- 2 \left(Q^\gamma_i / e \right) \mathrm{Re}\, \eta\, \hat{s}\, \frac{g_{V,i} g_{V,e}}{e^2} \Big] + i \leftrightarrow \bar{i} \Big\}^{-1} \quad . \tag{3.15}$$

Note that the previously simple decomposition (3.10) is now no longer true.

In the high energy regime $|q^2/M_Z^2| >> 1$, we can drop Γ_Z/M_Z. We also have

$$\eta \to \frac{1}{q^2} = -|\eta| \quad , \tag{3.16}$$

and

$$\mathrm{Re}\,\eta\hat{s} \quad , \quad |\eta|^2\hat{s}^2 \to 1 \quad . \tag{3.17}$$

Thus Eqs. (3.11), (3.14) and (3.15) become in the high energy limit

$$\begin{aligned}
A \overset{|q^2/M_Z^2| >> 1}{\approx} & \left\{ 2\sum_i \left(f^+_{i/p}(x_1) - f^-_{i/p}(x_1)\right) f_{\bar{i}/N}(x_2) \right. \\
& \times \left[\left(\frac{g_{V,i}g_{A,i}\left(g^2_{V,e} + g^2_{A,e}\right)}{e^4} - \left(Q^\gamma_i/e\right)\frac{g_{A,i}g_{V,e}}{e^2} \right) \right. \\
& \left. \left. + \left(\frac{g_{V,e}g_{A,e}\left(g^2_{V,i} + g^2_{A,i}\right)}{e^4} - \left(Q^\gamma_i/e\right)\frac{g_{V,i}g_{A,e}}{e^2} \right) \frac{2\cos\theta}{1+\cos^2\theta} \right] + i \leftrightarrow \bar{i} \right\} \\
& \times \left\{ \sum_i f_{i/p}(x_1) f_{\bar{i}/N}(x_2) \left[\left(\left(Q^\gamma_i/e\right)^2 + \frac{\left(g^2_{V,i} + g^2_{A,i}\right)\left(g^2_{V,e} + g^2_{A,e}\right)}{e^4} \right. \right. \right. \\
& \left. \left. - 2\left(Q^\gamma_i/e\right) \right) + 2\left(\frac{g_{V,i}\,g_{V,e}\,g_{A,i}\,g_{A,e}}{e^4} - \left(Q^\gamma_i/e\right)\frac{g_{A,e}g_{A,i}}{e^2} \right) \frac{2\cos\theta}{1+\cos^2\theta} \right] \\
& \left. + i \leftrightarrow \bar{i} \right\}^{-1}
\end{aligned} \tag{3.18}$$

$$A_1 \overset{|q^2/M_Z^2| \gg 1}{\approx} \left\{ 2\sum_i \left(f^+_{i/p}(x_1) - f^-_{i/p}(x_1) \right) f_{\bar{i}/N}(x_2) \right.$$

$$\times \left[\frac{g_{V,i}g_{A,i}\left(g^2_{V,e}+g^2_{A,e}\right)}{e^4} - \left(Q^\gamma_i/e\right)\frac{g_{A,i}g_{V,e}}{e^2} \right] + i \leftrightarrow \bar{i} \Big\}$$

$$\times \left\{ \sum_i f_{i/p}(x_1) f_{\bar{i}/N}(x_2) \left[\left(Q^\gamma_i/e\right)^2 + \frac{\left(g^2_{V,i}+g^2_{A,i}\right)\left(g^2_{V,e}+g^2_{A,e}\right)}{e^4} \right.\right.$$

$$\left.\left. - 2\left(Q^\gamma_i/e\right)\frac{g_{V,i}g_{V,e}}{e^2} \right] + i \leftrightarrow \bar{i} \right\}^{-1} \qquad (3.19)$$

$$A_2 \overset{|q^2/M_Z^2| \gg 1}{\approx} \left\{ 2\sum_i \left(f^+_{i/p}(x_1) - f^-_{i/p}(x_1) \right) f_{\bar{i}/N}(x_2) \right.$$

$$\times \left[\frac{g_{V,e}g_{A,e}\left(g^2_{V,i}+g^2_{A,i}\right)}{e^4} - \left(Q^\gamma_i/e\right)\frac{g_{V,i}g_{A,e}}{e^2} \right] + i \leftrightarrow \bar{i} \Big\}$$

$$\times \left\{ \sum_i f_{i/p}(x_1) f_{\bar{i}/N}(x_2) \left[\left(Q^\gamma_i/e\right)^2 + \frac{\left(g^2_{V,i}+g^2_{A,i}\right)\left(g^2_{V,e}+g^2_{A,e}\right)}{e^4} \right.\right.$$

$$\left.\left. - 2\left(Q^\gamma_i/e\right)\frac{g_{V,i}g_{V,e}}{e^2} \right] + i \leftrightarrow \bar{i} \right\}^{-1} \qquad (3.20)$$

3. Numerical Results

We now proceed to numerical evaluation of the low energy asymmetries given in Eqs. (3.8) and (3.9) within the context of the Weinberg-Salam model[9] for weak and electromagnetic interactions. We defer the high energy asymmetries (3.19) and (3.20) till later. With the standard assignment of right-handed quarks and leptons to singlets and left-handed

quarks and leptons to doublets of weak isospin, the couplings of the Z^o are given by

$$g_{V,\ell} = \frac{e}{4\sin\theta_W \cos\theta_W}\left(-1 + 4\sin^2\theta_W\right) \quad ,$$

$$g_{A,\ell} = \frac{e}{4\sin\theta_W \cos\theta_W} \quad ,$$

$$g_{V,i} = \frac{e}{4\sin\theta_W \cos\theta_W}\left(2T_{3,i} - 4\frac{Q_i^\gamma}{e}\sin^2\theta_W\right) \quad ,$$

$$g_{A,i} = \frac{e}{4\sin\theta_W \cos\theta_W}\left(-2T_{3,i}\right) \quad . \tag{3.21}$$

The third component of weak isospin, $T_{3,i}$, is $+1/2$ for $i = u,c,\ldots$ and $-1/2$ for $i = d,s,\ldots$. The mass of the neutral weak boson is related to $G_F = 1.02 \times 10^{-5}/M_N^2$ by

$$\frac{1}{M_Z^2} = \frac{\sqrt{2}\, G_F \sin^2\theta_W \cos^2\theta_W}{\pi\alpha} \quad . \tag{3.22}$$

We may now rewrite the low energy asymmetries (3.8) and (3.9) in the specific case of the Weinberg-Salam model:

$$A_1(x_1,x_2) \overset{|q^2/M_Z^2| \ll 1}{\approx} \frac{x_1 x_2 s G_F}{4\sqrt{2}\,\pi\alpha} \tag{3.23}$$

$$\times \frac{\sum_i \left(Q_i^\gamma/e\right)\left(-2T_{3,i}\right)\left(-1+4\sin^2\theta_W\right)\left[f^+_{i/p}(x_1) - f^-_{i/p}(x_1)\right] f_{\bar{i}/N}(x_2) + i \leftrightarrow \bar{i}}{\sum_i \left(Q_i^\gamma/e\right)^2 f_{i/p}(x_1)\, f_{\bar{i}/N}(x_2) + i \leftrightarrow \bar{i}}$$

and

$$A_2(x_1,x_2) \overset{|q^2/M_Z^2| \ll 1}{\approx} \frac{x_1 x_2 s G_F}{4\sqrt{2}\,\pi\alpha} \times \frac{\sum_i \left(Q_i^\gamma/e\right)\left(2T_{3,i} - 4\,\frac{Q_i^\gamma}{e}\sin^2\theta_W\right)\left[f^+_{i/p}(x_1) - f^-_{i/p}(x_1)\right] f_{\bar{i}/N}(x_2) + i \leftrightarrow \bar{i}}{\sum_i \left(Q_i^\gamma/e\right)^2 f_{i/p}(x_1)\, f_{\bar{i}/N}(x_2) + i \leftrightarrow \bar{i}} \tag{3.24}$$

The only quantities remaining unspecified are the quark distributions, and in particular the correlation between the spin direction of the proton and its quark partons, which is contained in the functions $f^+_{i/p}(x_1)$ and $f^-_{i/p}(x_1)$. Here we make the additional assumption that to a good approximation only the valence quarks in the nucleon correlate their spins with the overall nucleon spin direction. The "ocean" is assumed unpolarized. Numerical results for low energy asymmetries are presented here for two cases. First, the SU(6) wave function for the proton gives

$$\frac{f^+_{u/p}(x)}{f^+_{u/p}(x) + f^-_{u/p}(x)} = \frac{5}{6}$$

$$\frac{f^+_{d/p}(x)}{f^+_{d/p}(x) + f^-_{d/p}(x)} = \frac{1}{3} \tag{3.25}$$

Second, the x dependent form[10]

$$\frac{f^+_{u/p}(x)}{f^+_{u/p}(x) + f^-_{u/p}(x)} = \frac{1}{2}\left(1 + x^{0.39}\right)$$

$$\frac{f^+_{d/p}(x)}{f^+_{d/p}(x) + f^-_{d/p}(x)} = \frac{1}{2}\left(1 - \frac{1}{3}x^{0.23}\right), \tag{3.26}$$

will be used. In the latter case, the u quark spin is completely aligned with that of the proton at $x = 1$, while both the u and d quarks are completely uncorrelated at $x = 0$. Both sets of polarized quark distributions yield spin dependent structure functions which are in adequate agreement with the polarized electron-polarized proton deep inelastic scattering experiments.[11] Of course the second set is somewhat better in this regard, having been fit in part to these data. For the unpolarized quark parton distributions themselves we use the parametrization of Field and Feynman,[12] but with the "ocean" as modified by Berger.[13] This gives a good description of the muon pair production data in 400 GeV pN collisions.

Before examining the predicted low energy asymmetries in detail, let us discuss the expected sign of the effect. In the limit where $\sin^2\theta_W$ is very small, only left-handed leptons and quarks interact with the Z^o. For $u\bar{u} \to \ell\bar{\ell}$ the product of quark and lepton couplings is negative for both the photon and Z^o. However for dilepton masses less than M_Z, the photon and Z^o propagators are of opposite sign, so the amplitudes for the intermediate γ and Z^o interfere destructively (the same holds for $d\bar{d} \to \ell\bar{\ell}$) and decrease the cross section from what it would be from photon exchange alone. Consequently the asymmetry, defined as right-handed minus left-handed quark cross sections divided by their sum, is positive for all values of $\cos\theta$. The known value of $\sin^2\theta_W$ is small enough that this positive sign holds for the low energy A_1 and A_2 calculated below.

In Fig. 3.1 the predictions for $A_1(x_1,x_2)$ and $A_2(x_1,x_2)$ at low energies are shown for scattering of polarized protons on unpolarized protons with SU(6) spin wave functions for the valence quarks in the

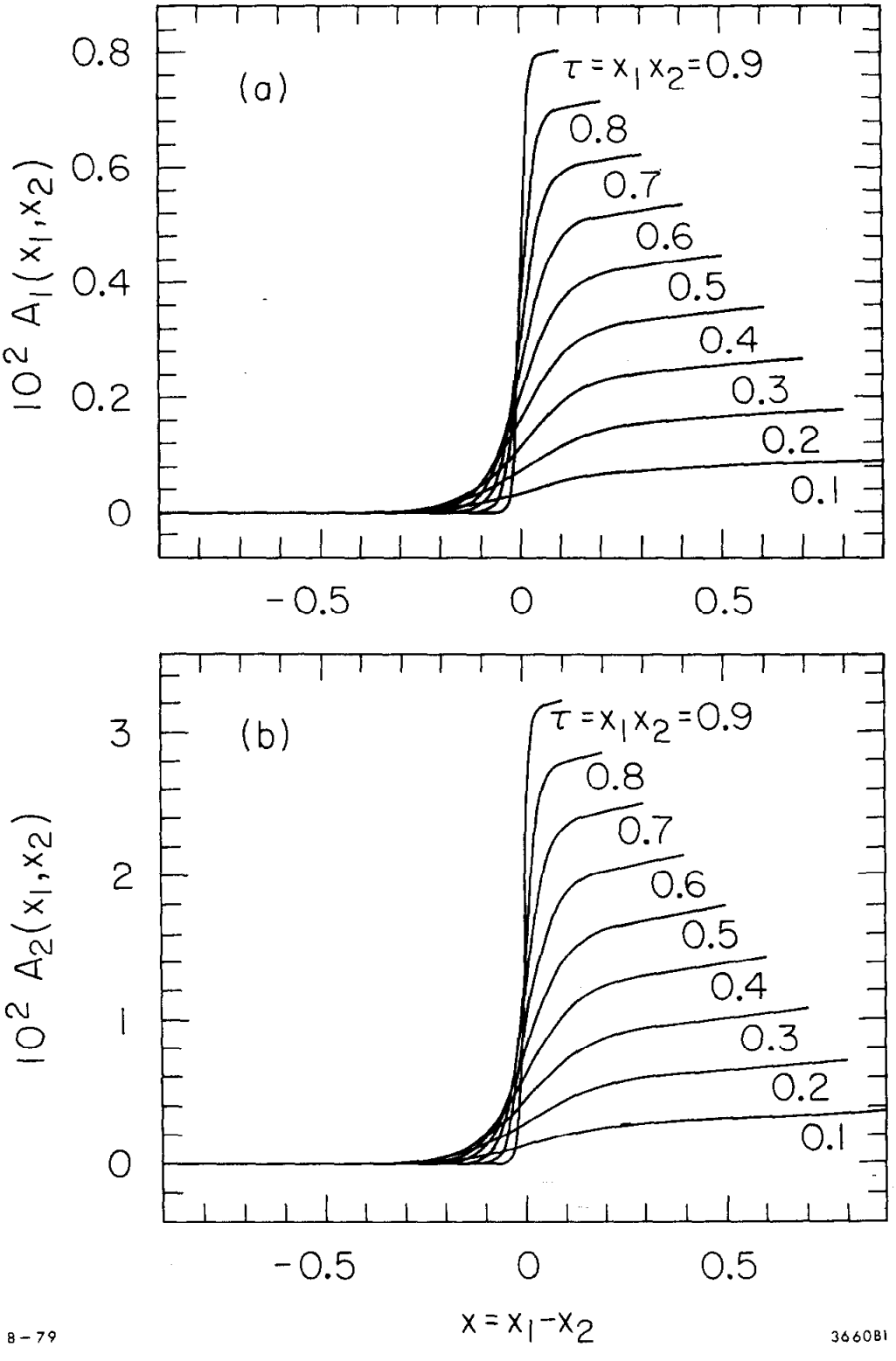

Fig. 3.1. The low energy parity violating asymmetries $A_1(x_1,x_2)$ and $A_2(x_1,x_2)$ for production of dileptons by longitudinally polarized protons on a proton target using the SU(6) spin wave function for the valence quarks in the proton. The center-of-mass energy squared is $s = 1000$ GeV^2, and $\sin^2\theta_W = 0.225$.

proton. The variables $x = x_1 - x_2$, the fractional momentum of the lepton pair along the polarized proton beam direction, and $\tau = |q^2|/s = x_1 x_2$ have been used. A value of $\sin^2\theta_W = 0.225$, representative of the results of recent experiments,[14] is employed in all graphs. An s value of 1000 GeV^2 has been chosen, with the asymmetries at other energies obtainable by scaling linearly in s.

The most obvious difference between the results for A_1 and A_2 at low energies is that the former is roughly an order of mangitude smaller. This is a consequence of the value of $\sin^2\theta_W$: for $\sin^2\theta_W = 1/4$ there is an exact vanishing of $g_{V,\ell}$ and hence of A_1 at low energies. The experimental value of $\sin^2\theta_W$ is close enough to 0.25 to severely suppress A_1.

For a given value of $\tau = x_1 x_2$ the values of $x = x_1 - x_2$ lie between $\tau - 1$ and $1 - \tau$. For negative values of x ($x_2 > x_1$) the dominant process is annihilation of valence quarks in the target with "ocean" antiquarks in the polarized proton. Since these antiquarks are unpolarized by assumption, the asymmetries are very small for $x < 0$.

At the opposite extreme, when x is near the maximum value of $1-\tau$, x_1 is near 1. In this regime, the cross section is dominated by valence u quarks in the polarized proton annihilating with antiquarks in the target. Since these u quarks are mostly aligned with the proton's spin, a maximum of the asymmetry is found.

In Figs. 3.2 and 3.3 we show low energy A_1 and A_2 for proton and neutron targets using the x dependent polarized quark distributions of Eq. (3.16). The results for proton targets are quite similar to those in Fig. 3.1, but are somewhat larger in magnitude, especially near $x = 1$. Using a neutron target (Fig. 3.3) rather than a proton target makes little difference in the asymmetries.

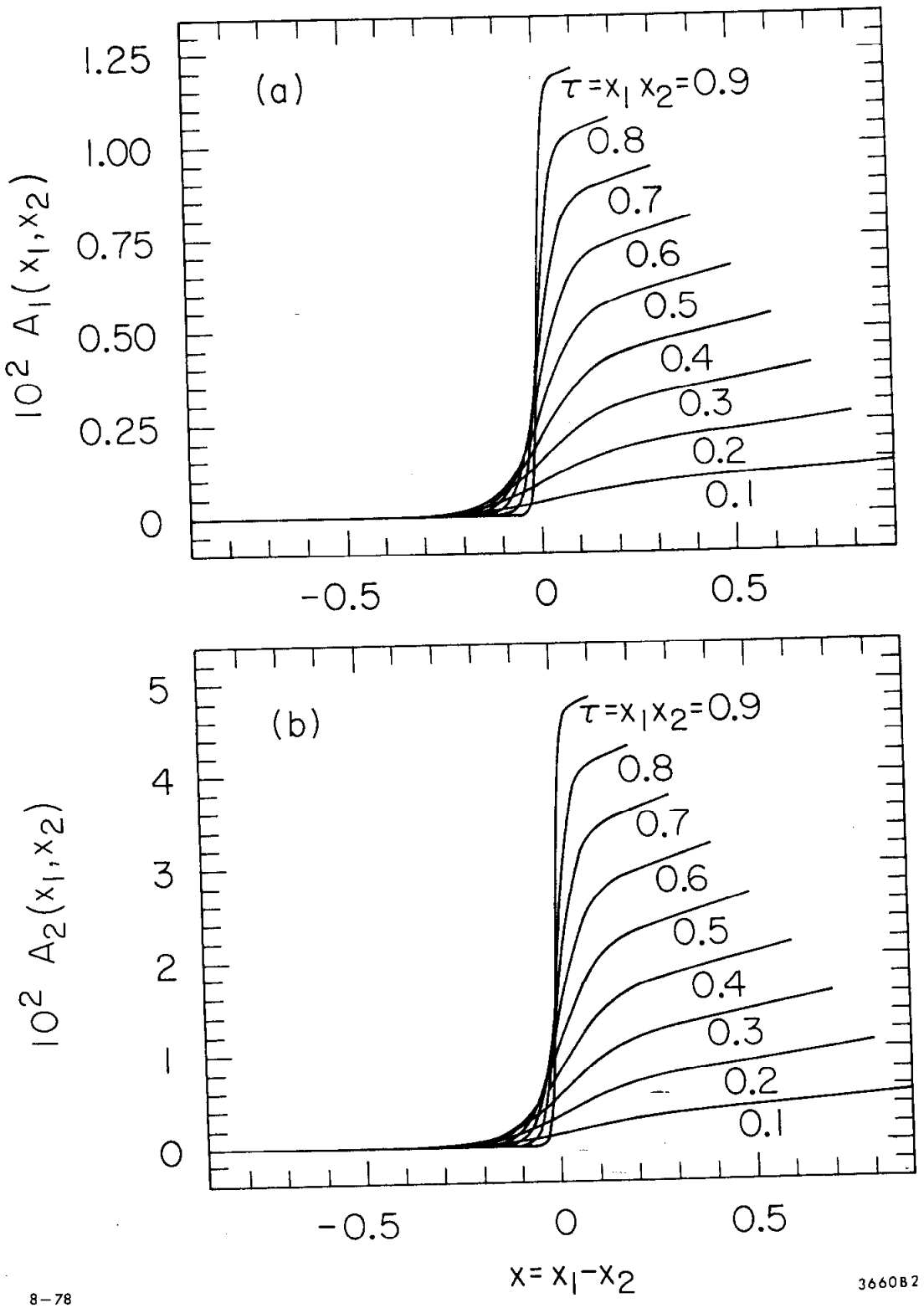

Fig. 3.2. Same as Fig. 3.1, but with x-dependent polarized quark distributions.

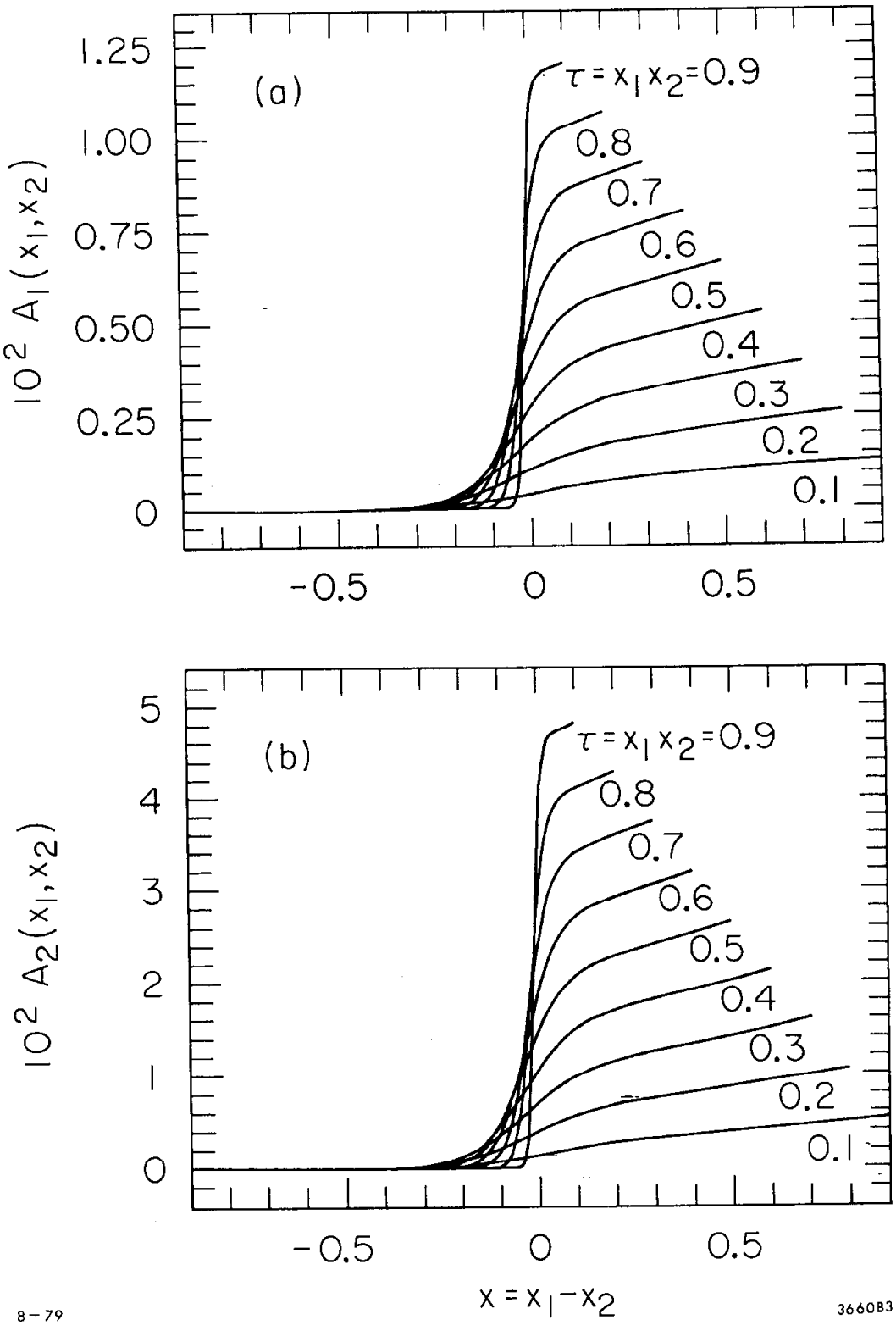

Fig. 3.3. Same as Fig. 3.1, but with x-dependent polarized quark distributions and a neutron target.

We next present numerical results for the high energy asymmetries A_1 and A_2 (cf. Eqs. (3.19) and (3.20)), also within the context of the Weinberg-Salam theory of electroweak interactions. Using the couplings of the quarks and leptons to the Z^o as given in Eq. (3.12), and parametrizing the quark structure functions as before, we show in Fig. 3.4 the parity violating asymmetries A_1 and A_2 for $pp \to \mu^+\mu^- X$. The x-dependent polarized quark distirbutions of Cheng and Fischbach have been used, and the s value is taken to be 6.4×10^5 GeV^2 (Isabelle energy).

Figure 3.4 shows that the asymmetries A_1 and A_2 at high energies become comparable to one another, and are of order 10^{-1} in magnitude. Note that the high energy asymmetries display different profiles in the τ-contours -- mainly because A_1 and A_2 in the high energy limit are no longer directly proportional to $\tau = x_1 x_2 s$ (see Eqs. (3.19) and (3.20)). The sign of the asymmetries is now opposite from the previous low-energy results.

4. Discussion

As shown in Sect. 2, the structure of the expression for the parity violating asymmetry for polarized proton production of lepton pairs is very similar to that for the asymmetry in polarized electron deep inelastic scattering. The asymmetry A_1, being independent of θ, is the analogue of the y independent term in the deep inelastic asymmetry. A_2, which has a coefficient $2\cos\theta/(1+\cos^2\theta)$, is correspondingly the analogue of the coefficient of $[1-(1-y)^2]/[1+(1-y)^2]$ in deep inelastic scattering.

Numerically, A_2 at low energies is at the hoped for 10^{-2} level in the Weinberg-Salam model for $|q^2| = 200$ GeV^2 ($\tau = |q^2|/s = 0.2$ at

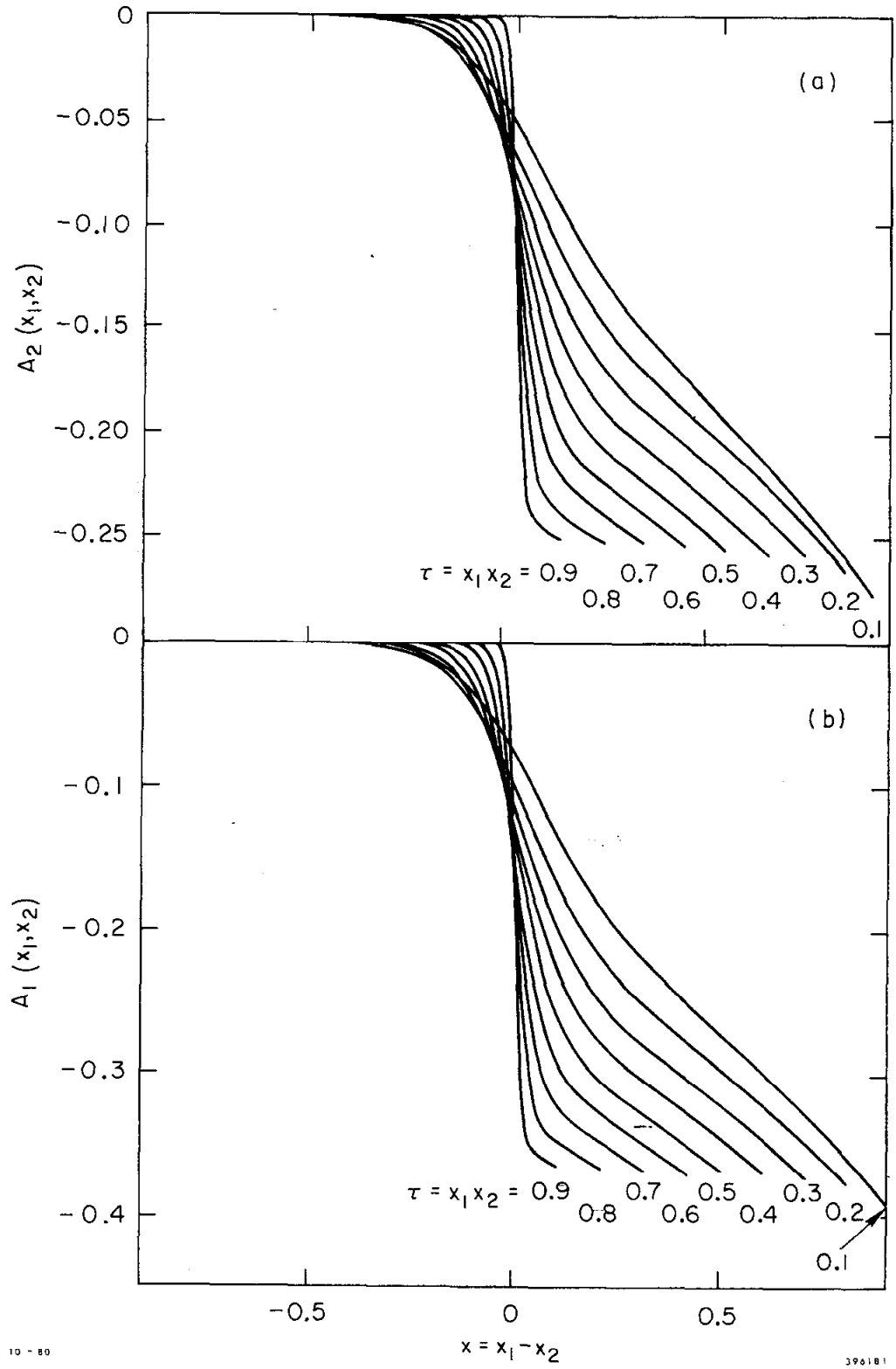

Fig. 3.4. The high energy parity violating asymmetries $A_1(x_1,x_2)$ and $A_2(x_1,x_2)$ for production of dileptons by longitudinally polarized protons on a proton target using the x-dependent polarized quark distributions. The center-of-mass energy squared is $s = 6.4 \times 10^5$ GeV^2, and $\sin^2\theta_W = 0.225$.

$s = 1000\ GeV^2$). However, because of the value of the weak mixing angle θ_W, at low energies A_1 is much smaller than A_2. Note that the low energy result $|A_1| << |A_2|$ is the reverse of the case in polarized electron deep inelastic scattering where the y independent term in the asymmetry (and analogue of A_1) is the dominant term. This comes about because the low energy result for A_1 involves the vector coupling of the Z^o to leptons times the axial coupling to quarks, whereas its deep inelastic analogue involves axial coupling to leptons times vector coupling to quarks. The experimental value of $\sin^2\theta_W \approx 0.225$ makes $g_{V,\ell}$, which is proportional to $(1 - 4\sin^2\theta_W)$, especially small.

Unfortunately, this situation makes the already difficult experimental measurement of these asymmetries doubly so. The asymmetry A_2 has a coefficient $2\cos\theta/(1+\cos^2\theta)$, and must be separated from the isotropic but much smaller (at low energies) asymmetry A_1 by measuring an angular distribution on top of the difference of beam polarizations required for isolating a parity violating effect. (At high (Isabelle) energies the asymmetries A_1 and A_2 are of comparable sizes. However, it is doubtful that polarized colliding proton beams will be available at Isabelle.)

Added to this is the question of whether the lowest order $q\bar{q} \to \ell\bar{\ell}$ diagram is to be trusted quantitatively as the mechanism for dilepton production in hadron collisions. The size of the experimental $\langle p_\perp \rangle$ values for the produced dileptons points toward higher order QCD effects being important,[2] e.g., $q\bar{q} \to$ gluon + $\ell\bar{\ell}$ and gluon + $q \to \ell\bar{\ell} + q$. The disagreement between the predicted Drell-Yan total cross section and that observed may also indicate quantitative problems for the lowest order model.[2] Thus, while measurement of a parity violating asymmetry

in dilepton production with polarized proton beams is of interest as another check of basic ideas on weak and electromagnetic interactions, the extraction therefrom of couplings of the Z^0 to quarks and leptons has quantitative uncertainties which correspond to those in the detailed theoretical understanding of dilepton production.

REFERENCES AND FOOTNOTES FOR CHAPTER III

* Most of the material in this chapter can be found in F. J. Gilman and T. Tsao, Phys. Rev. D21, 159 (1980).

1. S. D. Drell and T. M. Yan, Phys. Rev. Lett. 25, 316 (1970); ibid., 25, 902 (1970); and Ann. Phys. (N.Y.) 66, 578 (1971).
2. See the reviews of E. Berger, talk at the Orbis Scientiae, Coral Gables, January 1979 and SLAC-PUB-2314, 1979 (unpublished); and R. Stroynowski, in Proceedings of the SLAC Summer Institute on Particle Physics, edited by A. Mosher, SLAC, Stanford, California (1980).
3. R. W. Brown, K. O. Mikaelian and M. K. Gaillard, Nucl. Phys. B75, 112 (1974). See also R. Gustafson et al., Fermilab Proposal No. 583, 1978 (unpublished).
4. C. Prescott et al., Phys. Lett. 77B, 347 (1978); 84B, 524 (1979).
5. R. N. Cahn and F. J. Gilman, Phys. Rev. D17, 1313 (1978).
6. Our metric is such that q^2 is negative for the time-like virtual γ and Z^o four-momenta of relevance here; $\alpha = e^2/4\pi \approx 1/137$.
7. Since a quark with given helicity only annihilates with an antiquark of the opposite helicity, the proper antiquark actually occurs in the unpolarized target with probability $\frac{1}{2} f_{\bar{1}/N}(x_2)$. The factor of one-half cancels out in the ratio of cross sections that forms the asymmetry.
8. Although we have analyzed the asymmetry at the quark level by labeling in terms of the initial quark, the same formulae hold using the initial antiquark with appropriate changes in γ and Z^o

couplings. Thus the terms in Eq. (3.6) and thereafter involving antiquarks in place of quarks and vice versa ($i \leftrightarrow \bar{i}$) have the same form.

9. S. Weinberg, Phys. Rev. Lett. 19, 1264 (1967); A. Salam in Elementary Particle Theory: Relativistic Groups and Analyticity (Nobel Symposium No. 8), edited by N. Svartholm (Almqvist and Wisksell, Stockholm, 1968), p. 367.
10. H.-Y. Cheng and E. Fischbach, Phys. Rev. D19, 860 (1979).
11. M. J. Alguard et al., Phys. Rev. Lett. 37, 1261 (1976); 41, 70 (1978).
12. R. D. Field and R. P. Feynman, Phys. Rev. D5, 2590 (1977).
13. E. Berger, Ref. 2 and private communication.
14. C. Prescott et al., Ref. 4 and C. Baltay in Proceedings of the 19th International Conference on High Energy Physics, Tokyo, 1978, edited by S. Homma, M. Kawaguchi and H. Miyazawa (Physical Society of Japan, Tokyo, 1979), p. 882.

CHAPTER IV

POLARIZED-ELECTRON POSITRON ANNIHILATION NEAR THE Z^o MASS AND POLARIZED-ELECTRON ELECTRON SCATTERING

1. Introduction

In this chapter, we study the cross sections and parity violating and angular asymmetries that arise in polarized-electron positron annihilation when the center-of-mass collision energy is near the Z^o-pole. At such values of the collision energy, the Z^o can be physically produced (no longer virtual) and the reaction cross sections -- now overwhelmingly favored by Z^o exchange over γ exchange -- exhibit a typical Breit-Wigner resonance. Recall that at low energies, the parity violating asymmetries are given by the γ-Z interference term in the parity violating numerator, and dominated by the γ^2 term in the parity conserving denominator. This situation changes dramatically when we do polarization experiments near the Z^o-pole. Both the numerator and denominator terms of the asymmetry are dominated by the Z^{o2} parts of the cross section. As a result, the asymmetries are of order 10^{-1} to 1. This provides an ideal setting for studying Z^o physics. (It should also be emphasized that electron-positron annihilation provides a much cleaner probe into the detailed structure of the Z^o than any other process.)

In Sect. 2 we present and tabulate results for the decay width, and branching ratios of the Z^o. Also listed are the couplings of the Z^o to matter in the Weinberg-Salam theory.[1] These are used in Sect. 3 to give predictions for cross sections and asymmetries in the reactions $e^-e^+ \to \mu^-\mu^+$, $e^-e^+ \to u\bar{u}$ and $e^-e^+ \to d\bar{d}$. In Sect. 4 we consider the process

$e^-e^+ \to e^-e^+$, which is separate from the previous cases because of additional γ and Z^o exchange in the t-channel. We conclude in Sect. 5 with an examination of the reaction $e^-e^- \to e^-e^-$.

2. Decay Width and Branching Ratios of the Z^o

The lowest order diagram for the decay of the Z^o into matter is shown in Fig. 4.1. Let g_V and g_A be the vector and axial couplings, respectively, of the Z^o to a given fermion f. Then

$$\Gamma(Z^o \to f\bar{f}) = \frac{N_c M_Z}{12\pi}\left(g_V^2 + g_A^2\right) \quad . \tag{4.1}$$

The color factor N_c is equal to three for decay into a quark pair and is one for a lepton pair. We have treated the fermions as massless.

In the Weinberg-Salam model,

$$g_{V,e} = a\left(-1 + 4\sin^2\theta_W\right) \qquad g_{A,e} = +a \tag{4.2a}$$

$$g_{V,\nu} = +a \qquad g_{A,\nu} = -a \tag{4.2b}$$

$$g_{V,u} = a\left(1 - \frac{8}{3}\sin^2\theta_W\right) \qquad g_{A,u} = -a \tag{4.2c}$$

$$g_{V,d} = a\left(-1 + \frac{4}{3}\sin^2\theta_W\right) \qquad g_{A,d} = +a \tag{4.2d}$$

where

$$a \equiv \frac{e}{4\sin\theta_W \cos\theta_W} \quad . \tag{4.2e}$$

If we sum over the leptons and quarks in one 'generation,' we find for the Z^o width in the Weinberg-Salam model[2]

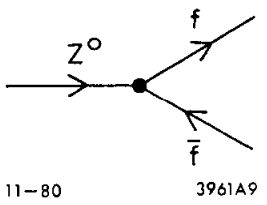

Fig. 4.1. Lowest order Feynman diagram for decay of Z^o into a fermion pair $f\bar{f}$.

$$\Gamma\left(Z^{o} \to e^{+}e^{-} + \nu_e\bar{\nu}_e + u\bar{u} + d\bar{d}\right) = \frac{\alpha M_Z}{3\sin^2\theta_W\cos^2\theta_W}\left(1 - 2\sin^2\theta_W + \frac{8}{3}\sin^4\theta_W\right). \tag{4.3}$$

The mass of the Z^o is related to $G_F = 1.02 \times 10^{-5}/M_N^2$ by

$$\frac{1}{M_Z^2} = \sqrt{2}\,\frac{G_F \sin^2\theta_W \cos^2\theta_W}{\pi\alpha} \quad . \tag{4.4}$$

For three 'generations' of leptons and quarks, we multiply by three to get

$$\Gamma(Z^{o} \to \text{all}) = \frac{\alpha M_Z}{\sin^2\theta_W\cos^2\theta_W}\left(1 - 2\sin^2\theta_W + \frac{8}{3}\sin^4\theta_W\right) \quad . \tag{4.5}$$

Numerically, when $\sin^2\theta_W = 0.225$, $M_Z = 89.6$ GeV and $\Gamma(Z^o \to \text{all}) = 2.57$ GeV. These numbers are used as input in the sections that follow. In Table 4.1 we list the branching ratios of Z^o into e^+e^-, $\nu_e\bar{\nu}_e$, $u\bar{u}$, and $d\bar{d}$ in the Weinberg-Salam model.

3. Cross Sections and Asymmetries for $e^-e^+ \to \mu^-\mu^+, q\bar{q}$

In this section we discuss the reaction $e^-e^+ \to f_i\bar{f}_i$, with $f_i = \mu, u, d$. The relevant Feynman diagram for this process is shown[3] in Fig. 4.2. In units of the point cross section $\sigma_{pt} = 4\pi\alpha^2/3s$ (where s is the center-of-mass energy squared), the spin average and summed cross section for $e^-e^+ \to f_i\bar{f}_i$ is

$$R_i \equiv \frac{\sigma\left(e^-e^+ \to f_i\bar{f}_i\right)}{\sigma_{pt}} \tag{4.6}$$

$$= N_c\left[(e_i/e)^2 + \frac{\left(g_{V,e}^2 + g_{A,e}^2\right)\left(g_{V,i}^2 + g_{A,i}^2\right)}{e^4}|\eta|^2 s^2 - 2(e_i/e)\,\frac{g_{V,e}g_{V,i}}{e^2}\,\mathrm{Re}\,\eta\, s\right],$$

TABLE 4.1

The branching ratios $\Gamma_i/\Gamma(Z^o \to \text{all})$ for $i = e^+e^-$, $\nu_e\bar{\nu}_e$, $u\bar{u}$, and $d\bar{d}$ in the Weinberg-Salam model with three 'generations' of leptons and quarks and $\sin^2\theta_W = 0.225$.

Decay Mode	Branching Ratio
e^+e^-	3.1%
$\nu_e\bar{\nu}_e$	6.1%
$u\bar{u}$	10.6%
$d\bar{d}$	13.6%

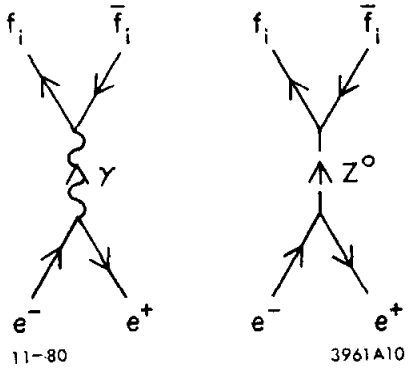

Fig. 4.2. Lowest order Feynman diagrams for $e^-e^+ \to f_i\bar{f}_i$.

where

$$\eta \equiv \frac{1}{s - M_Z^2 - iM_Z\Gamma} \quad , \tag{4.7}$$

and f_i is a particular fermion of charge e_i, with vector and axial couplings $g_{V,i}$ and $g_{A,i}$, respectively, to the Z^o. The Z^o mass and width is M_Z and Γ, respectively. The cross section in Eq. (4.6) contains a color factor N_c equal to three for f_i = quark and equal to one for f_i = lepton. The masses of all fermion have been neglected.

In Fig. 4.3(a),(b),(c) we plot R_i for $e^-e^+ \to \mu^-\mu^+$, $e^-e^+ \to u\bar{u}$, and $e^-e^+ \to d\bar{d}$ as a function of the total energy $E = \sqrt{s}$. These numerical results are all for the Weinberg-Salam model when $\sin^2\theta_W = 0.225$, and are representative of cross sections for any charged lepton, charge +2e/3 quark, and charge -e/3 quark, respectively, with conventional $SU(2) \times U(1)$ assignments. We see that, on resonance ($E \approx 89.6$ GeV), the quark cross sections are larger than the lepton cross section by roughly the color factor $N_c = 3$.

We now turn our attention to the differential scattering cross section for $e^-e^+ \to f_i\bar{f}_i$. For the annihilation of a longitudinally polarized electron (helicity $\lambda/2$) and the creation of a fermion (helicity $\lambda'/2$) the differential cross section is

$$\frac{d\sigma}{d\Omega}\,\lambda,\lambda'\left(e^-e^+ \to f_i\bar{f}_i\right) = \frac{\alpha^2 N_c}{8s}\left\{\left[(e_i/e)^2 + \frac{\left(g_{V,e}^2 + g_{A,e}^2 + 2\lambda g_{V,e}g_{A,e}\right)\left(g_{V,i}^2 + g_{A,i}^2 + 2\lambda' g_{V,i}g_{A,i}\right)}{e^4}\,|\eta|^2 s^2 - 2(e_i/e)\,\frac{\left(g_{V,e} + g_{A,e}\right)\left(g_{V,i} + \lambda' g_{A,i}\right)}{e^2}\,\mathrm{Re}\,\eta\, s\right]\left[(1+\cos^2\theta) + \lambda\lambda'\,2\cos\theta\right]\right\} \tag{4.8}$$

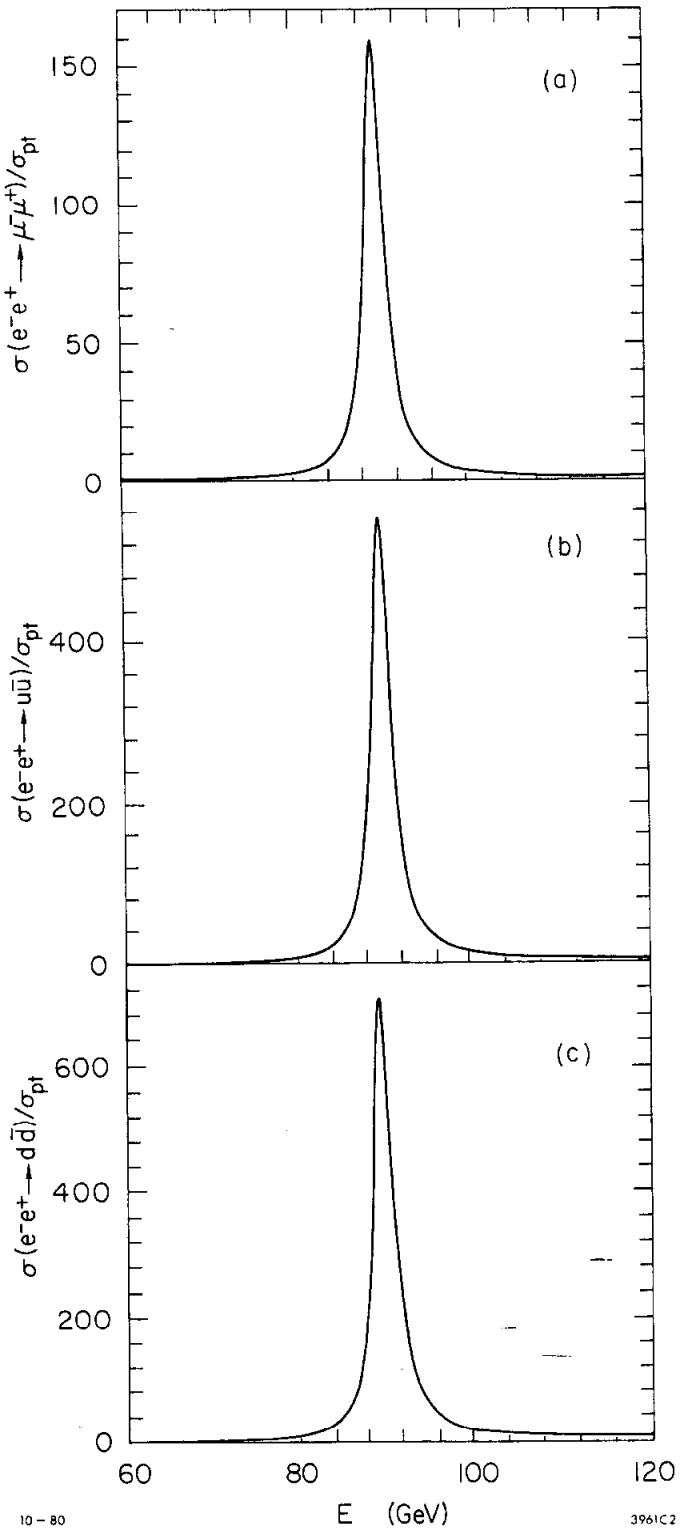

Fig. 4.3. Cross sections as a function of beam energy E for (a) $e^-e^+ \to \mu^-\mu^+$, (b) $e^-e^+ \to u\bar{u}$, and (c) $e^-e^+ \to d\bar{d}$, in units of σ_{pt} for the Weinberg-Salam model with $\sin^2\theta_W = 0.225$.

where

$$\lambda,\lambda' = \begin{cases} +1 & \text{right-handed electron, fermion} \\ -1 & \text{left-handed electron, fermion} \end{cases} . \qquad (4.9)$$

As usual, the fermion mass terms have been neglected. The angle θ is the scattering angle between the incoming electron and outgoing fermion (lepton or quark).

Even with unpolarized beams there is a forward-backward asymmetry ($2\cos\theta$ term) in $e^-e^+ \to f_i\bar{f}_i$. If we define $d\sigma(\theta)$ as the spin-averaged and summed differential cross section, the forward-backward asymmetry is defined as

$$A_{FB} \equiv \frac{d\sigma(\theta=0) - d\sigma(\theta=\pi)}{d\sigma(\theta=0) + d\sigma(\theta=\pi)} = \frac{\text{coefficient of } 2\cos\theta}{\text{coefficient of } 1+\cos^2\theta} \qquad (4.10)$$

$$A_{FB} = \frac{2\,\dfrac{g_{A,e}g_{A,i}}{e^2}\left[2\,\dfrac{g_{V,e}g_{V,i}}{e^2}|\eta|^2 s^2 - (e_i/e)\,\mathrm{Re}\,\eta\, s\right]}{\left[(e_i/e)^2 + \dfrac{\left(g_{V,e}^2+g_{A,e}^2\right)\left(g_{V,i}^2+g_{A,i}^2\right)}{e^4}|\eta|^2 s^2 - 2(e_i/e)\,\dfrac{g_{V,e}g_{V,i}}{e^2}\,\mathrm{Re}\,\eta\, s\right]} \qquad (4.11)$$

This forward-backward asymmetry is plotted in Fig. 4.4(a),(b),(c) for $e^-e^+ \to \mu^-\mu^+$, $e^-e^+ \to u\bar{u}$, and $e^-e^+ \to d\bar{d}$ -- all for the Weinberg-Salam theory. The total center-of-mass energy E has been taken from 0 to 125 GeV. Note that in all three cases the angular asymmetry is of order -1 when E is 60 to 75 GeV, i.e., below the mass of the Z^o, and is very small at the Z^o mass. This is because $g_{V,e}$ in the Weinberg-Salam model is proportional to $(-1+4\sin^2\theta_W)$, and the value of 0.225 that we use for $\sin^2\theta_W$ makes $g_{V,e}$ close to vanishing.

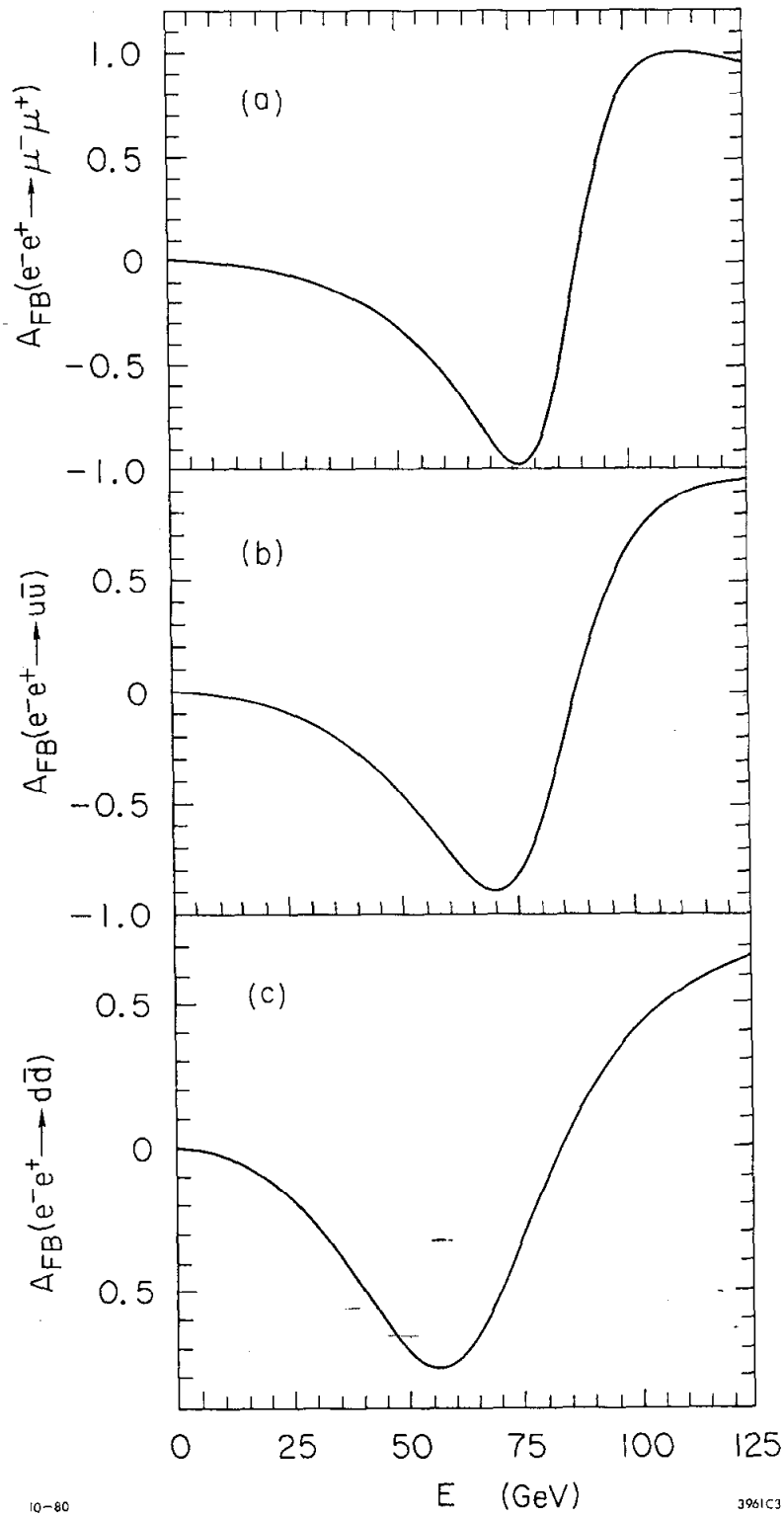

Fig. 4.4. Forward-backward asymmetry A_{FB} as a function of total center-of-mass energy E for the reactions (a) $e^-e^+ \to \mu^-\mu^+$, (b) $e^-e^+ \to u\bar{u}$, and (c) $e^-e^+ \to d\bar{d}$, in the Weinberg-Salam model with $\sin^2\theta_W = 0.225$.

Since the forward-backward asymmetry is not a parity violating quantity, it need not arise solely from the presence of the Z^o. However, the angular asymmetry induced electromagnetically by two γ exchange is only a few percent and rises logarithmically with energy. Thus these two γ background effects will not be important around 60 to 75 GeV. Of course, the quarks can only be observed through their hadron fragments. Unscrambling the jets due to different quarks may be very difficult experimentally.

We can sum over quark helicities[4] in Eq. (4.8) and form a parity violating asymmetry for a polarized electron beam by taking the difference of positive and negative helicity cross sections divided by their sum:

$$A = \frac{d\sigma_{\lambda=+} - d\sigma_{\lambda=-}}{d\sigma_{\lambda=+} + d\sigma_{\lambda=-}} \quad . \tag{4.12}$$

This has the angular decomposition

$$A \equiv \frac{A_1 + A_2 \dfrac{2\cos\theta}{1+\cos^2\theta}}{1 + A_{FB} \dfrac{2\cos\theta}{1+\cos^2\theta}} \quad . \tag{4.13}$$

At low energies ($E \leq 25$ GeV), the forward-backward asymmetry A_{FB} is small (cf., Fig. 4.4(a),(b),(c)), and the second term in the denominator may be neglected relative to the first term. In terms of Z^o couplings, the parity violating asymmetries A_1 and A_2 are given by

$$A_1 = \frac{2\left[\dfrac{g_{V,e}g_{A,e}\left(g_{V,i}^2 + g_{A,i}^2\right)}{e^4}|\eta|^2 s^2 - (e_i/e)\dfrac{g_{A,e}g_{V,i}}{e^2}\,\mathrm{Re}\,\eta\, s\right]}{\left[(e_i/e)^2 + \dfrac{\left(g_{V,e}^2 + g_{A,e}^2\right)\left(g_{V,i}^2 + g_{A,i}^2\right)}{e^4}|\eta|^2 s^2 - 2(e_i/e)\dfrac{g_{V,e}g_{V,i}}{e^2}\,\mathrm{Re}\,\eta\, s\right]} \tag{4.14}$$

$$A_2 = \frac{2\left[\frac{g_{V,i}g_{A,i}\left(g_{V,e}^2+g_{A,e}^2\right)}{e^4}|\eta|^2 s^2 - (e_i/e)\,\frac{g_{V,e}g_{A,i}}{e^2}\,\mathrm{Re}\,\eta\, s\right]}{\left[(e_i/e)^2 + \frac{\left(g_{V,e}^2+g_{A,e}^2\right)\left(g_{V,i}^2+g_{A,i}^2\right)}{e^4}|\eta|^2 s^2 - 2(e_i/e)\,\frac{g_{V,e}g_{V,i}}{e^2}\,\mathrm{Re}\,\eta\, s\right]} \tag{4.15}$$

Notice that $A_1 = A_2$ for final states $f_i = \mu^-$ or τ^-. In Fig. 4.5 we present the asymmetry for this case for the Weinberg-Salam model, while Fig. 4.6(a),(b) show A_1 for f_i = u and d, and Fig. 4.7(a),(b) do the same for A_2.

For both A_1 and A_2 their largest magnitude generally occurs at an energy near the Z^o pole, in distinction to the previous forward-backward asymmetry A_{FB}. The parity violating asymmetries are negative at the Z^o-pole and generally substantial (< -0.2), but are not quite as large as the non-parity violating forward-backward asymmetry at its maximum below the Z^o mass. In the case of quark final states, we again must face the problem of sorting out different flavors by observation of their hadron fragments. Otherwise, we must observe a particular hadron and average over the quark flavors being produced.

4. Polarization Asymmetry for $e^+e^- \to e^+e^-$

In this section we give the differential cross section and parity violating asymmetry for polarized-electron positron elastic scattering. The lowest order Feynman diagrams which contribute to this process is shown in Fig. 4.8. The formulae are now slightly more complicated because of t-channel diagrams in addition to the usual s-channel annihilation diagrams. The differential cross section for a longitudinally

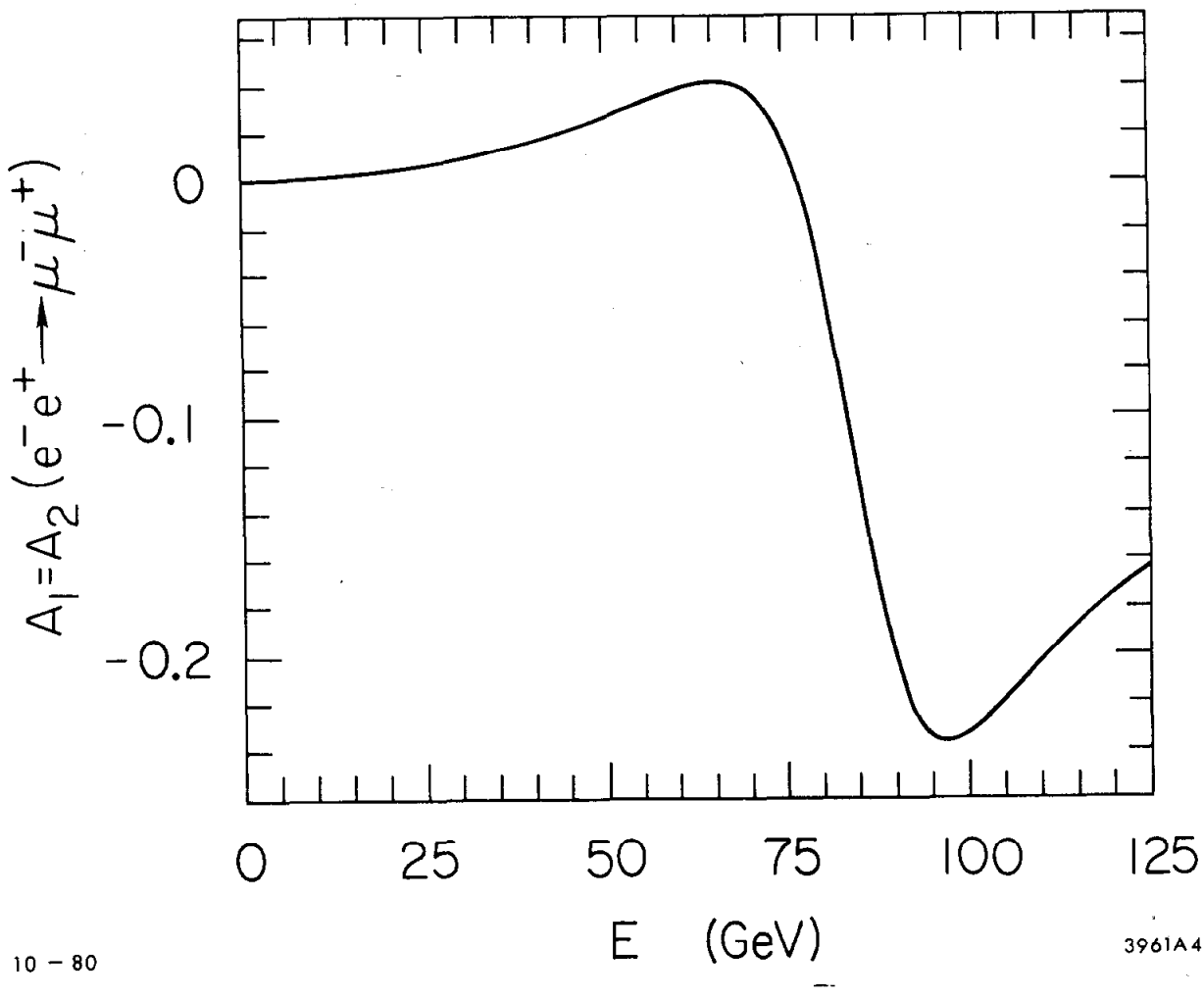

Fig. 4.5. Parity violating asymmetry as a function of total center-of-mass energy E for $e^-e^+ \to \mu^-\mu^+$ in the Weinberg-Salam model with $\sin^2\theta_W = 0.225$.

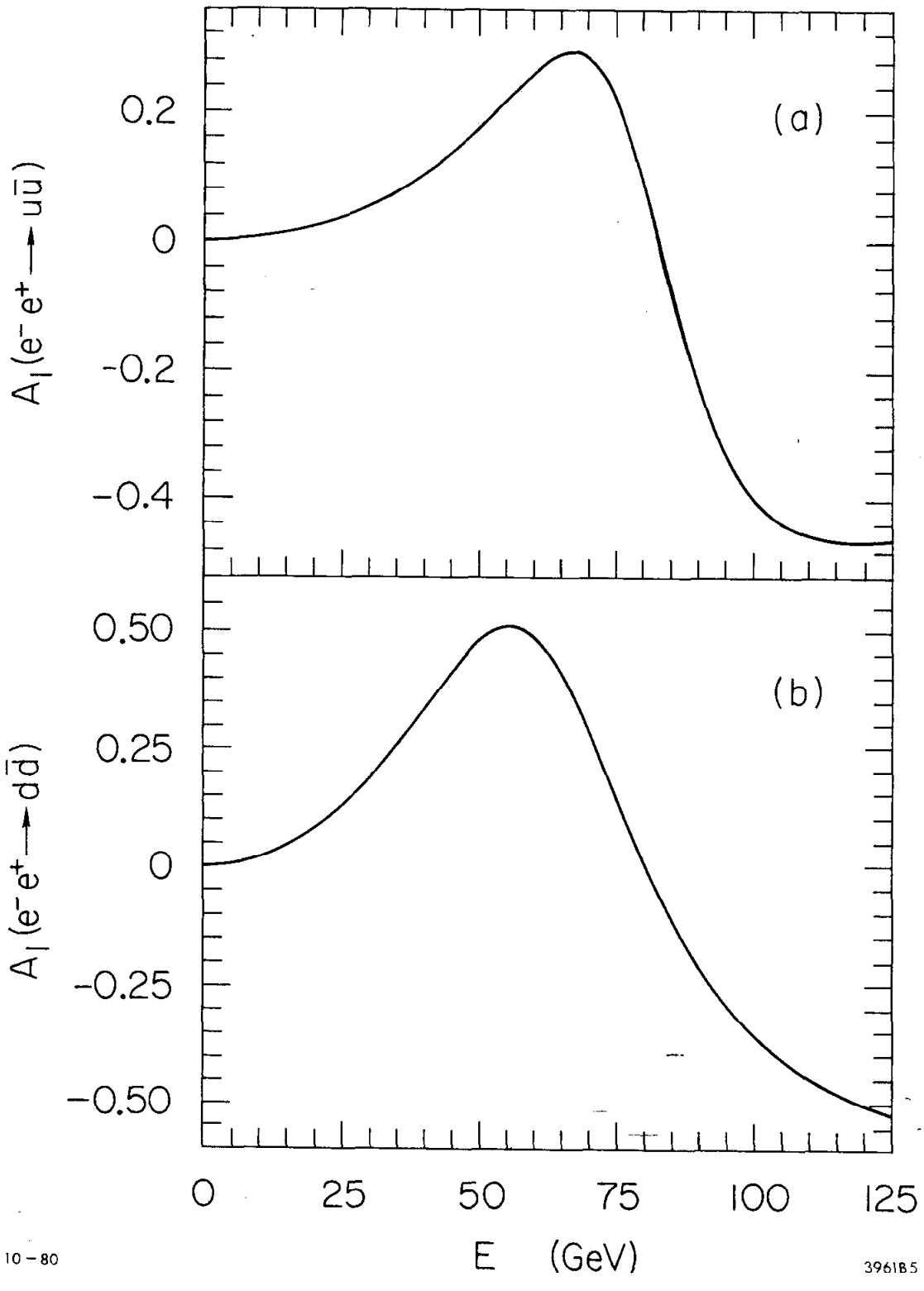

Fig. 4.6. Parity violating asymmetry A_1 as a function of total center-of-mass energy E for (a) $e^-e^+ \to u\bar{u}$, and (b) $e^-e^+ \to d\bar{d}$, in the Weinberg-Salam model with $\sin^2\theta_W = 0.225$.

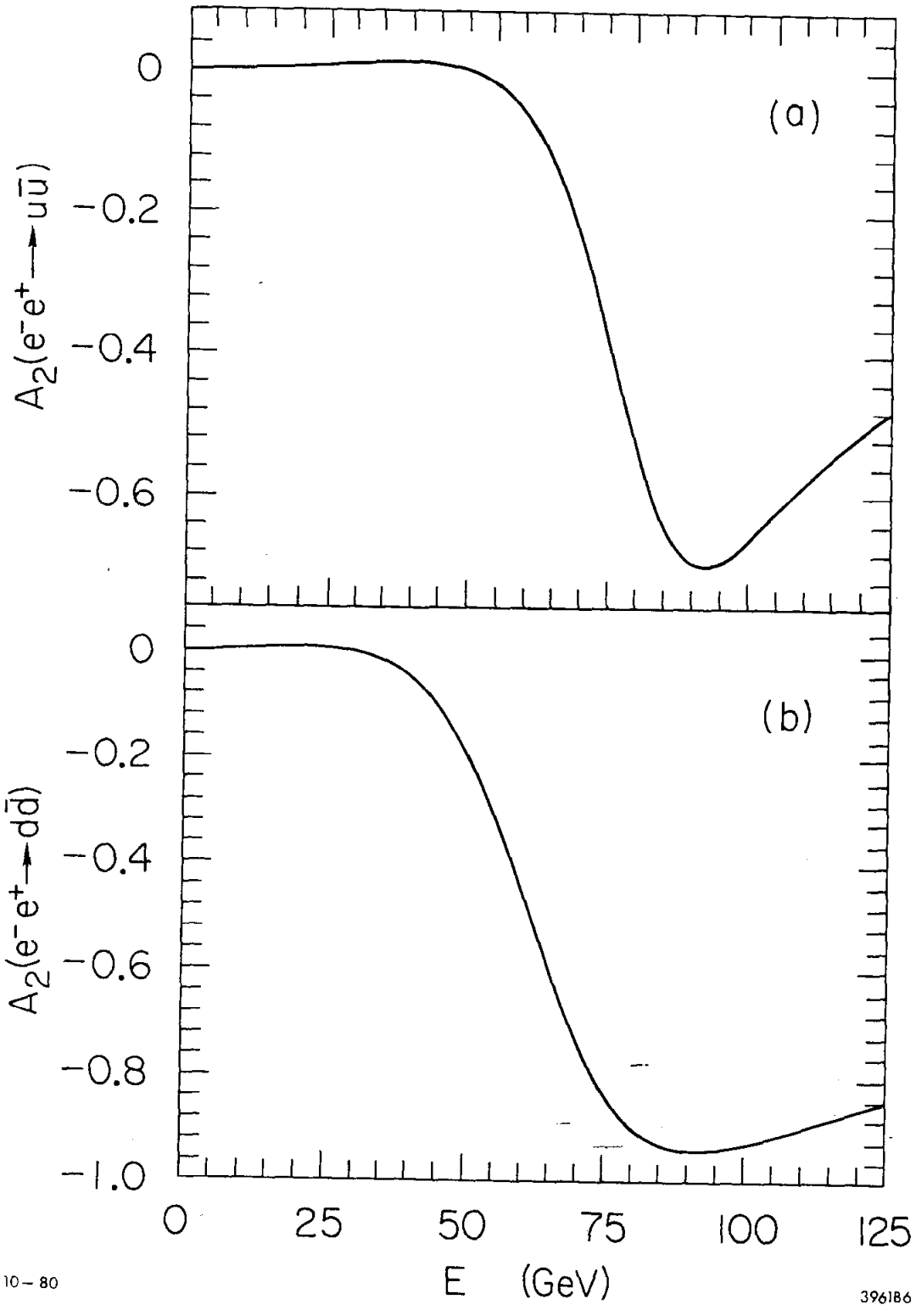

Fig. 4.7. Parity violating asymmetry A_2 as a function of total center-of-mass energy E for (a) $e^-e^+ \to u\bar{u}$, and (b) $e^-e^+ \to d\bar{d}$, in the Weinberg-Salam model with $\sin^2\theta_W = 0.225$.

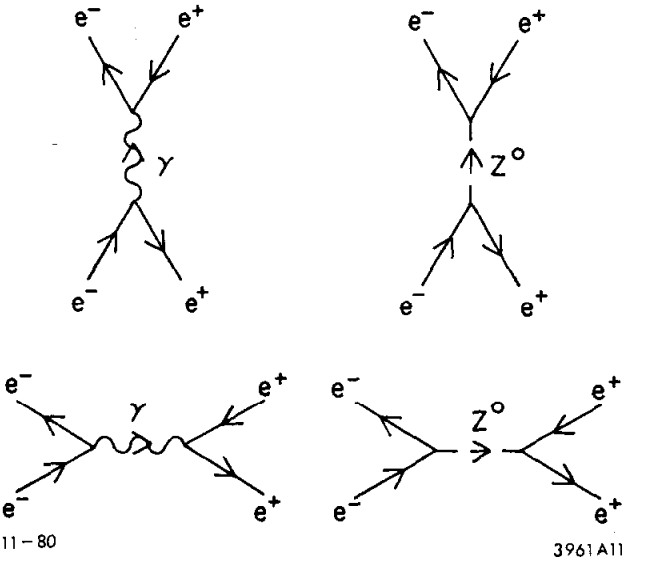

Fig. 4.8. Lowest order Feynman diagrams for $e^+e^- \rightarrow e^+e^-$.

polarized e^- beam is[5]

$$\frac{4s}{\alpha_{ch}^2}\frac{d\sigma_\lambda}{d\Omega}\left(e^+e^- \to e^+e^-\right) = 2s^2\left[\frac{1}{t^2} + \rho^2\left(\alpha^2 - \beta^2\right) + \frac{2\rho}{t}\left(g_{V,e}^2 + g_{A,e}^2\right)\right]$$

$$+ \frac{(1-\cos\theta)^2}{2}\left[1 + |\eta|^2 s^2\left(\alpha^2 - \beta^2\right) + \mathrm{Re}\ \eta s\left(g_{V,e}^2 - g_{A,e}^2\right)\right]$$

$$+ \frac{(1+\cos\theta)^2}{2}\left[\left(1 - \frac{s}{t}\right)^2 + |\eta - \rho|^2 s^2\left(\alpha^2 + \beta^2\right)\right]$$

$$+ \lambda(1+\cos\theta)^2 |\eta - \rho|^2 s^2 \alpha\beta \qquad (4.16)$$

where η here differs slightly from its previous definition by a factor of e^2:

$$\eta = \frac{1}{e^2}\frac{1}{s - M_Z^2 - iM_Z\Gamma} \quad . \qquad (4.17)$$

We also have

$$\rho = \frac{1}{e^2}\frac{1}{t^2 + M_Z^2} \quad , \qquad (4.18)$$

$$t = \frac{s(1-\cos\theta)}{2} \quad , \qquad (4.19)$$

$$\alpha = g_{V,e}^2 + g_{A,e}^2 \quad , \qquad (4.20)$$

$$\beta = 2g_{V,e}\, g_{A,e} \quad . \qquad (4.21)$$

arity violating asymmetry[6] is

$$\frac{d\sigma_{\lambda=+} - d\sigma_{\lambda=-}}{d\sigma_{\lambda=+} + d\sigma_{\lambda=-}} \tag{4.22}$$

$$\frac{(1+\cos\theta)^2 \, |\eta-\rho|^2 s^2 \alpha\beta}{\left\{2s^2\left[\frac{1}{t^2} + \rho^2(\alpha^2-\beta^2) + \frac{2\rho}{t}\left(g_{V,e}^2 - g_{A,e}^2\right)\right]\right.}$$

$$\frac{(1-\cos\theta)^2}{2}\left[1 + |\eta|^2 s^2(\alpha^2-\beta^2) + \mathrm{Re}\ \eta s\left(g_{V,e}^2 - g_{A,e}^2\right)\right]$$

$$\left. - \frac{(1+\cos\theta)^2}{2}\left[\left(1 - \frac{s}{t}\right)^2 + |\eta-\rho|^2 s^2(\alpha^2+\beta^2)\right]\right\} \tag{4.23}$$

Fig. 4.9 we show $A(e^+e^- \to e^+e^-)$ as a function of the total center-energy E in the Weinberg-Salam model ($\sin^2\theta_W = 0.225$) for center-scattering angle $\theta = \pi/2$. The maximal asymmetry occurs near the and is about -0.2.

arization Asymmetry for $e^-e^- \to e^-e^-$

o conclude this chapter we present results for the differential section and polarization asymmetry in $e^-e^- \to e^-e^-$. This reaction be studied at an electron-positron machine such as LEP. Rather, uires a machine such as the proposed SLAC Single Pass Collider electrons in both beams.

There are four diagrams (Fig. 4.10) for this reaction -- two annel) direct graphs and two (u-channel) cross graphs which are ired by the Pauli exclusion principle. The differential scattering s section[7] for a polarized-electron beam is

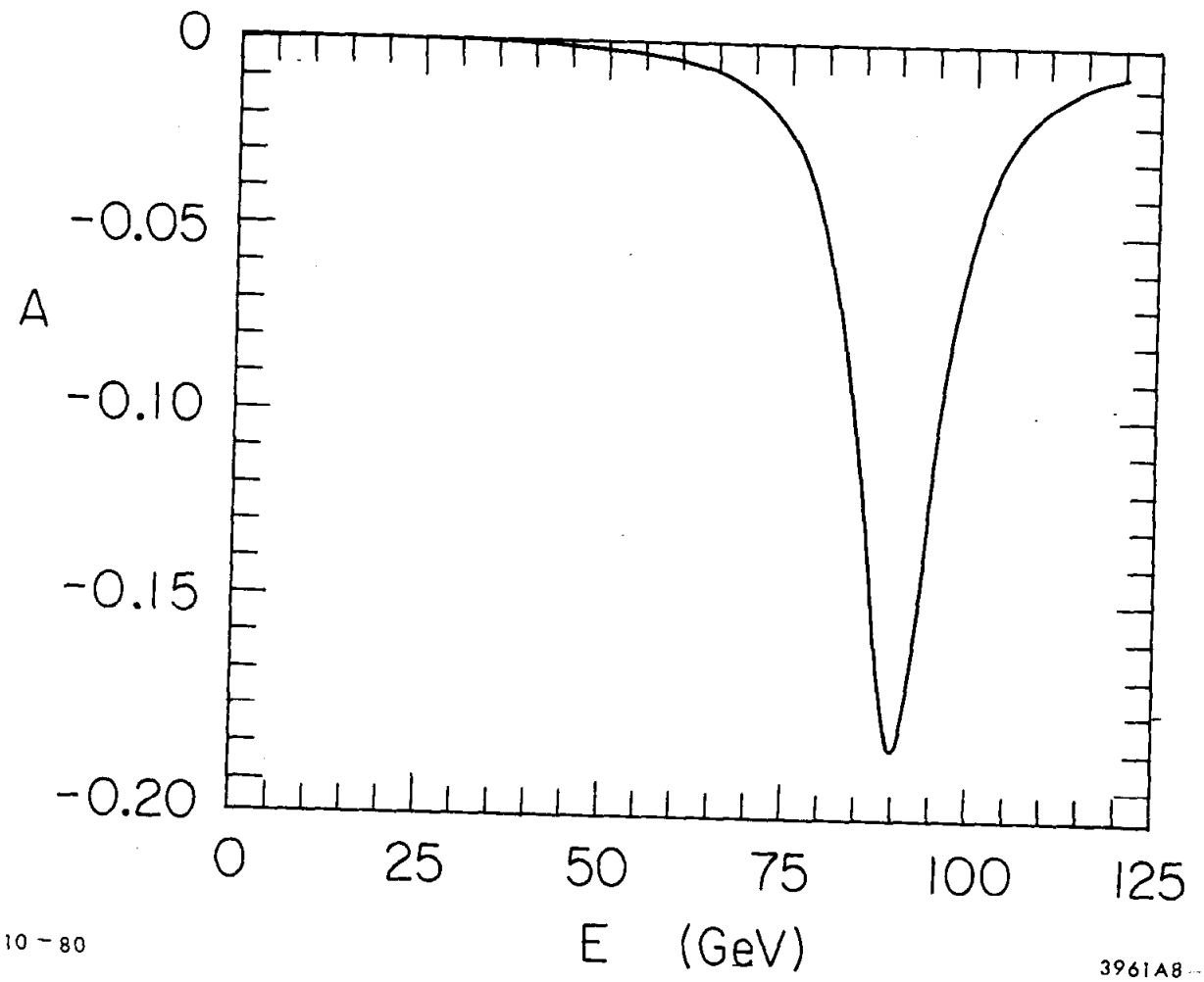

Fig. 4.9. Parity violating asymmetry as a function of total center-of-mass energy E for $e^+e^- \to e^+e^-$ in the Weinberg-Salam model with $\sin^2\theta_W = 0.225$. The center-of-mass scattering angle is $\pi/2$.

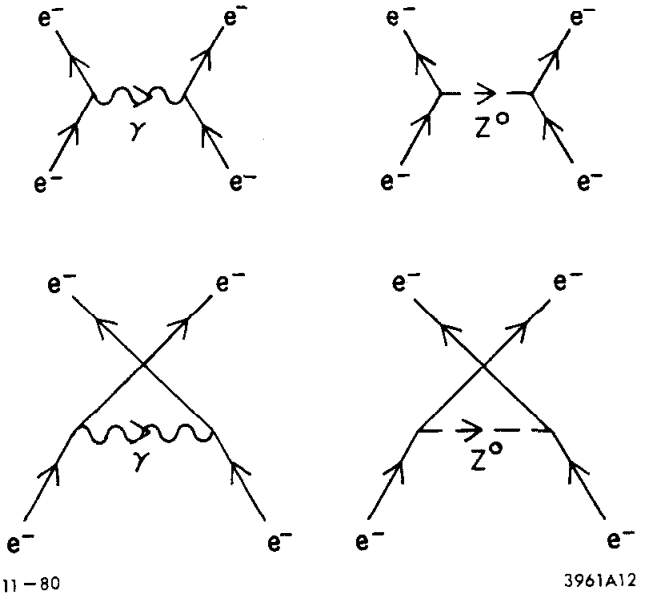

Fig. 4.10. Lowest order Feynman diagrams for $e^-e^- \rightarrow e^-e^-$.

$$\frac{4}{\alpha_{ch}^2}\frac{d\sigma_\lambda}{d\Omega}\left(e^-e^- \to e^-e^-\right) = 2s\left[\frac{1}{t_1}+\frac{1}{t_2}+\left(\rho_1+\rho_2\right)\left(g_{V,e}+\ g_{A,e}\right)^2\right]^2$$

$$+\ \frac{s(1+\cos\theta)^2}{2}\left[\frac{1}{t_1}+\rho_1\left(g_{V,e}^2-g_{A,e}^2\right)\right]^2$$

$$+\ \frac{s(1-\cos\theta)^2}{2}\left[\frac{1}{t_2}+\rho_2\left(g_{V,e}^2-g_{A,e}^2\right)\right]^2 \quad . \tag{4.24}$$

Here we have defined

$$t_1 = \frac{s(1-\cos\theta)}{2} \quad , \tag{4.25}$$

$$t_2 = \frac{s(1+\cos\theta)}{2} \quad , \tag{4.26}$$

$$\rho_1 = \frac{1}{t_1+M_Z^2}\ \frac{1}{e^2} \quad , \tag{4.27}$$

$$\rho_2 = \frac{1}{t_2+\ M_Z^2}\ \frac{1}{e^2} \quad . \tag{4.28}$$

The parity violating asymmetry is

$$A = \frac{d\sigma_{\lambda=+}-\ d\sigma_{\lambda=-}}{d\sigma_{\lambda=+}+\ d\sigma_{\lambda=-}} \tag{4.29}$$

$$= \frac{8\,g_{V,e}\,g_{A,e}\left(\rho_1+\rho_2\right)\left[\frac{1}{t_1}+\frac{1}{t_2}+\left(\rho_1+\rho_2\right)\left(g_{V,e}^2+g_{A,e}^2\right)\right]}{\left\{2\left[\left(\frac{1}{t_1}+\frac{1}{t_2}+\left(\rho_1+\rho_2\right)\left(g_{V,e}^2+g_{A,e}^2\right)\right)^2+4\left(\rho_1+\rho_2\right)^2 g_{V,e}^2\,g_{A,e}^2\right]\right.}$$

$$+\ \frac{(1+\cos\theta)^2}{2}\left[\frac{1}{t_1}+\rho_1\left(g_{V,e}^2-g_{A,e}^2\right)\right]^2$$

$$\left.+\ \frac{(1-\cos\theta)^2}{2}\left[\frac{1}{t_2}+\rho_2\left(g_{V,e}^2-g_{A,e}^2\right)\right]^2\right\} \quad . \tag{4.30}$$

In Fig. 4.11 we exhibit the asymmetry $A(e^-e^- \to e^-e^-)$ as a function of total center-of-mass energy E for the Weinberg-Salam model with $\sin^2\theta_W = 0.225$. The center-of-mass scattering angle has been chosen to be $\theta = \pi/2$. Note that the asymmetry is negative and only at the 4% level even when $E \approx M_Z$. This is a consequence of the fact that the Z^o is not resonantly produced in the t-channel and hence the large effects of the Z^o-pole are never realized.

6. Summary

In this chapter we have presented formulae for cross sections, and for parity violating and angular asymmetries for $e^-e^+ \to \mu^-\mu^+$, $e^-e^+ \to u\bar{u}$, and $e^-e^+ \to d\bar{d}$ near the Z^o mass. Numerical results were given in the Weinberg-Salam model. As expected, all asymmetries are large and are of order 10^{-1} to 1 in magnitude. The polarization asymmetry for $e^+e^- \to e^+e^-$ was also studied and is approximately -0.2 at the Z^o-pole for $\sin^2\theta_W = 0.225$ and $\theta_{c.m.} = \pi/2$. Finally, the polarization asymmetry for the reaction $e^-e^- \to e^-e^-$ is much smaller than the previously considered s-channel annihilation polarization asymmetries.

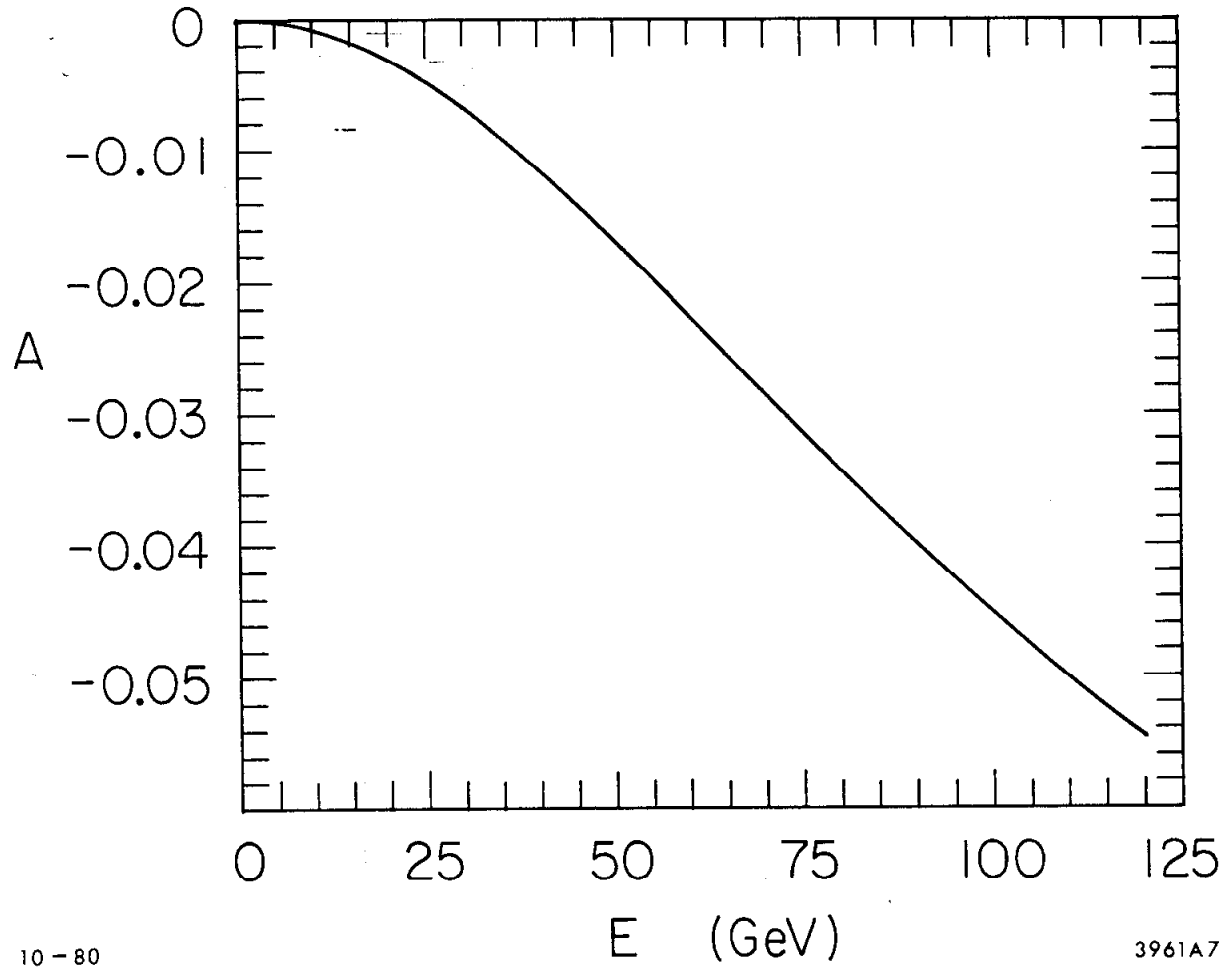

Fig. 4.11. Parity violating asymmetry as a function of total center-of-mass energy E for $e^-e^- \to e^-e^-$ in the Weinberg-Salam model with $\sin^2\theta_W = 0.225$. The center-of-mass scattering angle is $\pi/2$.

REFERENCES AND FOOTNOTES FOR CHAPTER IV

1. S. Weinberg, Phys. Rev. Lett. 19, 1264 (1967); A. Salam, in Elementary Particle Theory: Relativistic Groups and Analyticity (Nobel Symposium No. 8), edited by N. Svartholm (Almqvist and Wiksell, Stockholm, 1968), p. 367.

2. Here $\alpha = e^2/4 \approx 1/137$ is the fine structure constant.

3. Figure 4.2 does not apply for $f_i = e^-$ because of additional contributions due to γ and Z^o exchange in the t-channel, nor for $f_i = \nu_e$ because of W exchange in the t-channel. We consider the case $f_i = e^-$ separately in Sect. 3 of this chapter.

4. An equivalent parity violating quantity may be formed by taking an unpolarized e^- beam and measuring the helicity of the final state f_i (e.g., forming the polarization asymmetry for the f_i). If instead the helicity of the final state $\bar{f}_i$ is detected then there is an overall sign change. This possibility is studied in the article by Field and Richter, in CERN Yellow Report No. 76-18, Physics with Very High Energy e^+e^- Colliding Beams.

5. The case for unpolarized beams is presented in the reference in Footnote 4. Here and in Eq. (4.24) α_{ch} is the fine structure constant.

6. See also R. Budny, Phys. Lett. 55B, 227 (1975).

7. The transversely polarized case is considered in R. Budny, Stanford University Preprint, ITP-499 (1975).

CHAPTER V

PARAMETERS OF THE SIX-QUARK MODEL*

1. Introduction

The neutral kaon system has played an important role in elementary particle physics. The small measured value of the K_L-K_S mass difference and the near absence of a strangeness changing neutral current in kaon decays led Glashow, Iliopoulos and Maiani to propose a fourth charmed quark.[1] Later Gaillard and Lee estimated the mass of the charm quark[2] by comparing the experimental value of the K_L-K_S mass difference with the value calculated in the four-quark Weinberg-Salam model.[3] This estimate gave a value for the charm quark mass close to the value later obtained from charmonium spectroscopy.

The K°-$\bar{K}^\circ$ system is the only place where CP violation has been observed. In the Weinberg-Salam model with four quark flavors and one Higgs doublet there is no CP violation.[4] However, as was first pointed out by Kobayashi and Maskawa,[5] CP violation is possible in the six-quark model. At present there is experimental evidence for five quark flavors, the fifth b-quark, with charge -1/3, and its antiparticle are the constituents of the T family of particles. A sixth quark t, with charge 2/3, is required in the Weinberg-Salam model if the left-handed fields are to be assigned to the standard weak SU(2) doublets

$$\begin{pmatrix} u \\ d' \end{pmatrix}_L , \quad \begin{pmatrix} c \\ s' \end{pmatrix}_L , \quad \begin{pmatrix} t \\ b' \end{pmatrix}_L . \tag{5.1}$$

The right-handed fields are assigned to SU(2) singlets. The primed fields in Eq. (5.1) are not mass eigenstates but are related to them by a unitary transformation. With the standard choice of quark fields this transformation has the form[5]

$$\begin{pmatrix} d' \\ s' \\ b' \end{pmatrix} = \begin{pmatrix} c_1 & -s_1c_3 & -s_1s_3 \\ s_1c_2 & c_1c_2c_3 - s_2s_3e^{i\delta} & c_1c_2s_3 + s_2c_3e^{i\delta} \\ s_1s_2 & c_1s_2c_3 - c_2s_3e^{i\delta} & c_1s_2s_3 - c_2c_3e^{i\delta} \end{pmatrix} \begin{pmatrix} d \\ s \\ b \end{pmatrix}. \quad (5.2)$$

Here $s_i = \sin\theta_i$ and $c_i = \cos\theta_i$ where $i\varepsilon\{1,2,3\}$. By adjusting the phases of the quark fields, the phase δ can be moved from one location in the matrix to another; however, δ cannot be completely eliminated from the matrix. It follows that a non-zero value for the phase δ will result in CP violation. The Cabibbo-type angles θ_1, θ_2 and θ_3 are chosen to lie in the first quadrant. With this convention the quadrant of the phase δ has physical significance and cannot be specified by convention. Experimental information from beta decay give $s_1^2 \simeq 0.05$. This combined with measurements of hyperon decays give the limit $s_3 \lesssim 0.5$ on violations of universality.[6,7]

The phenomenological implications of the six-quark model for CP violation in the neutral kaon system and elsewhere have been studied by Ellis, Gaillard and Nanopoulos[8] and were found to be compatible with experiments. The constraints imposed by the measured value of the K_L-K_S mass difference and the CP violation parameter ε on the parameters θ_2, θ_3 and δ of the six-quark model have also been studied.[9,10] In these calculations the K^o-$\bar{K}^o$ mass matrix is derived from the lowest order box diagram in Fig. 5.1, neglecting strong interaction corrections.

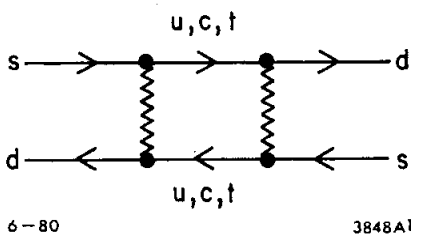

Fig. 5.1. Box diagram contributing to K^O-$\bar{K}^O$ mixing in the six-quark model.

The effective Hamiltonian for $\Delta S = 1$ weak nonleptonic decays is computed in the six-quark model by successively treating the W-boson, t, b and c quarks as heavy and removing their fields from explicitly appearing in the theory.[11,12] Strong interaction effects, as described by quantum chromodynamics (QCD), are taken into account by summing the leading logarithms in these large masses using renormalization group[13] techniques. The resulting effective Hamiltonian is a sum of Wilson coefficients[14] multiplied by renormalized local four-quark operators. Diagrams with heavy quark loops, so-called Penguin-type diagrams, induce local four-quark operators with a chiral structure $(V-A)\otimes(V+A)$ into the effective Hamiltonian.[15] Although the magnitude of the coefficients of these operators is small compared with those of the $(V-A)\otimes(V-A)$ operators, it has been suggested that these operators have matrix elements for nonleptonic decays of kaons and hyperons which are greatly enhanced and that these $(V-A)\otimes(V+A)$ matrix elements make important contributions to nonleptonic decay amplitudes.[15] If this is the case, then an understnading of the $\Delta I = \frac{1}{2}$ rule is possible because the $(V-A)\otimes(V+A)$ operators are purely isospin one half. The phase δ enters the weak current through couplings of the heavy quarks. Consequently if the $(V-A)\otimes(V+A)$ operators are important for the $\Delta I = \frac{1}{2}$ rule they can contribute significantly to CP violating $K \to \pi\pi$ decay amplitudes.[16] In fact, if most of the magnitude of the $K \to \pi\pi$ (I=0) amplitude is due to the contribution of the $(V-A)\otimes(V+A)$ operators, then through a redefinition of kaon phases to comply with the phase convention that the $K \to 2\pi$ (I=0) amplitude be real, these operators make a contribution to the CP violation parameter ε' which may be large enough for upcoming experiments to detect.[17] In

addition, through the redefinition of the kaon phases, the $(V-A)\otimes(V+A)$ operators can make a contribution to the CP violation parameter which is somewhat smaller, but still comparable to that coming from the box diagram of Fig. 5.1. Strong interaction corrections to the box diagram have recently been calculated[18] in the six-quark model using similar techniques. These corrections are significant for both the real and the imaginary parts of the kaon mass matrix.

In this chapter we discuss the restrictions the neutral kaon system imposes on the parameters of the six-quark model, including the recently calculated strong interaction corrections to the effective Hamiltonian for $\Delta S = 1$ weak nonleptonic decays and the effective $\Delta S = 2$ Hamiltonian for K^o-$\bar{K}^o$ mixing. Particular attention is given to the effects of the strong interaction corrections. We review the uncertainties associated with the theoretical predictions for ϵ and the K_L-K_S mass difference. The effects of these uncertainties on the angular constraints are also discussed. In addition, we examine how the CP violation parameter ϵ' and the b-quark lifetime depend on the six-quark model parameters. Upcoming experiments will attempt to measure these quantities and are likely to play an important role in testing the six-quark model as well as determining the values of its parameters.

2. The Neutral Kaon System in the Six-Quark Model

To leading order in the large W-boson t-quark, b-quark and c-quark masses the effective $|\Delta S| = 2$ Hamiltonian for K^o-$\bar{K}^o$ mixing has the form[19]

$$\mathcal{H}_{\text{eff}}^{|\Delta S|=2} = \frac{-G_F^2}{16\pi^2} (\bar{s}_\alpha d_\alpha)_{V-A} (\bar{s}_\beta d_\beta)_{V-A}$$

$$\times \Big[\eta_1 m_c^2 s_1^2 c_2^2 (c_1 c_2 c_3 - s_2 s_3 e^{-i\delta})^2$$

$$+ \eta_2 m_t^2 s_1^2 s_2^2 (c_1 s_2 c_3 + c_2 s_3 e^{-i\delta})^2$$

$$+ 2 \eta_3 m_c^2 \ell n \left(\frac{m_t^2}{m_c^2}\right) s_1^2 s_2 c_2 (c_1 c_2 c_3 - s_2 s_3 e^{-i\delta})(c_1 s_2 c_3 + c_2 s_3 e^{-i\delta}) \Big]$$

$$+ \text{h.c.} \quad . \tag{5.3}$$

The coefficients η_1, η_2 and η_3 have been calculated[18] in the leading logarithmic approximation and depend on the running strong interaction coupling constant α_s evaluated at the heavy mass scales and at the renormalization point mass. The matrix elements of this effective Hamiltonian are evaluated in an effective theory of strong interactions[19] with three light quark flavors u, d and s. The t, b and c quarks have been treated as heavy and their fields removed from explicitly appearing in the theory.

The kaon mass matrix element is

$$M_{12} = \langle K^\circ | H_{\text{eff}}^{|\Delta S|=2} | \bar{K}^\circ \rangle \quad . \tag{5.4}$$

The real part of this matrix element is

$$\begin{aligned} \mathrm{Re}M_{12} = \frac{-G_F^2}{16\pi^2} \langle K^o | (\bar{d}_\alpha s_\alpha)_{V-A} \, (\bar{d}_\beta s_\beta)_{V-A} | \bar{K}^o \rangle (2\pi)^3 \\ \times \Big[\eta_1 m_c^2 s_1^2 c_2^2 \Big\{ (c_1 c_2 c_3 - s_2 s_3 c_\delta)^2 - s_2^2 s_3^2 s_\delta^2 \Big\} \\ + \eta_2 m_t^2 s_1^2 s_2^2 \Big\{ (c_1 s_2 c_3 + c_2 s_3 c_\delta)^2 - c_2^2 s_3^2 s_\delta^2 \Big\} \\ + 2\eta_3 m_c^2 \ell n \left(\frac{m_t^2}{m_c^2} \right) s_1^2 c_2 s_2 \Big\{ (c_1 c_2 c_3 - s_2 s_3 c_\delta)(c_1 s_2 c_3 + c_2 s_3 c_\delta) \\ + c_2 s_2 s_3^2 s_\delta^2 \Big\} \Big] \quad . \end{aligned} \tag{5.5}$$

This is related to the difference between the K_S and K_L masses by

$$m_S - m_L \simeq 2\mathrm{Re}M_{12} \quad . \tag{5.6}$$

The experimental value of this mass difference,[20] $m_S - m_L = -3.52 \times 10^{-12}$ MeV, imposes a constraint on the six-quark model parameters through Eqs. (5.5) and (5.6). To proceed further we must evaluate the matrix element of the renormalized local four-quark operator $(\bar{d}_\alpha s_\alpha)_{V-A} \, (\bar{d}_\beta s_\beta)_{V-A}$ between K^o and $\bar{K}^o$ states. This matrix element has a dependence on the renormalization point mass μ which is cancelled by the μ dependence of the coefficients η_1, η_2 and η_3 (at least when they are computed exactly). We wish to pick μ near the typical light hadronic mass scale, where simple quark-model-type estimates of the K^o-$\bar{K}^o$ matrix element may have some validity. But we also want μ large enough so that a leading logarithmic computation of the coefficients η_1, η_2 and η_3 is sensible.

It is instructive to note that the relation

$$\langle K^o | (\bar{d}_\alpha s_\alpha)_{V-A} \; (\bar{d}_\beta s_\beta)_{V-A} | \bar{K}^o \rangle$$

$$= \sum_{\substack{\text{complete} \\ \text{set } \{n\}}} \langle K^o | (\bar{d}_\alpha s_\alpha)_{V-A} | n \rangle \langle n | (\bar{d}_\beta s_\beta)_{V-A} | \bar{K}^o \rangle \qquad (5.7)$$

is invalid because the operator $(\bar{d}_\alpha(x) s_\alpha(x))_{V-A} \; (\bar{d}_\beta(x) s_\beta(x))_{V-A}$ -- where the space-time dependence has been made explicit -- requires additional subtractions to make its matrix elements finite, while $(\bar{d}_\alpha(x) s_\alpha(x))_{V-A} \; (\bar{d}_\beta(y) s_\beta(y))_{V-A}$, with $x \neq y$, does not.[21] At order α_s in the strong interactions these additional subtractions arise because of diagrams like that in Fig. 5.2. However, there does exist a systematic approximation procedure for the matrix element $\langle K^o | (\bar{d}_\alpha s_\alpha)_{V-A} \; (\bar{d}_\beta s_\beta)_{V-A} | \bar{K}^o \rangle$ within which Eq. (5.7) has some significance. In the large N_c limit,[22] where N_c is the number of colors, the diagram in Fig. 5.2 is suppressed by a factor of $(1/N_c)^2$ compared to the free field (no strong interactions) diagram shown in Fig. 5.3. Generalizing this to an arbitrary order in α_s we find that Eq. (5.7) is valid for the leading term in the $1/N_c$ expansion for the matrix element $\langle K^o | (\bar{d}_\alpha s_\alpha)_{V-A} \; (\bar{d}_\beta s_\beta)_{V-A} | \bar{K}^o \rangle$. Each of the matrix elements $\langle n | (\bar{d}_\beta s_\beta)_{V-A} | \bar{K}^o \rangle$ appearing on the right-hand side of Eq. (5.7), can be written as the sum of two terms. One arises from connected diagrams and the other arises from possible disconnected diagrams. To leading order in $1/N_c$ the connected piece only gets a contribution from the vacuum state $|n\rangle = |0\rangle$, while the disconnected piece only gets a contribution from the two particle state $|n\rangle = |K^o \bar{K}^o\rangle$. Therefore, to leading order in $1/N_c$, the sum on the right-hand side of Eq. (5.7) truncates to just two terms

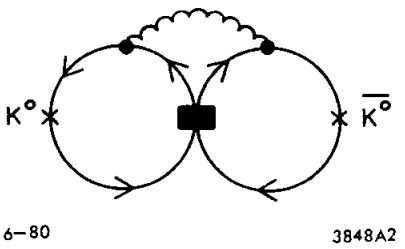

Fig. 5.2. Order α_s correction to the matrix element $\langle K^o|(\bar{d}_\alpha s_\alpha)_{V-A}(\bar{d}_\beta s_\beta)_{V-A}|\bar{K}^o\rangle$, which vanishes in the large N_c limit. The black box denotes the action of the local four-quark operator $(\bar{d}s)_{V-A}(\bar{d}s)_{V-A}$.

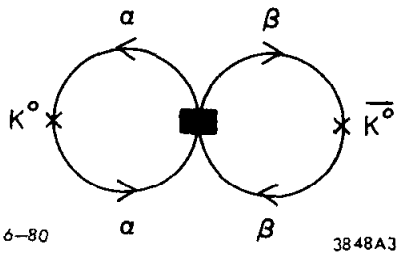

Fig. 5.3. Lowest order contribution to the matrix element $\langle K^o | (\bar{d}_\alpha s_\alpha)_{V-A} (\bar{d}_\beta s_\beta)_{V-A} | \bar{K}^o \rangle$. The black box denotes the action of the local four-quark operator $(\bar{d}s)_{V-A}(\bar{d}s)_{V-A}$. Here α and β denote the color quantum number carried by a quark line, where $\alpha,\beta \in \{1,2,3\}$.

$$\langle K^o|(\bar{d}_\alpha s_\alpha)_{V-A}\ (\bar{d}_\beta s_\beta)_{V-A}|\bar{K}^o\rangle \underset{N_c\to\infty}{\longrightarrow} \langle K^o|(\bar{d}_\alpha s_\alpha)_{V-A}|0\rangle\langle 0|(\bar{d}_\beta s_\beta)_{V-A}|\bar{K}^o\rangle$$

$$+\ \langle 0|(\bar{d}_\alpha s_\alpha)_{V-A}|\bar{K}^o\rangle\langle K^o|(d_\beta s_\beta)_{V-A}|0\rangle$$

$$= 2\langle K^o|(\bar{d}_\alpha s_\alpha)_{V-A}\ 0\rangle\langle 0|(\bar{d}_\beta s_\beta)_{V-A}|\bar{K}^o\rangle$$

$$= \frac{f_K^2\, m_K}{(2\pi)^3} \quad . \tag{5.8}$$

It is convenient to parameterize the K^o-$\bar{K}^o$ matrix element in terms of a quantity B, in the following fashion:

$$\langle K^o|(\bar{d}_\alpha s_\alpha)_{V-A}\ (\bar{d}_\beta s_\beta)_{V-A}|\bar{K}^o\rangle = B\left(\frac{4}{3}\right)\frac{f_K^2\, m_K}{(2\pi)^3} \quad . \tag{5.9}$$

We have just seen that in the large N_c limit B is independent of μ and has the value B = 3/4. If the naive valence quark model or the vacuum insertion approximation is used to evaluate the matrix element $\langle K^o|(\bar{d}_\alpha s_\alpha)_{V-A}\ (\bar{d}_\beta s_\beta)_{V-a}|\bar{K}^o\rangle$, then B = 1. Shrock and Treiman performed a bag model computation of the matrix element and found $B \simeq 0.4$.[23] All the above approximations neglect the renormalization point dependence of the matrix element. However, if one of these approximations for the matrix element is used in Eq. (5.5), the resulting expression for the K_L-K_S mass difference will not be very sensitive to the value of the renormalization point, μ.[24] This is because η_1, η_2 and η_3 are proportional, in the leading logarithmic approximation,[18] to $[\alpha_s(\mu^2)]^{-2/9}$ and thus depend only weakly on the value of the renormalization point mass.

The imaginary part of the mass matrix element is

$$\mathrm{Im}M_{12} = \frac{-G_F^2}{16\pi^2} \langle K^o | (\bar{d}_\alpha s_\alpha)_{V-A} (\bar{d}_\beta s_\beta)_{V-A} | \bar{K}^o \rangle (2\pi)^3 2s_2c_2s_3s_\delta$$
$$\times \left[\eta_1 m_c^2 s_1^2 (-c_1c_2^2c_3 + s_2c_2s_3c_\delta) + \eta_2 m_t^2 s_1^2 (c_1s_2^2c_3 + s_2c_2s_3c_\delta)\right.$$
$$\left. + \eta_3 m_c^2 \ell n (m_t^2/m_c^2)\, s_1^2 (c_1c_2^2c_3 - c_1s_2^2c_3 - 2s_2c_2s_3c_\delta)\right] . \qquad (5.10)$$

Let

$$\varepsilon_m = \frac{\mathrm{Im}M_{12}}{\mathrm{Re}M_{12}} , \qquad (5.11)$$

with $\mathrm{Re}M_{12}$ given by Eq. (5.5) and $\mathrm{Im}M_{12}$ by Eq. (5.10). Note that ε_m is independent of the matrix element $\langle K^o | (\bar{d}_\alpha s_\alpha)_{V-A} (\bar{d}_\beta s_\beta)_{V-A} | \bar{K}^o \rangle$ because it is cancelled in the ratio given by Eq. (5.11). Within the standard phase convention, where the $K \to 2\pi$ (I=0) amplitude is chosen to be real (apart from final state $\pi\pi$ interactions), the imaginary part of the width transition matrix element, $\mathrm{Im}\Gamma_{12}$, is negligible compared with $\mathrm{Im}M_{12}$.[25] The CP violation parameter ε, defined by[26]

$$\varepsilon \equiv \frac{i\mathrm{Im}\Gamma_{12} - \mathrm{Im}M_{12}}{(\Gamma_S - \Gamma_L)/2 + i(m_S - m_L)} , \qquad (5.12)$$

then simplifies to

$$\varepsilon \simeq \frac{1}{2\sqrt{2}} \left(\frac{\mathrm{Im}M_{12}}{\mathrm{Re}M_{12}}\right) e^{i\pi/4} . \qquad (5.13)$$

The phase, $\pi/4$, originates from the experimental relation[20] between the mass and width differences $m_S - m_L \simeq -(\Gamma_S - \Gamma_L)/2$. Equation (5.6) has been used to relate the mass difference between kaon eigenstates to ReM_{12}. In Eq. (5.13) ImM_{12}/ReM_{12} cannot simply be replaced by ε_m because the choice of quark fields in Eq. (5.2) does not give a real $K \to 2\pi$ (I=0) amplitude. The effective Hamiltonian for $\Delta S = 1$ weak nonleptonic decays has been calculated[11,12] in the six-quark model by successively treating the W-boson, t-quark, b-quark and c-quark as heavy and removing their fields from explicitly appearing in the theory. The resulting effective Hamiltonian density, $\mathcal{H}_{eff}^{\Delta S=1} = \sum_i C_i Q_i$, is a sum of Wilson coefficients. C_i times local four quark operators Q_i constructed out of the light u, d and s quark fields. The leading logarithms of the W-boson and heavy quark masses were summed using renormalization group techniques and contribute to the Wilson coefficients C_i. The isospin ½ operator Q_6 arises from Penguin-type diagrams and has the (V-A)⊗(V+A) chiral structure which may lead to enhanced matrix elements.[11] Let f be the fraction of the $K \to 2\pi$ (I=0) amplitude that comes from the matrix elements of Q_6. If f is large, then the $K \to 2\pi$ (I=0) amplitude has a non-negligible CP violating phase, $e^{i\xi}$, where [11]

$$\xi \simeq \frac{f\ ImC_6}{ReC_6} \quad . \tag{5.14}$$

The $K \to 2\pi$ (I=0) amplitude would be real if the strange quark field is redefined by $s \to e^{i\xi} s$, in Eq. (5.2). At the same time

$$\frac{ImM_{12}}{ReM_{12}} \to \varepsilon_m + 2\xi \quad , \tag{5.15}$$

so that[11]

$$\varepsilon \simeq \frac{1}{2\sqrt{2}} (\varepsilon_m + 2\xi)\ e^{i\pi/4} \quad . \tag{5.16}$$

The experimental value[20] $\varepsilon \simeq (2.3 \times 10^{-3})\ e^{i\pi/4}$ places a further constraint on the values of the parameters θ_2, θ_3 and δ of the six-quark model. This constraint, unlike that imposed by the K_L-K_S mass difference, does not depend on the value of the matrix element $\langle K^o | (\bar{d}_\alpha s_\alpha)_{V-A}\ (\bar{d}_\beta s_\beta)_{V-A} | \bar{K}^o \rangle$.

The CP violation parameter ε' is defined by[26]

$$\varepsilon' \equiv \frac{i}{\sqrt{2}} e^{i(\delta_2 - \delta_0)} \frac{\mathrm{Im}A_2}{A_0} \quad , \tag{5.17}$$

where A_0 and A_2 are the isospin zero and isospin two $K \to 2\pi$ amplitudes respectively; δ_2 and δ_0 are the $I = 2$ and $I = 0$ $\pi\pi$ phase shifts. The matrix elements of the $I = \frac{1}{2}$ operator Q_6 cannot contribute to the $I = 2$ amplitude A_2. However, by redefining the phase of the strange quark field to make the amplitude A_0 real, A_2 picks up an imaginary part. The experimental values[25] for the phase shifts δ_0 and δ_2 along with $\mathrm{Re}A_2/A_0 \approx 1/20$ yields[11]

$$\varepsilon' \simeq \frac{1}{20\sqrt{2}}\ e^{i\pi/4}\ (-\xi) \quad . \tag{5.18}$$

Experimentally[25] $|\varepsilon'/\varepsilon| \lesssim 1/50$; however, upcoming experiments[17] should be capable of detecting a non-zero value for ε'/ε at the fraction of a percent level.

In principle the experimental value of the K_L-K_S mass difference can be used in Eqs. (5.6) and (5.7) to determine the angle θ_2 as a function of δ and θ_3. The measured value of ε can then be used (cf., Eqs. (5.16), (5.14), (5.11), (5.10) and (5.5)) to determine δ as a function of θ_3. The net result is that the angles θ_2 and δ can be expressed as functions (perhaps multivalued) of the angle θ_3. In practice, there are a number of uncertainties introduced by the dependence of the theoretical expressions for m_S-m_L and ε on additional parameters besides the angles θ_1, θ_2, θ_3 and δ. We need the neavy W-boson, t-quark, b-quark and c-quark masses. For the c-quark and b-quark masses[27] we use the values 1.5 GeV and 4.5 GeV derived from charmonium and upsilon spectroscopy. Since the value of the t-quark mass is presently unknown, it is treated as an additional parameter. The mass of the W-boson is taken to be 78 GeV. The QCD corrections depend on the strong interaction running coupling constant evaluated at the large W-boson, t-quark, b-quark and c-quark masses. In the leading logarithmic approxiamtion

$$\alpha_s(Q^2) = \frac{12\pi}{33 - 2N_f} \frac{1}{\ell n(Q^2/\Lambda^2)} \quad . \tag{5.19}$$

We use $\Lambda^2 = 0.1\ \mathrm{GeV}^2$ and $\Lambda^2 = 0.01\ \mathrm{GeV}^2$, which are consistent with results from deep inelastic scattering.[28] When the leading logarithmic approximation is valid, the results should not be very sensitive to the precise value of Λ^2. In Eq. (5.19), N_f is the number of quark flavors being equal to 6, 5 and 4 at the mass scales of the t, b and c-quarks respectively. The constraints imposed by the K_L-K_S mass difference depend on the value of the matrix element $\langle K^o | (\bar{d}_\alpha s_\alpha)_{V-A} (\bar{d}_\beta s_\beta)_{V-A} | \bar{K}^o \rangle$ or equivalently, if Eq. (5.9) is used, on the parameter B.[29]

In Fig. 5.4, s_2, s_δ and ε'/ε are plotted as functions of s_3 for $s_\delta > 0$. Solutions for $s_\delta < 0$ also exist[30] and will be discussed later. For Fig. 5.4 we use $m_t = 30$ GeV, $B = 1$ and $f = 0.75$. The values of the quantities η_1, η_2, η_3 and C_6 are taken from Refs. 18 and 11 of Chapter V,[31] with the renormalization point chosen so that $\alpha_s(\mu^2) = 1$. Some features of these graphs can be understood from the expressions for $\mathrm{Re}M_{12}$ and $\mathrm{Im}M_{12}$ given in Eqs. (5.5) and (5.10). While Eqs. (5.5) and (5.10) are quite complicated, a considerable simplification occurs for s_3 near zero. Treating s_3 and s_1 as small quantities we have

$$\mathrm{Re}M_{12} \propto \left\{\eta_1 m_c^2 c_2^4 + \eta_2 m_t^2 s_2^4 + 2\eta_3 m_c^2 \ell n\ (m_t^2/m_c^2)\ c_2^2 s_2^2\right\} \quad , \qquad (5.20a)$$

and

$$\mathrm{Im}M_{12} \propto 2 s_2 c_2 s_3 s_\delta \left\{-\eta_1 m_c^2 c_2^2 + \eta_2 m_t^2 s_2^2 + \eta_3 m_c^2 \ell n \left(\frac{m_t^2}{m_c^2}\right)(c_2^2 - s_2^2)\right\} . \qquad (5.20b)$$

The constant of proportionality in Eq. (5.20) is independent of θ_2, θ_3 and δ. For small s_3 the constraints imposed by the K_L-K_S mass difference and ε depend on δ only through its sine. Thus the sign of c_δ is irrelevant at small s_3. Note also that the K_L-K_S mass difference constraint gives a simple quadratic equation for s_2^2. This quadratic equation has at most one positive solution for s_2^2. Therefore, s_δ is a single valued hyperbolic function of s_3 in the region of small s_3. The measured value of the phase of ε implies that s_δ is positive[16] for small s_3. Away from $s_3 \approx 0$ the solutions for s_δ and s_2 become double valued and depend on the sign of c_δ. For $c_\delta < 0$, there is a cancellation between the terms which

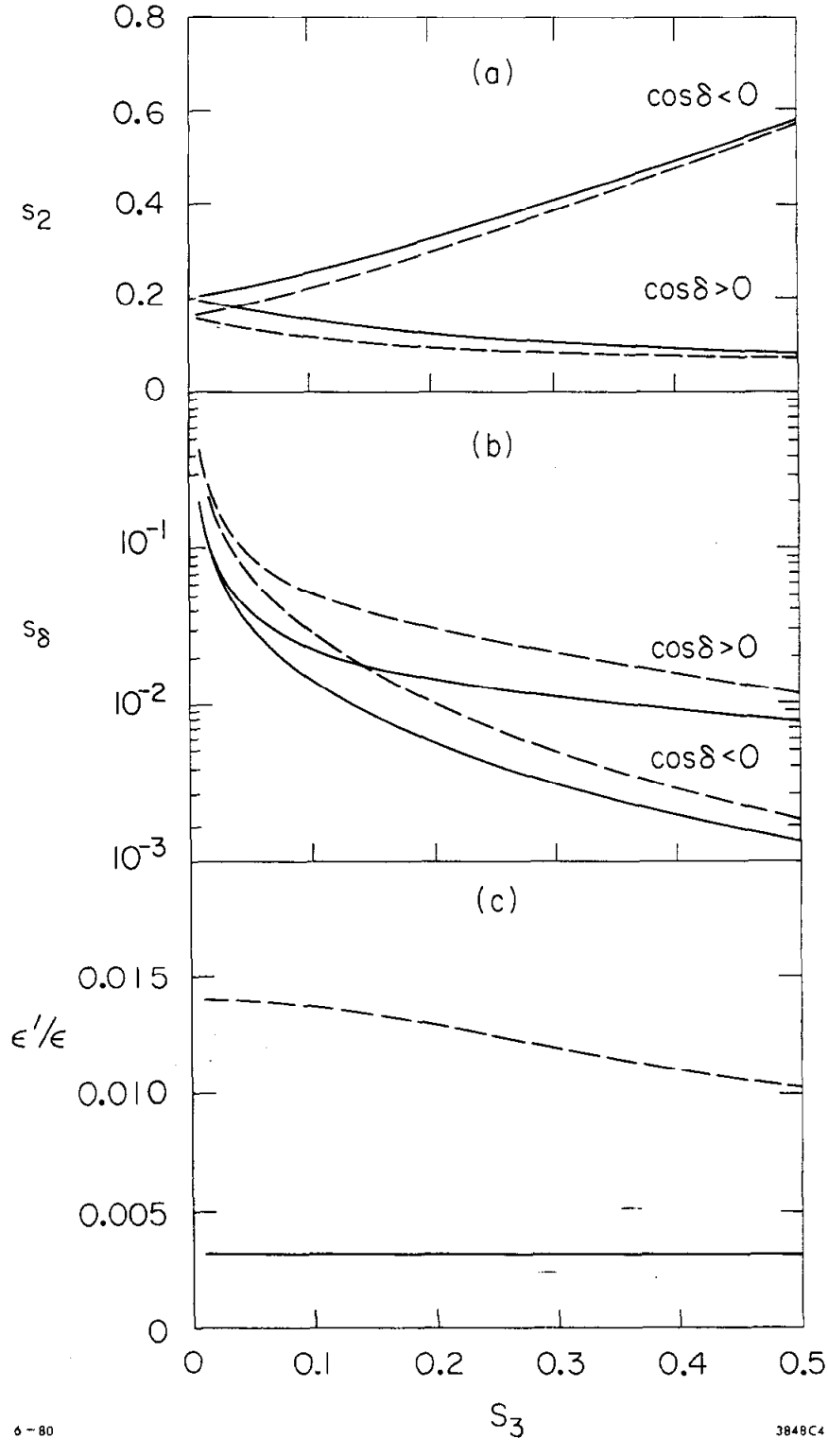

Fig. 5.4. Graphs of (a) s_2, (b) s_δ and (c) ε'/ε as functions of s_3 when δ lies in the upper half plane. The parameters m_t = 30 GeV, B = 1 and f = 0.75 are used. Dashed lines are for Λ^2 = 0.1 GeV^2 and solid lines are for Λ^2 = 0.01 GeV^2. ε'/ε has almost the same value (to within 10%) for $c_\delta < 0$ and $c_\delta > 0$.

form the coefficient of m_t^2 in Eq. (5.5). The mass difference constraint then implies that for fixed s_3, s_2 should be larger for the case $c_\delta < 0$ than for $c_\delta > 0$. From Eq. (5.10) we see that ImM_{12} is proportional to $s_2 s_2 s_\delta$. The ϵ constraint gives rise to the opposite behavior for s_δ, i.e., larger values of s_δ occurring for $c_\delta > 0$.

The general dependence of s_2 and s_δ on Λ^2 can also be inferred from the expressions for ReM_{12} and ImM_{12} (cf., Eqs. (5.5) and (5.10)). Recall from Ref. 18 of Chapter V that η_2 and η_3 do not depend significantly on Λ^2; however, η_1 becomes smaller as Λ^2 decreases from 0.1 GeV^2 to 0.01 GeV^2. Thus the smaller value of Λ^2 widens the gap between the four-quark model prediction for $m_S - m_L$ and its experimental value. This results in larger values of s_2. Therefore, at a given value of s_3, s_2 increases while s_δ decreases as Λ^2 is changed from 0.1 GeV^2 to 0.01 GeV^2.

The quantity ϵ'/ϵ plotted in Fig. 5.4(c) does not depend strongly on s_3. This is because both ϵ' and ϵ are proportional to $s_2 s_3 s_\delta$ so this factor cancels out in their ratio. The principal Λ^2 dependence of ϵ'/ϵ arises from the Λ^2 dependence of ReC_6. The Wilson coefficient ReC_6 increases significantly[11] (i.e., by more than a factor of two) when Λ^2 decreases from 0.1 GeV^2 to 0.01 GeV^2. This results in a corresponding decrease in ϵ'/ϵ. Note that ϵ'/ϵ is virtually independent of the sign of c_δ. This is because both ϵ and ϵ' are proportional to the factor $s_2 s_3 s_\delta$.

The plots in Fig. 5.4 were calculated using $B = 1$, which corresponds to the valence quark model or the vacuum insertion approximation for the matrix element $\langle K^o | (\bar{d}_\alpha s_\alpha)_{V-A} (\bar{d}_\beta s_\beta)_{V-A} | \bar{K}^o \rangle$. In Fig. 5.5 we show s_2, s_δ and ϵ'/ϵ as functions of s_3 for the same parameters as used in Fig. 5.4.

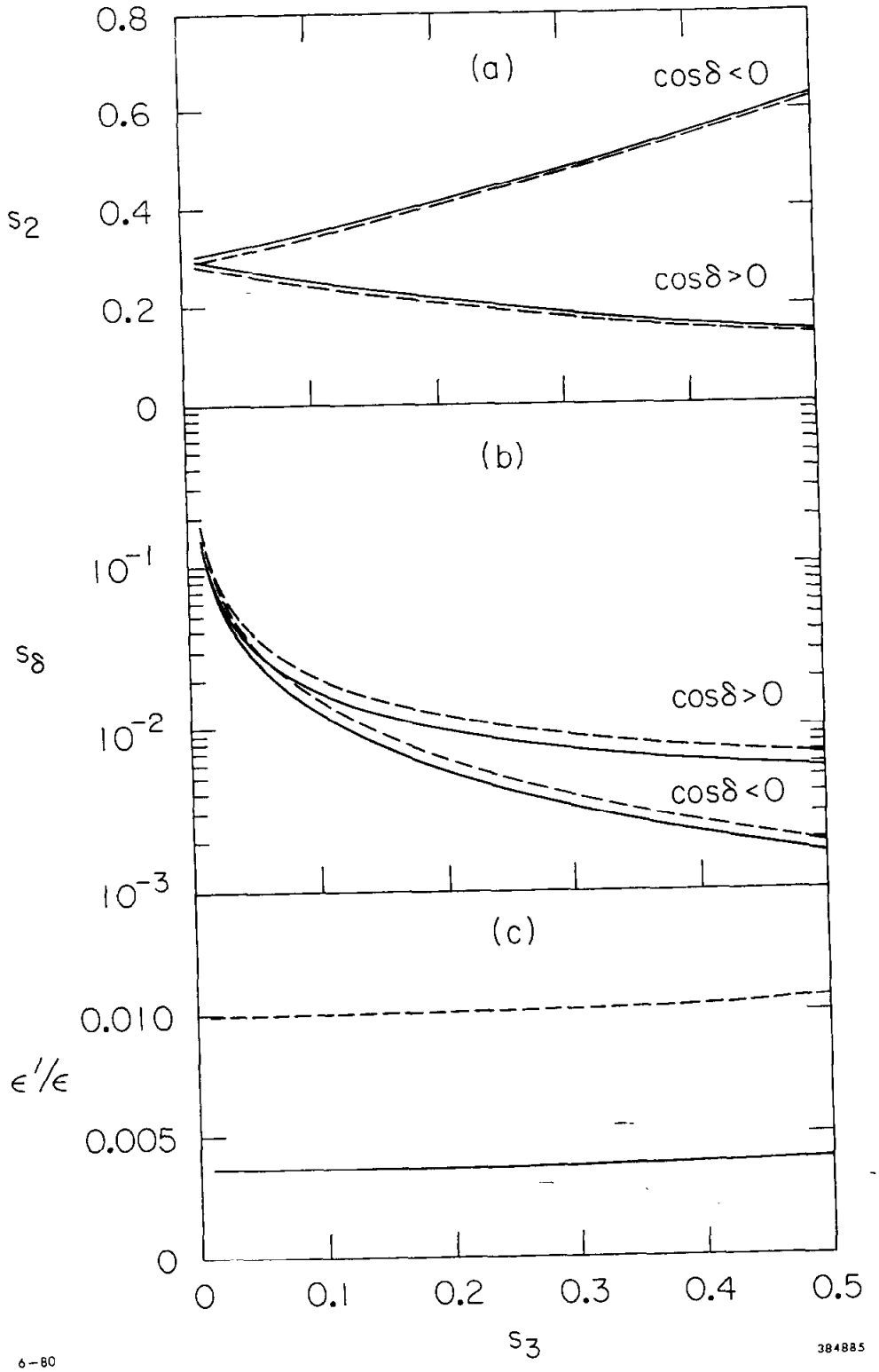

Fig. 5.5. Graphs of (a) s_2, (b) s_δ and (c) ε'/ε as function of s_3 when δ lies in the upper half plane. The parameters m_t = 30 GeV, B = 0.4 and f = 0.75 are used. Dashed lines are for Λ^2 = 0.1 GeV^2 and solid lines are for Λ^2 = 0.01 GeV^2. ε'/ε has almost the same value (to within 10%) for $c_\delta < 0$ and $c_\delta > 0$.

except that here B = 0.4. This B value corresponds to a bag model evaluation[23] of the matrix element $\langle K^o|(\bar{d}_\alpha s_\alpha)_{V-A}\ (\bar{d}_\beta s_\beta)_{V-A}|\bar{K}^o\rangle$. The smaller value of B increases the discrepancy between the four-quark model prediction and the measured value of $m_S - m_L$. This leads to generally larger values of s_2 and a diminished sensitivity to Λ^2.

Results[32] from PETRA indicate that the t-quark mass must be greater than 15 GeV. For t-quark masses less than 30 GeV, larger values of s_2 than those shown in Figs. 5.4 and 5.6 will be needed to fulfill the mass difference constraint. In turn, the measured value of ε then gives smaller values for s_δ. If the mass of the t-quark is much larger than 30 GeV, it will be necessary to include higher order terms in m_t^2/m_W^2 which have been neglected in our analysis.

In Fig. 5.6 we plot s_2, $|s_\delta|$ and ε'/ε as a function of s_3 for δ in the lower half plane. These solutions exist if the expression within the square brackets of Eq. (5.10) is ngeative. This occurs only for $c_\delta < 0$, when s_3 is so large that the term proportional to m_t^2 is negative and dominates the square brackets in Eq. (5.10). Note that s_2 and s_δ are double valued functions of s_3. At fixed s_3, the larger value of s_2 in Fig. 5.6(a) corresponds to the smaller value of $|s_\delta|$ in Fig. 5.6(b). This is in consonance with being proportional to $s_2 s_3 s_\delta$.

Allowed regions of s_2 and s_δ are confined to a limited range in s_3 when $s_\delta < 0$. The size of this region depends on Λ^2. Decreasing Λ^2 will increase the magnitude of the terms not proportional to m_t^2 in the expression for $\mathrm{Im}M_{12}$ (cf., Eq. (5.10)) and will also decrease the magnitude of the corresponding terms in the expression for $\mathrm{Re}M_{12}$ (cf., Eq. (5.5)). This causes the allowed region to begin at larger values of s_3.

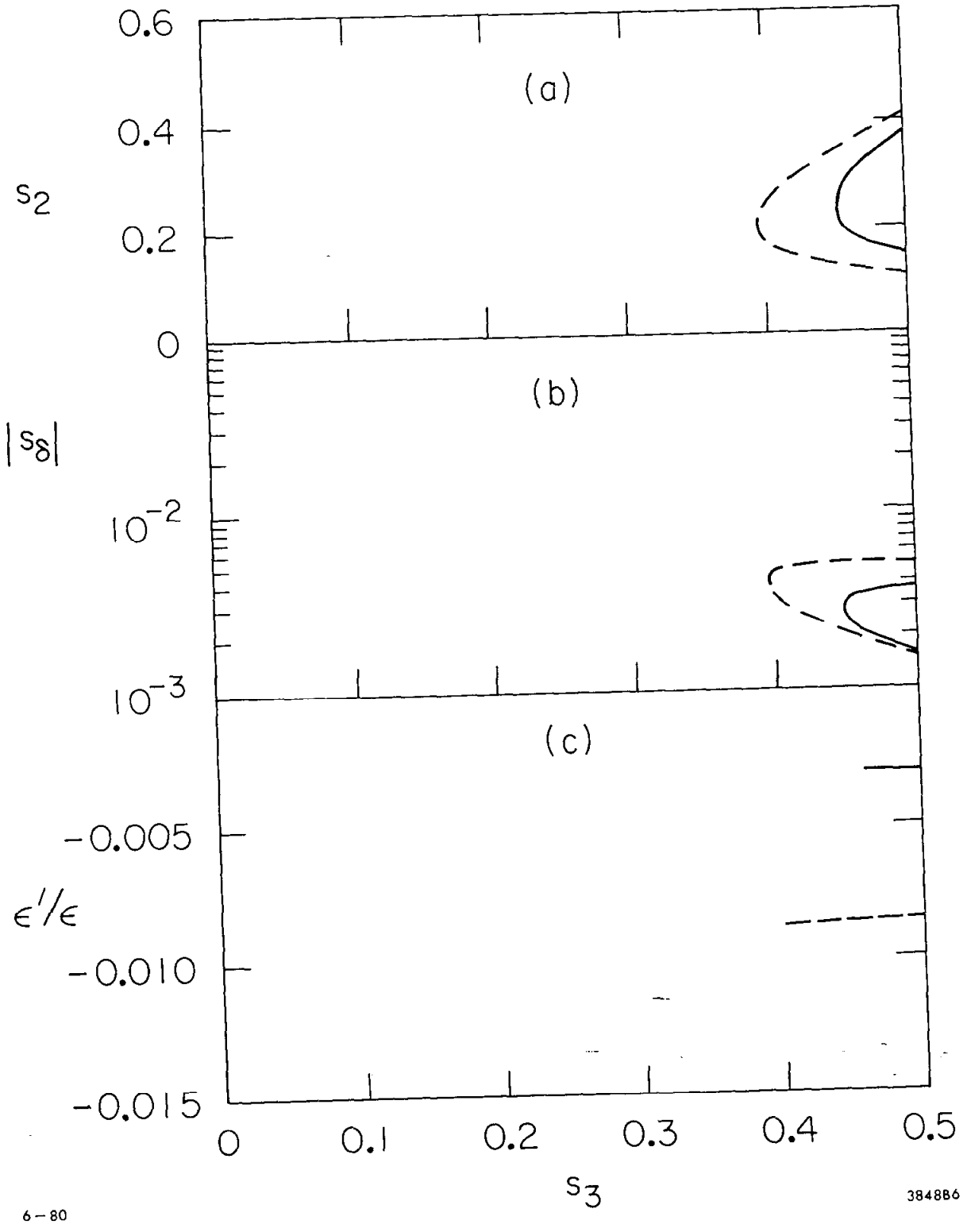

Fig. 5.6. Graphs of (a) s_2, (b) $|s_\delta|$ and (c) ε'/ε as functions of s_3 when δ lies in the lower half plane. The parameters m_t = 30 GeV, B = 1.0 and f = 0.75 are used. Dashed lines are for Λ^2 = 0.1 GeV^2 and solid lines are for Λ^2 = 0.01 GeV^2. Note these regions exist only for $c_\delta < 0$.

The size of the allowed range of angles also depends on B and m_t. In order that the mass difference constraint be satisfied, a smaller value for B will require that the coefficient of m_t^2 in the square brackets of Eq. (5.5) be larger. Hence, regions with δ in the lower half plane will be moved to larger values of s_3 as B is decreased. For $B = 0.4$, there are no regions with $s_\delta < 0$ that are compatible with the universality bound, $s_3 \lesssim 0.5$. Similarly, smaller values of m_t result in smaller allowed regions than those shown in Fig. 5.6. This is because the coefficient of m_t^2 in the square brackets of Eqs. (5.5) and (5.10) must increase as m_t decreases, pushing these regions to larger values of s_3.

When δ lies in the upper half plane, ε'/ε is positive. As shown in Fig. 5.6(c), ε'/ε is negative when δ lies in the lower half plane. Information on the quadrant of δ will thus be obtained if upcoming experiments measure ε'/ε. For δ in the lower half plane, only a small region of allowed values of s_2 and s_δ exists. The measurement of a negative value for ε'/ε would be extremely fortuitous, providing very stringent constraints on the parameters of the six-quark model.

In Figs. 5.4, 5.5 and 5.6 we use the value $f = 0.75$ for the fraction of the $K \to 2\pi$ (I=0) amplitude arising from the matrix elements of Q_6. The constraints imposed on the parameters of the six-quark model by the experimental values of the K_L-K_S mass difference and the CP violation parameter ε are not very sensitive to the value of f chosen. However, the predicted value of ε'/ε depends crucially on f, being proportional to it. The parameter f is strongly dependent on the renormalization point. This renormalization point dependence arises because the operator Q_6 is induced only through QCD corrections and because its Wilson

coefficient receives contributions mainly from integrations over virtual momenta in the limited range $\mu^2 \lesssim p^2 \lesssim m_c^2$. We use a large value of f since this allows an understanding of the $\Delta I = \frac{1}{2}$ rule. We do not know exactly what choice of renormalization point, if any, corresponds to this value of f. It is, therefore, necessary to examine the sensitivity of our results to the value of $\alpha_s(\mu^2)$ used. As mentioned above, η_1, η_2 and η_3 depend weakly on the value of $\alpha_s(\mu^2)$. However, the quantities ImC_6 and ReC_6 both depend on $\alpha_s(\mu^2)$ and, for ReC_6 the dependence is very strong. Since our constraints on the angles θ_2, θ_3 and δ do not depend strongly on the value of ξ, the renormalization point dependence of ReC_6 does not introduce a great uncertainty in these angles. However ε' is proportional to ξ and so our predictions for ε'/ε must be interpreted very qualitatively. Several authors[12,33,34] adopt another approach to calculating ε'/ε which does not use a leading logarithmic calculation of ReC_6. Rather, they rely on an estimate of the matrix element $\langle 2\pi(I=0)|Q_6|K^o\rangle$ which is combined with the experimental value of the isospin zero amplitude A_0 and the calculated value of ImC_6 to make a prediction for ξ.[35] This approach also involves an implicit choice of μ, namely that for which the estimate of the matrix element $\langle 2\pi(I=0)|Q_6|K^o\rangle$ is valid. Predictions for ε'/ε are, however, now not as sensitive to the value of $\alpha_s(\mu^2)$ used to compute C_6, since ImC_6 is much less sensitive to variations of $\alpha_s(\mu^2)$ than ReC_6. This approach generally leads to somewhat smaller values of ε'/ε than we have found.

Finally, it is instructive to compare the QCD corrected values of s_2 and s_δ (cf., Figs. 5.4 and 5.6) with the uncorrected values. In Figs. 5.7 and 5.8, s_2 and s_δ are plotted as functions of s_3 for $m_t = 30$ GeV,

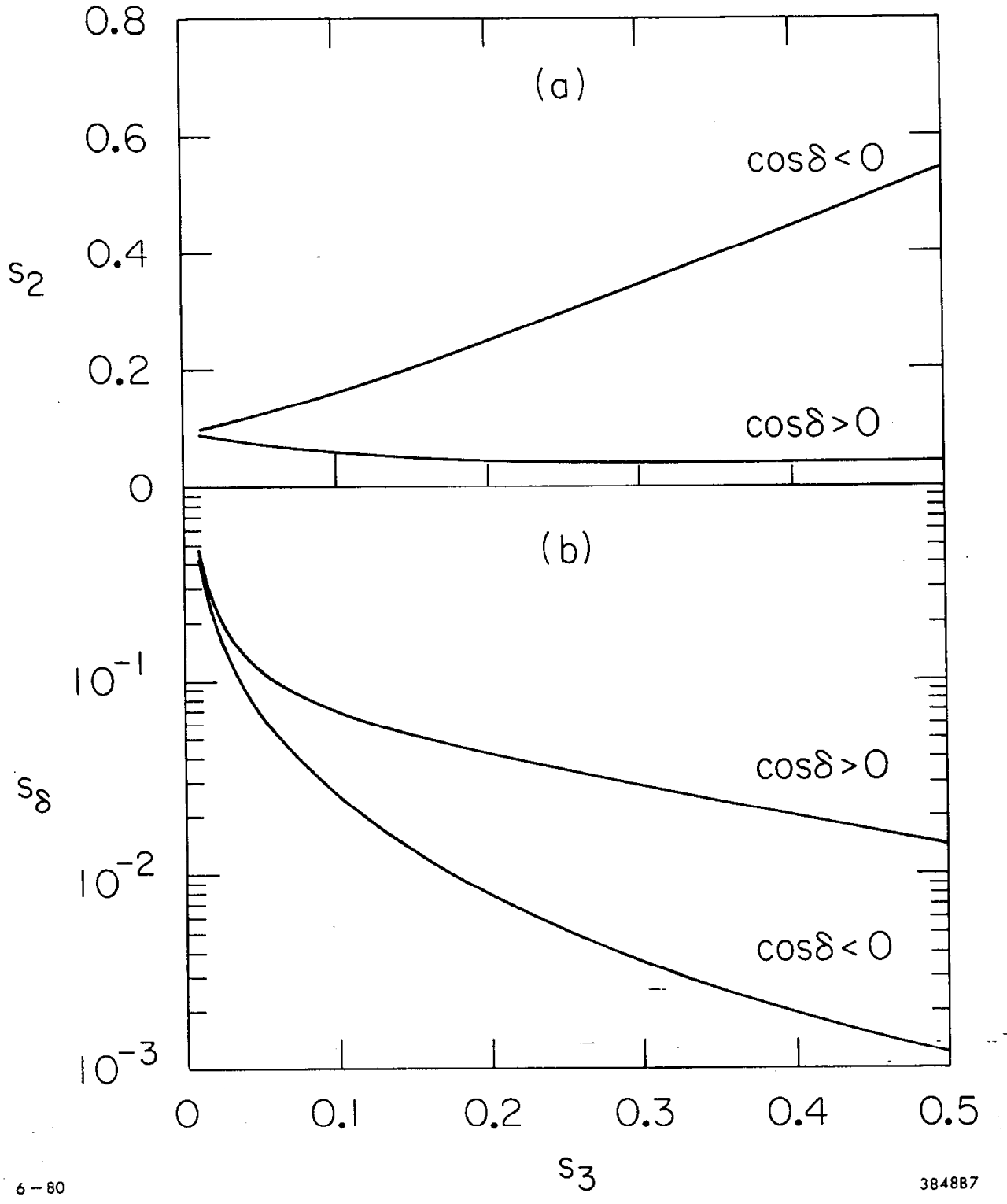

Fig. 5.7. Graphs of (a) s_2 and (b) s_δ as functions of s_3, for δ in the upper plane, in the free quark model (i.e., no strong interactions). The parameters m_t = 30 GeV and B = 1.0 are used. In the absence of strong interactions f = 0 and ε'/ε = 0.

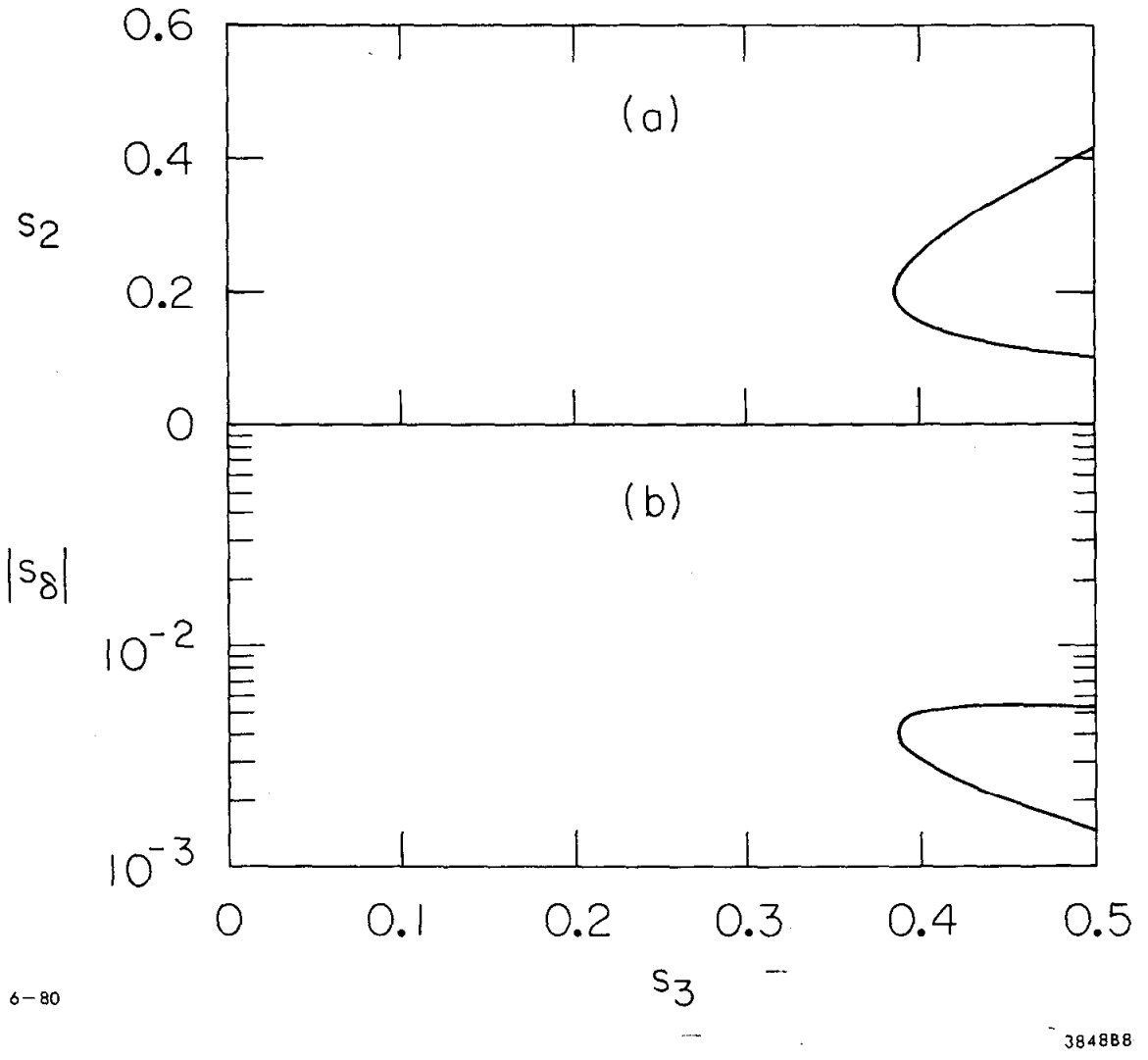

Fig. 5.8. Graphs of (a) s_2 and (b) $|s_\delta|$ as functions of s_3, for δ in the lower half plane, in the free quark model (i.e., no strong interactions). The parameters m_t = 30 GeV and B = 1.0 and f = 0 are used.

$B = 1$, and $f = 0$ for the case of no QCD corrections.[36] In the absence of QCD corrections, the quantities η_1, η_2 and η_3 are all equal to one. Since the QCD corrected values of η_1, η_2 and η_3 are smaller than one, the mass difference constraint gives rise to smaller values of s_2 in Fig. 5.7(a) than in Fig. 5.4(a). The ϵ constraint then gives rise to generally larger values of s_δ in Fig. 5.7(b) than in Fig. 5.4(b). The allowed region of angles, for which δ lies in the lower half plane, are shown in Fig. 5.8. This region is about the same size as the negative s_δ region in Fig. 5.6 corresponding to $\Lambda^2 = 0.1$ GeV^2 but considerably larger than the $\Lambda^2 = 0.01$ GeV^2 region of negative s_δ.

3. B Meson Decays

The observation of B meson decays should soon be possible at CESR. The rates for these weak decays depend on the parameters of the six-quark model. If we view inclusive B meson decays as arising from b-quark decay, in which the light quark constituent of the meson acts only as a spectator, then the dependence of the B meson lifetime on the six-quark model parameters is easily calculated.[37] The total width for b-quark decay can be written as the sum of two terms

$$\Gamma_b = \Gamma(b \to c) + \Gamma(b \to u) \qquad (5.21)$$

The first term arises from the diagrams in Fig. 5.9 and is given by

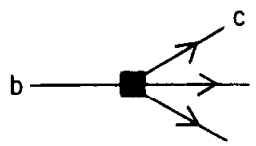

Fig. 5.9. Diagram illustrating decays which contribute to the partial decay width $\Gamma(b \to c)$. The unlabeled final state fermions are: $e\bar{\nu}_e$, $\mu\bar{\nu}_\mu$, $\tau\bar{\nu}_\tau$, $d\bar{u}$, $s\bar{u}$, $d\bar{c}$, and $s\bar{c}$. The black box represents a local four-fermion vertex.

$$\Gamma(b \to c) = \frac{G_F^2 m_b^5}{192\pi^3}\left[(c_1c_2s_3 + s_2c_3c_\delta)^2 + s_2^2c_3^2s_\delta^2\right] \tag{5.22}$$

$$\times \left(2f\left(\frac{m_c}{m_b}\right) + \phi(m_c,m_\tau;m_b) + 3\eta f\left(\frac{m_c}{m_b}\right)\left\{c_1^2 + s_1^2c_3^2\right\}\right.$$

$$\left. + 3\eta\phi(m_c,m_c;m_b)\left\{s_1^2c_2^2 + (c_1c_2c_3 - s_2s_3c_\delta)^2 + s_2^2s_3^2s_\delta^2\right\}\right) \quad .$$

The second term in Eq. (5.21) arises from the diagrams in Fig. 5.10 and is given by

$$\Gamma(b \to u) = \frac{G_F^2 m_b^5}{192\pi^3}\left[s_1^2s_3^2\right]\left(2 + f\left(\frac{m_\tau}{m_b}\right) + 3\eta\left\{c_1^2 + s_1^2c_3^2\right\}\right. \tag{5.23}$$

$$\left. + 3\eta f\left(\frac{m_c}{m_b}\right)\left\{s_1^2c_2^2 + (c_1c_2c_3 - s_2s_3c_\delta)^2 + s_2^2s_3^2s_\delta^2\right\}\right) \quad .$$

The kinematical functions f and ϕ appearing in Eqs. (5.22) and (5.23) take into account the phase space suppression due to the non-negligible masses of the c-quark and the τ-lepton.[38] The function f(x) is given by

$$f(x) = 1 - 8x^2 + 8x^6 - x^8 - 24x^4 \ln x \quad . \tag{5.24}$$

The other function $\phi(m_1,m_2;m_b)$ is quite complicated, but when $m_1 = m_2$, it simplifies to

$$\phi(m,m;m_b) = g\left(\frac{2m}{m_b}\right) \tag{5.25}$$

where

$$g(x) = \left(1 - \frac{7}{2}x^2 - \frac{1}{8}x^4 - \frac{3}{16}x^6\right)(1-x^2)^{\frac{1}{2}}$$

$$+ 3x^4\left(1 - \frac{x^4}{16}\right)\ln\left(\frac{1 + \sqrt{1-x^2}}{x}\right) \quad . \tag{5.26}$$

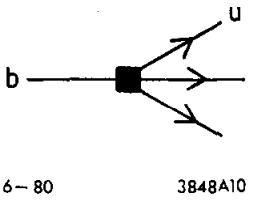

Fig. 5.10. Diagram illustrating decays which contribute to the partial decay width $\Gamma(b \to u)$. The unlabeled final state fermions are: $e\bar{\nu}_e$, $\mu\bar{\nu}_\mu$, $\tau\bar{\nu}_\tau$, $d\bar{u}$, $s\bar{u}$, $d\bar{c}$, and $s\bar{c}$. The black box represents a local four-fermion vertex.

The factor η which appear in Eqs. (5.22) and (5.23) arises because of the strong interaction corrections to the effective Hamiltonian for non-leptonic b-quark decays. This Hamiltonian is derived by a two-step process in which the W-boson and the t-quark are removed from explicitly appearing. The mechanism which gives an enhancement of the matrix elements of the $(V-A)\otimes(V+A)$ four-quark operators over the matrix elements of the $(V-A)\otimes(V-A)$ operators in the nonleptonic kaon and hyperon decays is expected to be absent in B-meson decays.[39] Neglecting Penguin-type diagrams and using the leading logarithmic approximation we have[40]

$$\eta = \frac{1}{3}\left(2f_+^2 + \frac{1}{f_+^4}\right) \tag{5.27}$$

where

$$f_+ = \left[\frac{\alpha_s(M_W^2)}{\alpha_s(m_t^2)}\right]^{6/21}\left[\frac{\alpha_s(m_t^2)}{\alpha_s(m_b^2)}\right]^{6/23} . \tag{5.28}$$

In the preceding section the experimental values for the K_L-K_S mass difference and the CP violation parameter ε were used to write s_δ and s_2 as functions of s_3. Using these results $\Gamma(b\to u)$ and $\Gamma(b\to c)$ can also be expressed as functions of s_3.[41] In Figs. 5.11 and 5.12 the ratio $\Gamma(b\to u)/\Gamma(b\to c)$ and the b-quark lifetime $\tau_b = 1/\Gamma_b$ are plotted as a function of s_3.

The plots in Fig. 5.11 corresponds to allowed values of δ in the upper half plane. When δ lies in the lower half plane it is a double-valued function of s_3. Figure 5.12 exhibits the same plots for this case. In Figs. 5.11 and 5.12 we use solutions for s_2 and s_δ shown in Figs. 5.4 and 5.6. Recall that the previous calculation used as parameters

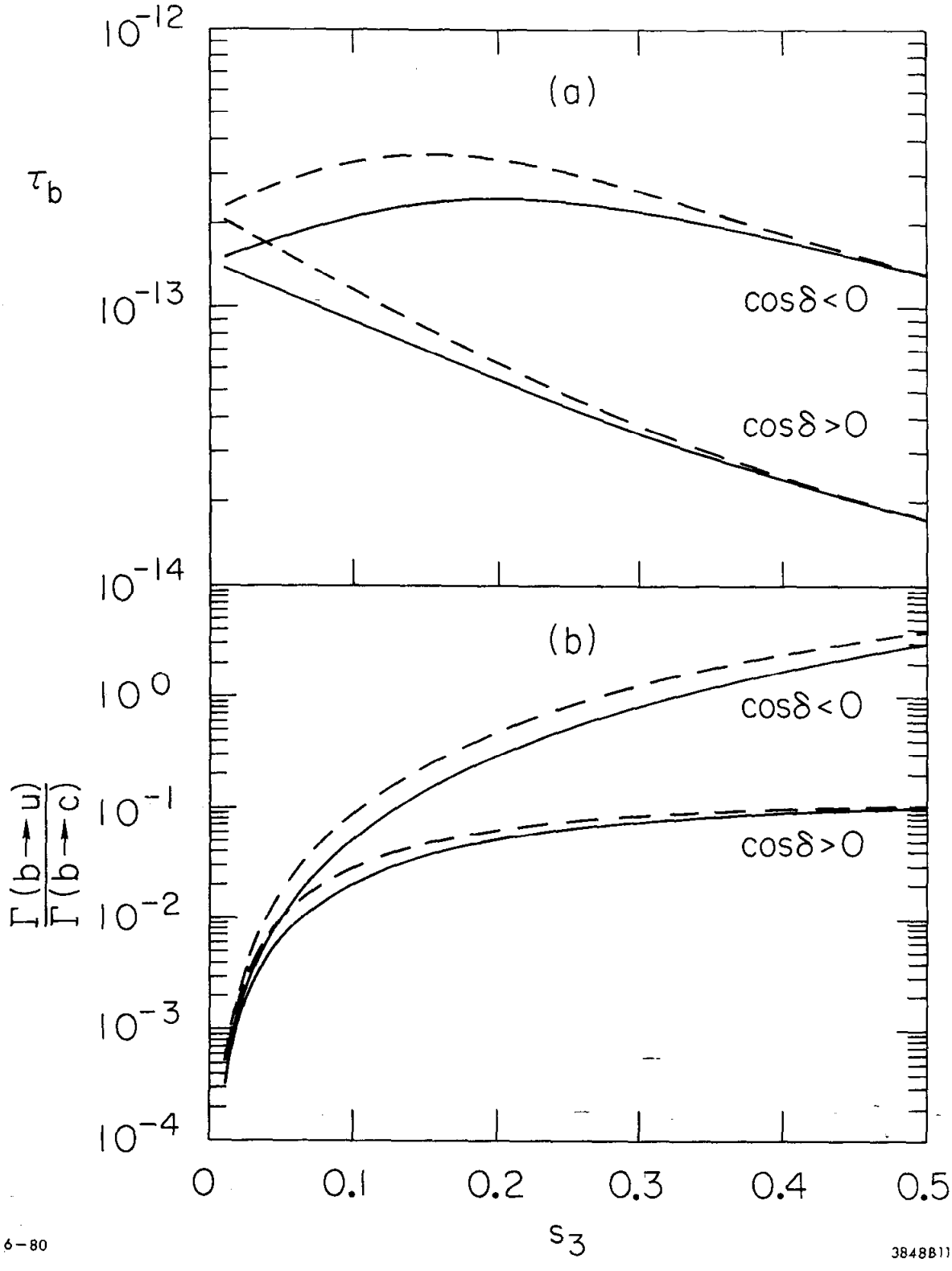

Fig. 5.11. Plot of (a) the b-quark lifetime τ_b (in seconds) and (b) the ratio of u-quark production to c-quark production $\Gamma(b \to u)/\Gamma(b \to c)$ for the allowed values of the six-quark model parameters shown in Figs. 5.4(a) and 5.4(b). Dashed lines are for $\Lambda^2 = .1$ GeV^2 and solid lines are for $\Lambda^2 = .01$ GeV^2.

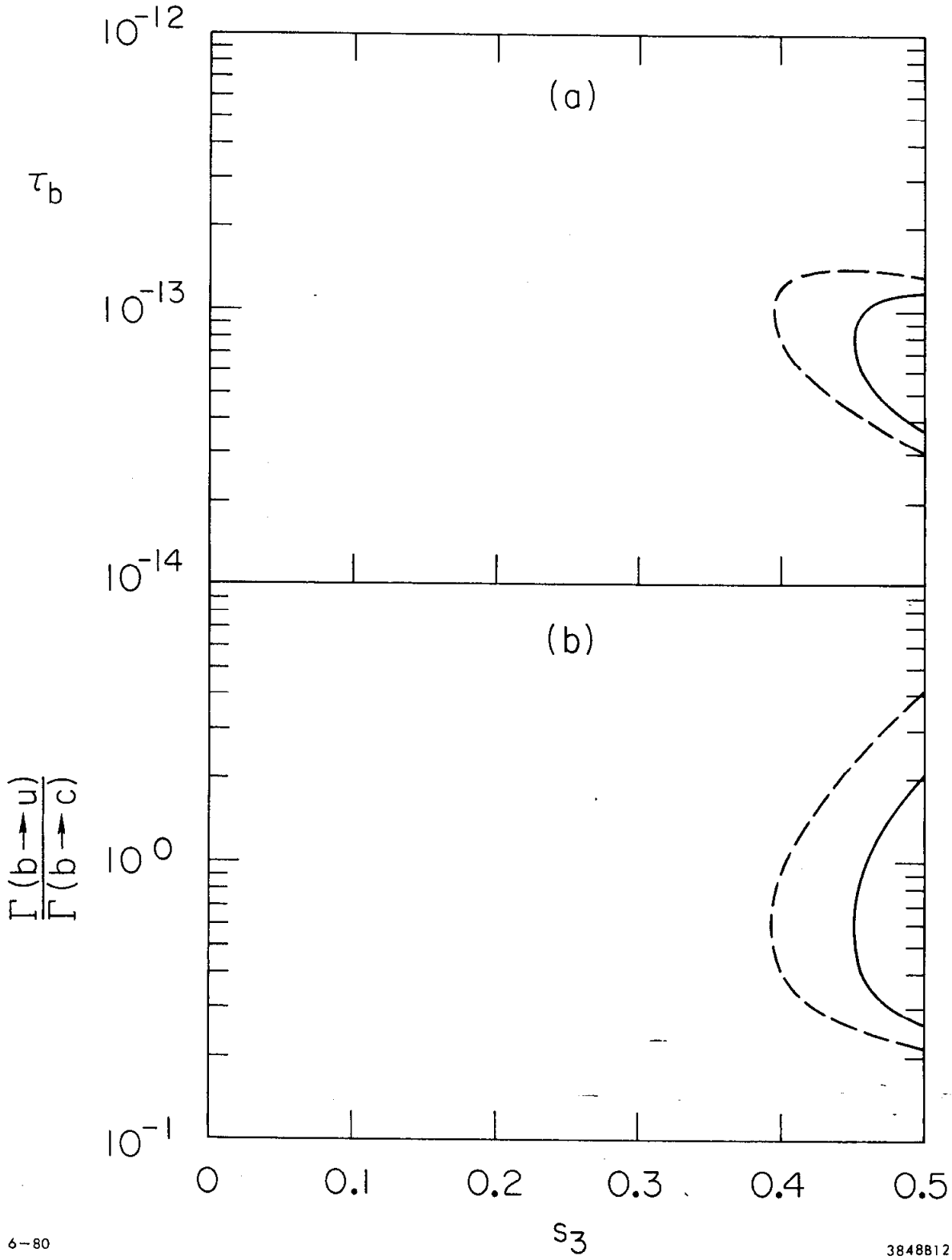

Fig. 5.12. Plot of (a) the b-quark lifetime τ_b (in seconds) and (b) the ratio of u-quark production to c-quark production $\Gamma(b \to u)/\Gamma(b \to c)$ for the allowed values of the six-quark model parameters shown in Figs. 5.6(a) and 5.6(b). Dashed lines are for $\Lambda^2 = .1$ GeV^2 and solid lines are for $\Lambda^2 = .01$ GeV^2.

m_t = 30 GeV, B = 1 and f = 0.75. As in Sect. 2, we choose m_c and m_b to be equal to 1.5 GeV and 4.5 GeV respectively. The partial decay widths $\Gamma(b \to u)$ and $\Gamma(b \to c)$ also depend on the τ-lepton mass which has the experimental value m_τ = 1.8 GeV. However, we use $m_\tau = m_c$ since the kinematical function $\phi(m_\tau, m_c; m_b)$ simplifies for this case. This approximation has no significant effect on any of our predictions. The general features of the graphs in Figs. 5.11 and 5.12 are largely determined by the expressions in the square brackets of Eqs. (5.22) and (5.23). Taking the limit $s_3 \to 0$ in these equations reveals that for very small s_3 $\Gamma(b \to u)$ is negligible and $\Gamma(b \to c)$ is roughly proportional to s_2^2. The constant of proportionality is independent of δ so that in the small s_3 limit the b-quark lifetime is independent of the sign of c_δ. Since s_2 is larger for Λ^2 = 0.01 GeV^2 than for Λ^2 = 0.1 GeV^2 (see Fig. 5.4(a)) the b-quark lifetime is smaller for Λ^2 = 0.01 than for Λ^2 = 0.1, in the region of small s_3. Away from small s_3 the b-quark lifetime, τ_b, and the ratio $\Gamma(b \to u)/\Gamma(b \to c)$ both depend on the quadrant of δ. For $c_\delta > 0$ there is no cancellation between the two terms in the square brackets of Eq. (5.22) so $\Gamma(b \to c)$ grows with s_3. Note also that $\Gamma(b \to u)$ grows as s_3 increases so that the b-quark lifetime decreases as s_3 increases. However, Fig. 5.11(a) shows that for $c_\delta < 0$ and δ in the upper half plane the b-quark lifetime is not as sensitive to the value of s_3. This is because the two terms in the square brackets of Eq. (5.22) cancel against each other, yielding a smaller $\Gamma(b \to c)$ than when $c_\delta > 0$. Note that $\Gamma(b \to u)$ still grows with s_3 and when s_3 is near the universality bound 0.5 the ratio $\Gamma(b \to u)/\Gamma(b \to c)$ becomes larger than one. So far we have been considering δ in the upper half plane. The only allowed regions when δ lies in the

lower half plane is for $c_\delta < 0$ (cf., Figs. 5.6). Since s_2 and s_δ are double valued functions of s_3 in this region, the b-quark lifetime and $\Gamma(b \to u)/\Gamma(b \to c)$ are also double valued functions of s_3. The upper branches in Fig. 5.6(a) correspond to the upper branches in Figs. 5.12(a) and 5.12(b). This is because the values of s_2 and s_3 are closer to each other in the upper branches of Fig. 5.6(a), yielding a stronger cancellation between the two terms in the square brackets of Eq. (5.22) and hence smaller values for $\Gamma(b \to c)$ than the lower branches of Fig. 5.6(a) give.

In Fig. 5.13 we plot τ_b and $\Gamma(b \to u)/\Gamma(b \to c)$ as functions of s_3 for the same choice of parameters as in Fig. 5.5 (i.e., $m_t = 30$ GeV, $B = 0.4$, $f = 0.75$). For a given s_3, s_2 is generally larger in Fig. 5.5(a) than in Fig. 5.4(a); therefore the b-quark lifetime is smaller in Fig. 5.13(a) than in Fig. 5.10(a). The general dependence of the b-quark lifetime on the mass of the t-quark can be deduced in a similar fashion. At fixed s_3, a value of m_t smaller than 30 GeV gives rise to a larger value of s_2 than is shown in Fig. 5.4(a). Therefore, when m_t is less than 30 GeV, the b-quark lifetime will generally be smaller than shown in Fig. 5.11(a).

It is interesting to compare the predictions shown in Figs. 5.11(a) and 5.12 with those of the free quark model shown in Fig. 5.14 (for δ in the upper half plane), where strong interaction effects are neglected. The parameter η defined in Eq. (5.27) is equal to one in the free quark model; the QCD corrections cause η to increase slightly. Most of the effects of the QCD corrections on the b-quark lifetime, τ_b, and the ratio of u-quark to c-quark production, $\Gamma(b \to u)/\Gamma(b \to c)$, is due to the QCD corrections to the allowed values of the six-quark model parameters θ_2, θ_3 and δ. For δ in the upper half plane, the QCD corrections tend to

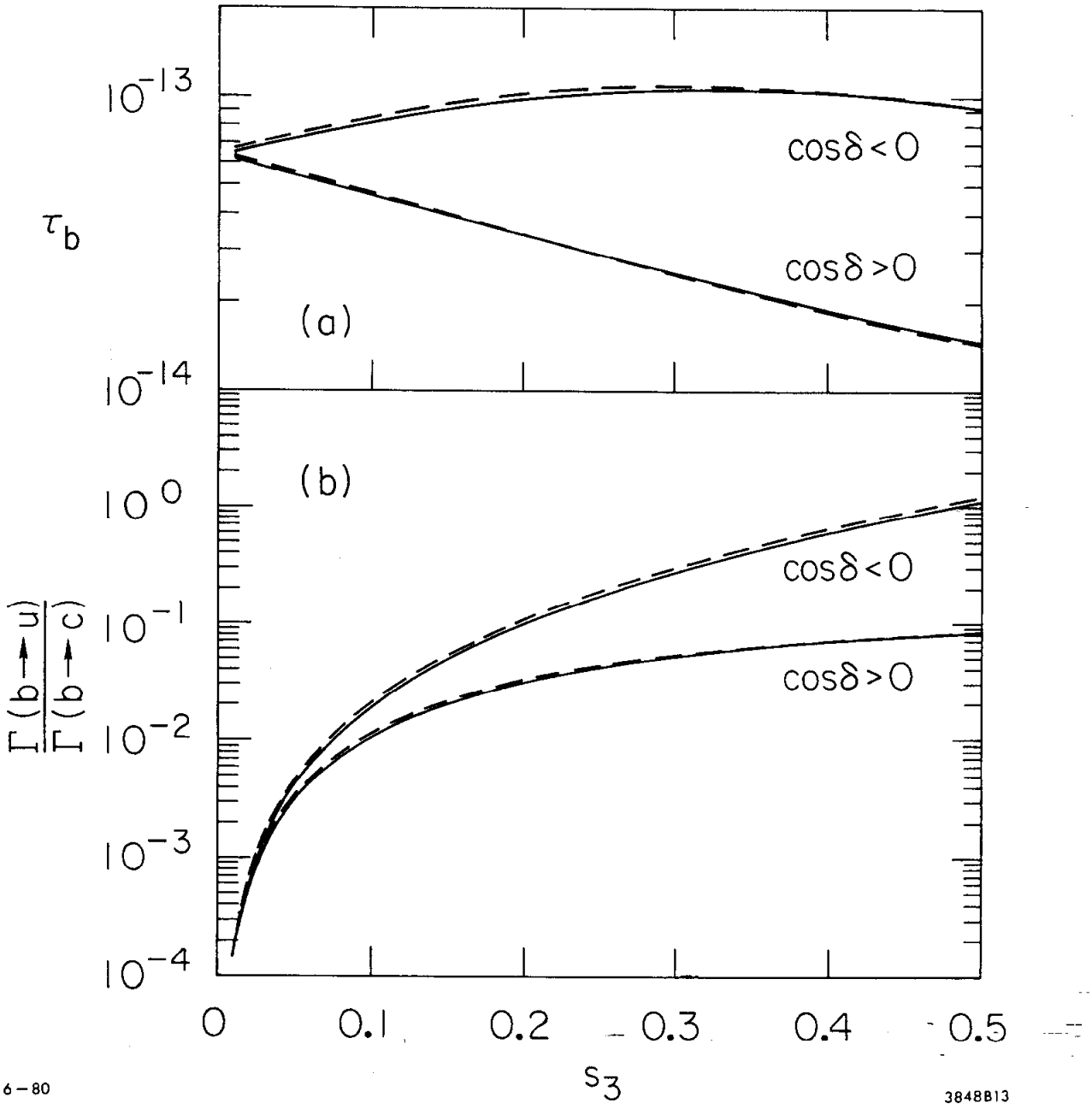

Fig. 5.13. Plot of (a) the b-quark lifetime τ_b (in seconds) and (b) the ratio of u-quark production to c-quark production $\Gamma(b \to u)/\Gamma(b \to c)$ for the allowed values of the six-quark model parameters shown in Figs. 5.5(a) and 5.5(b). Dashed lines are for $\Lambda^2 = .1$ GeV^2 and solid lines are for $\Lambda^2 = .01$ GeV^2.

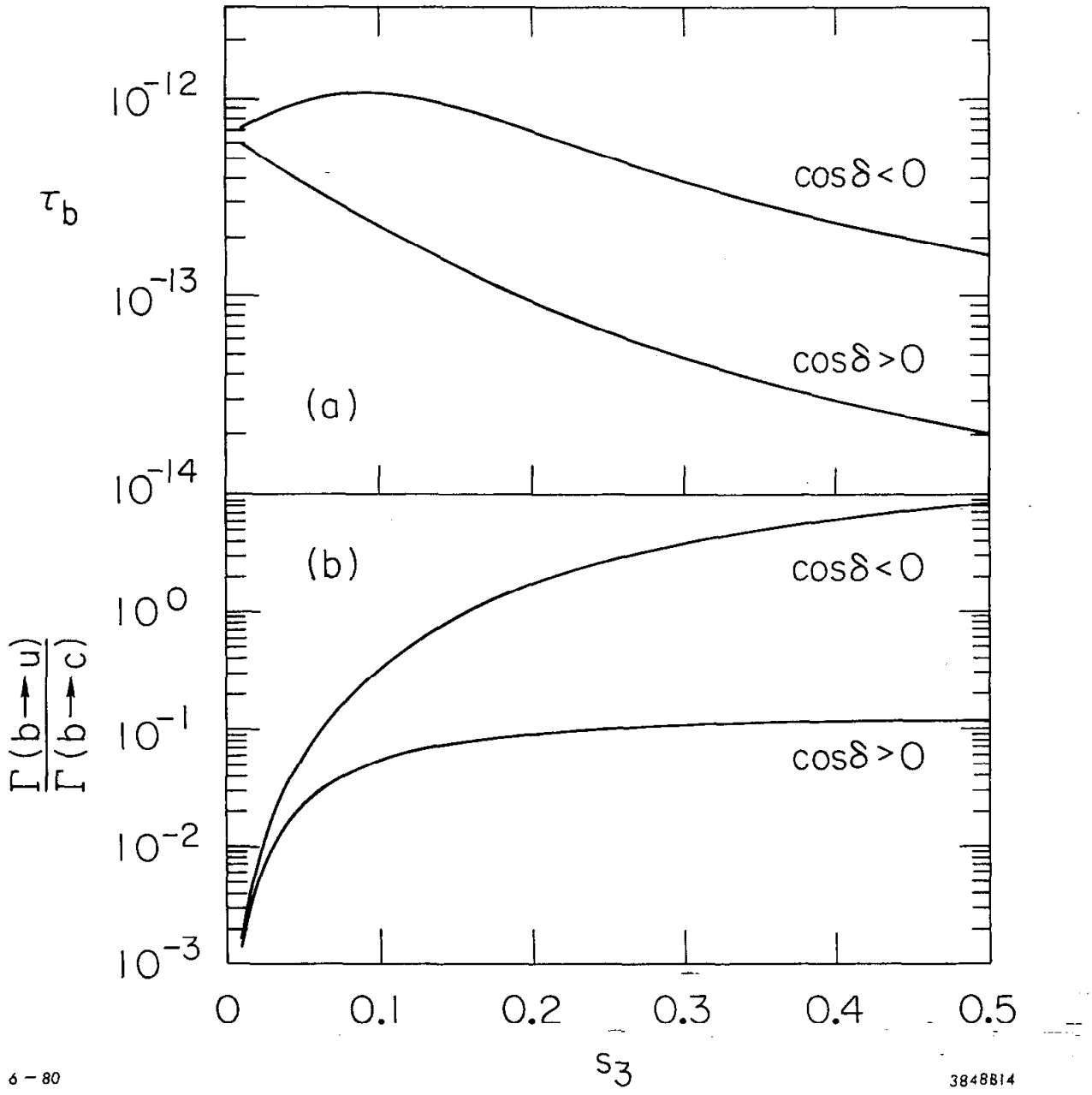

Fig. 5.14. Plot of (a) the b-quark lifetime τ_b (in seconds) and (b) the ratio of u-quark production to c-quark production $\Gamma(b \to u)/\Gamma(b \to c)$ for the values of the six-quark model parameters shown in Figs. 5.7(a) and 5.7(b).

increase the value of s_2 (at fixed s_3) so the b-quark lifetime in Fig. 5.14(a) is generally larger than in Fig. 5.11(a). When δ is in the lower half plane the b-quark lifetime and the ratio $\Gamma(b \to u)/\Gamma(b \to c)$ in the free quark model (i.e., no strong interactions) resemble those shown in Fig. 5.12 with $\Lambda^2 = 0.1$ GeV^2.

4. Summary

In this chapter we examined the constraints on parameters of the six-quark model imposed by the experimental values of the K_L-K_S mass difference and the CP violation parameter ϵ. Unlike previous work in which QCD effects were neglected, we have made use of calculations[11,18] where strong interaction effects are taken into account by summing the large logarithms in the W-boson, t-quark, b-quark and c-quark masses using renormalization group techniques. For the W-boson, t-quark and b-quark we have confidence in this procedure; however, treating the c-quark mass as large and using it as an expansion parameter is dubious at best. For example, in calculating the K_L-K_S mass difference, dispersive contributions were neglected[42] because they do not contribute to leading order in m_c^2. Such contributions arise when the two u-quarks in the loop of Fig. 5.1 bind to form a low mass hadronic state. Nevertheless, we have included strong interaction effects in a systematic way and in principle some of the higher order effects could be calculated. This is an improvement over the use of the free quark model.

The presence of many additional parameters (e.g., m_t, the matrix element $\langle K^o | (\bar{d}s)_{V-A} \, (\bar{d}s)_{V-A} | \bar{K}^o \rangle$, and Λ^2) whose values are not precisely known introduce further uncertainties in the constraints on the

parameters θ_2, θ_3 and δ of the six-quark model. We have explored the effects of varying these ancillary parameters.

Using the allowed values of the six-quark model parameters θ_2, θ_3 and δ we then calculated the CP violation parameter ε', the b-quark lifetime and the ratio of u-quark production to c-quark production in b-quark decays. There exists a small region of θ_2-θ_3-δ-space for which δ lies in the lower half plane and ε'/ε is negative. Since this region for $s_\delta < 0$ is much more restrictive than for $s_\delta > 0$, a measured negative value for ε'/ε in upcoming experiments would provide very stringent limits on the six-quark model parameters.[43] Within the picture where B meson decay results from a b-quark decaying into free quarks, with the final state quarks dressing themselves into hadrons with unit probability, the b-quark lifetime is equal to the B meson lifetime. We found the b-quark lifetime to be typically from 10^{-14} sec to 3×10^{-13} sec. We also found that when $c_\delta < 0$ the ratio of u-quark to c-quark production can be greater than one at large s_3.

REFERENCES AND FOOTNOTES FOR CHAPTER V

* Most of the results in this chapter can be found in B. D. Gaiser, T. Tsao and M. B. Wise, "Parameters of the Six-Quark Model, SLAC-PUB-2523, to be published in Annals of Physics.

1. S. L. Glashow, J. Iliopoulos and L. Maiani, Phys. Rev. D2, 1285 (1970).
2. M. K. Gaillard and B. W. Lee, Phys. Rev. D10, 897 (1974).
3. S. Weinberg, Phys. Rev. Lett. 19, 1264 (1967); A. Salam, in Elementary Particle Theory: Relativistic Groups and Analyticity (Nobel Symposium No. 8), edited by N. Svartholm (Almqvist and Wiksell, Stockholm, 1968), p. 367.
4. In the four-quark model with additional Higgs, CP violation can occur. See, for example, S. Weinberg, Phys. Rev. Lett. 37, 657 (1976); and P. Sikivie, Phys. Lett. 65B, 141 (1976).
5. M. Kobayashi and T. Maskawa, Prog. Theor. Phys. 49, 652 (1973).
6. R. E. Shrock and L. L. Wang, Phys. Rev. Lett. 41, 1692 (1978).
7. The constraints imposed on the parameters of the six-quark model by the upper limit on the decay width for $K_L \to \mu^+\mu^-$ have been discussed in: R. E. Shrock and M. B. Voloshin, Phys. Lett. 88B, 192 (1979).
8. J. Ellis, M. K. Gaillard and D. V. Nanopoulos, Nucl. Phys. B109, 213 (1976).
9. V. Barger, W. F. Long and S. Pakvasa, Phys. Rev. Lett. 42, 1589 (1979).
10. R. E. Shrock, S. B. Treiman and Ling-Lie Wang, Phys. Rev. Lett. 42, 1589 (1979).

11. F. J. Gilman and M. B. Wise, Phys. Rev. D20, 2392 (1979).

12. B. Guberina and R. D. Peccei, Nucl. Phys. B163, 289 (1980).

13. M. Gell-Mann and F. Low, Phys. Rev. 95, 1300 (1954); E. C. G. Stueckelberg and A. Peterman, Helv. Phys. Acta. 26, 499 (1953); C. G. Callan, Phys. Rev. D2, 1541 (1970); K. Symanzik, Commun. Math. Phys. 18, 227 (1970).

14. K. G. Wilson, Phys. Rev. 179, 1499 (1969).

15. A. I. Vainshtein, V. I. Zakharov and M. A. Shifman, Zh. Eksp. Teor. Fiz. Pis'ma Red. 22, 123 (1975) [JETP Lett. 22, 65 (1975)]; M. A. Shifman, A. I. Vainshtein and V. I. Zakharov, Nucl. Phys. B120, 316 (1977) and ITEP-63, ITEP-64 (1976), unpublished.

16. F. J. Gilman and M. B. Wise, Phys. Lett. 83B, 83 (1979).

17. R. Bernstein et al., Fermilab experiment E-617.

18. F. J. Gilman and M. B. Wise, SLAC-PUB-2473 (1980) (to appear in Phys. Lett.).

19. For a detailed discussion of what is meant by an effective theory of strong interactions see Sect. 3 of: E. Witten, Nucl. Phys. B104, 445 (1976).

20. Particle Data Group, Phys. Lett. 75B, 1 (1978).

21. We are grateful to K. Lane for an interesting discussion on this point.

22. For a review of the large N_c limit see: E. Witten, Nucl. Phys. B160, 57 (1979); S. Coleman, SLAC-PUB-2484 (1980).

23. R. E. Shrock and S. B. Treiman, Phys. Rev. D19, 2148 (1979).

24. If the large N_c limit or the free quark model is used for both the matrix elements $\langle K^o|(\bar{d}_\alpha s_\alpha)_{V-A}\ (\bar{d}_\beta s_\beta)_{V-A}|\bar{K}^o\rangle$ and the Wilson coefficients η_1, η_2 and η_3, then the resulting expression for the K_L-K_S mass difference is independent of μ.

25. See for example, K. Kleinknecht, in: Proceedings of the XVIIth International Conference on High Energy Physics (London, 1974), edited by J. R. Smith (Science Research Council, Rutherford Lab., 1974), pp. 111-123.

26. T. D. Lee and C. S. Wu, Am. Rev. Nucl. Sci. 16, 511 (1966).

27. The quantities m_c and m_t appearing in Eq. (5.3) are actually the running c-quark and t-quark masses. These are independent of the renormalization point μ and are most appropriately associated with spectroscopy. See Ref. 18.

28. J. G. H. Degroot et al., Phys. Lett. 82B, 292 (1979); 82B, 456 (1979); Z. Phys. C1, 142 (1979).

29. The constraints also depend on f_K and s_1^2. We use f_K = .159 GeV and s_1^2 = 0.0519.

30. J. S. Hagelin, Harvard University preprint, HUTP-80/A018 (1980), unpublished.

31. The values of C_6 given in Ref. 11 were calculated with M_W = 85 GeV, however, they will not differ significantly from the values of C_6 when M_W = 78 GeV is used.

32. For a review see: B. H. Wiik, DESY 79/84 (1979).

33. V. V. Prokhorov, Yad. Fiz. 30, 111 (1979).

34. J. S. Hagelin, Harvard University preprint, HUTP-80/A081 (1979), unpublished.

35. The quantity ξ can also be written as $\xi \approx \left[\frac{\mathrm{Im}C_6\langle\pi\pi(I=0)|Q_6|K^o\rangle}{A_o e^{i\delta_o}}\right]$.

36. The free quark model results are quite sensitive to the value of s_1^2 used. For example, if $s_1^2 = 0.059$ is used solutions with δ in the upper half plane would not exist for arbitrarily small s_3.

37. A similar picture when applied to D meson decays makes the unsuccessful prediction $\tau(D^o) = \tau(D^+)$. A possible explanation for the observed difference in lifetimes relies on a prominent role for the spectator in D^o decays. If this is the case, then we would expect our predictions to work only for charged B decays. See: M. Bander, D. Silverman and A. Soni, Phys. Rev. Lett. 44, 7 (1980).

38. See, for example, H. Harari, SLAC-PUB-2234 (1978), unpublished.

39. L. F. Abbott, P. Sikivie and M. B. Wise, Phys. Rev. D21, 768 (1980).

40. See, for example, A. Ali, J. G. Körner and G. Kramer, Z. Phys. C1, 269 (1979).

41. Similar discussions of b-quark decays in the six-quark model are given in Refs. 9 and 10, and in: H. Harari, SLAC-PUB-2234 (1978), unpublished; V. Barger, W. F. Long and S. Pakvasa, J. Phys. G5, L147 (1979).

42. Such contributions are discussed in: L. Wolfenstein, Nucl. Phys. B160, 501 (1979). Including these contributions would act much like a change in the parameter B.

43. If the parameter f is negative then ε'/ε will be negative for δ in the upper half plane. However, in this case the Penguin-type diagrams do not hlep explain the $\Delta I = \frac{1}{2}$ rule but rather act to suppress the $\Delta I = \frac{1}{2}$ enhancement.